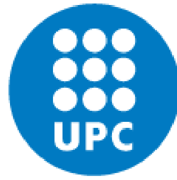

UNIVERSITAT POLITÈCNICA DE CATALUNYA
BARCELONATECH
Departament d'Enginyeria Electrònica

Dielectric charge control in contactless capacitive MEMS

Dissertation presented as a *compendium of publications*
in partial fulfillment of the requirements for the degree of
Doctor in Electronic Engineering

Sergi Gorreta Mariné

Co-advisors: Dr. Manuel Domínguez Pumar
Dr. Joan Pons Nin

June 2017

Electronic Engineering Department

To my parents.

Acknowledgments

First and foremost, I would like to offer my sincere thanks to my advisors, Manuel Domínguez and Joan Pons. I have been working with them since the third year of my degree and they have been supportive throughout this incredible journey of nine years making my Ph.D experience stimulating and productive. Also, I am hugely appreciative to the Professor Luis Castañer for involving me in the "Mars team" and sharing his enormous knowledge, expertise and management skills. And, of course, I wish to express my most sincere gratitude to Vicente Jiménez for nurturing my enthusiasm for electronics and his continuous help and assistance in numerous ways during all these years.

I would like to express my deep gratitude to those who have made this journey much more enjoyable. I am especially grateful to Albert Orpella and Eva Vidal for their confidence and their fidelity. Special thanks to the colleagues from the D213 and neighboring buildings with whom I have had the pleasure to share good moments: Jordi Ricart, Elisenda Bou, Gema López, Éric Calle, Raul Gómez, Albert Mestres, Joan Capdevila, Kike Barajas, Teresa Atienza, Chenna Bheesayagari, Lukasz Kowalski, Arnau Coll, Chen Jin and Gerard Masmitja. I also thank the technicians: Santi Pérez and Miguel García for their professionalism, their huge knowledge and the good moments spent together.

Finally I will not forget to thank the people who have had tremendous influence in my life: my family and my always-willing friends. They have been my biggest support for everything and have been there for me no matter what. All of them have made me the person I am today, and have helped all of my dreams come true. Although I really need to find a better way to express my gratitude, thank you all so much!

Abstract

Micro-Electro-Mechanical Systems, or MEMS, has been a continuously growing technology during the last decades. Since 1959, when the theoretical physicist Richard Feynman introduced the concept of nanotechnology in his famous talk "There is plenty of room at the bottom", several companies and researchers have been involved in the permanent improving of these devices. MEMS is the technology of microscopic devices, particularly those with moving parts and it is widely used in both sensing and actuating applications. In this regard, a large number of microsensors for almost every possible sensing modality have been developed, including pressure, inertial forces, chemical species, magnetic fields, etc. Accordingly to this, MEMS can be found today in many real applications across multiple markets, such as automotive, consumer, defense, industrial, medical, telecommunications, etc. The main advantages for the use of MEMS in front of other classical technologies are small size, low cost, high isolation and low power consumption.

However, there are still some reliability issues hindering the use of MEMS devices in some applications. Mechanical and electrical phenomena involving such micro-scale structures have been matter of study during the last years, being *dielectric charging* the most important in the case of electrostatically actuated MEMS. The charge accumulated in dielectric layers has a significant impact on the behavior of such devices by altering the electric field distribution in the structure and causing some undesirable effects such as shifts of the Capacitance-Voltage (C-V) characteristic and even permanent stiction of movable mechanical parts, so that the device becomes permanently damaged. Thus, detection and control of dielectric charge are of capital importance due to their strong influence on device performance and reliability.

In order to face this challenge, in this Thesis dielectric charge phenomena have been studied under bipolar voltage actuation and several different control

strategies have been proposed. These control schemes have demonstrated to be useful to set the dielectric charge to a desired level for contactless MEMS such as varactors, electrostatic positioners or microphone MEMS. Furthermore, these methods have provided the first active compensation of charge trapping generated by ionizing radiation in any device.

The first approach to control trapped charge proposed consisted in alternating voltage polarity, depending on the sampled value of the device capacitance. This method demonstrated the feasibility of compensating horizontal shifts of the C-V by charge injection while paving the way for the second control proposed. For the implementation of this second method, which was later patented worldwide, two voltage waveforms were introduced for both monitoring and controlling the net trapping charge. This method resulted in a true sigma-delta modulator capable of providing control for both signs of net trapped charge.

Finally, two further methods were proposed which improved the performance of the second control. The first one implemented a second-order sigma-delta control and the last one introduced some modifications in the feedback loop to allow continuous capacitance control while dielectric charge is being also controlled.

Resumen

Los sistemas micro-electromecánicos, conocidos como MEMS, constituyen una alternativa tecnologíca que ha experimentado un gran crecimiento en las últimas décadas. Desde que en 1959, cuando el físico teórico Richard Feynman introdujo el concepto de nanotecnología en su famosa conferencia “There is plenty of room at the bottom”, multitud de investigadores y empresas se han dedicado al desarrollo y la mejora permanente de este tipo de dispositivos. Las principales ventajas del uso de MEMS frente otras tecnologías más clásicas radican en su menor tamaño, su reducido coste y su bajo consumo. En tanto MEMS se refiere habitualmente a tecnologías micrométricaa de dispositivos que presentan partes móbiles, éstos son extensamente utilizados en aplicaciones tanto de detección como de actuación. Así, se ha desarrollado un gran número de microsensores MEMS, cubriendo prácticamente todas las modalidades de detección, incluyendo presión, fuerzas inerciales, sustancias químicas, campos magnéticos, etc. Hoy en día, se utilizan dispositivos MEMS en aplicaciones de mercados como automoción, industria, medicina, telecomunicaciones, defensa, etc.

Sin embargo, existen aún problemas de fiabilidad que limitan el uso de los MEMS en determinadas aplicaciones. Los fenómenos mecánicos y eléctricos que se producen en estas estructuras micrométricas han sido objeto de estudio durante los últimos años, siendo el más destacado el producido por la carga eléctrica acumulada en las capas dieléctricas que forman parte de los MEMS actuados electrostáticamente. Esta acumulación de carga altera la distribución de campo eléctrico en el dispositivo, afectando el comportamiento y las prestaciones de éste y causando efectos no deseados, como desplazamientos de la característica Capacidad-Tensión (C-V) e incluso colapsos indeseados de las partes móviles, que pueden conllevar daños permanentes. En consecuencia, la detección y el control de la carga acumulada en dieléctricos de MEMS son temas de vital importancia, debido a su enorme impacto en el rendimiento y la fiabilidad de los dispositivos.

Esta Tesis aborda este desafío, primero estudiando y modelizando la dinámica de la acumulación de carga dieléctrica cuando el dispositivo se actúa con tensiones bipolares, y, a continuación, proponiendo y evaluando estrategias de control de dicha carga. Se han demostrado estrategias que, por primera vez, permiten mantener un nivel de carga prefijado en dispositivos MEMS que operan en estado abierto, como varactores, posicionadores electrostáticos o micrófonos MEMS. Además, estos controles han permitido realizar la primera demostración de compensación activa de carga generada por radiaciones ionizantes en dispositivos MEMS.

El primer control propuesto consistía en alternar la polaridad de la tensión de actuación, dependiendo del valor de capacidad del dispositivo medido periódicamente. Con el uso de este método se demostró la factibilidad de compensar desplazamientos horizontales de la C-V mediante la inyección de carga debida a la actuación y se abrió el camino para la concepción de un segundo método mejorado. Para la implementación de este segundo método, que fue patentado más tarde, se propusieron dos formas de onda para actuar el dispositivo, que permiten tanto la monitorización como el control de la carga atrapada. Este método se basa en la modulación sigma-delta de primer orden y permite, por primera vez, controlar la carga neta atrapada en el dieléctrico.

Finalmente, se han propuesto dos métodos de control más, con el objetivo de introducir mejoras sobre los ya comentados. El primero de ellos implementa una modulación sigma-delta de segundo orden, mientras que en el segundo se introducen algunas modificaciones en el lazo de ralimentación que permiten el control de la capacidad del dispositivo al mismo tiempo que el control de la carga neta atrapada.

Sometimes it's not enough to know
what things mean,
sometimes you have to know
what things don't mean.

Bob Dylan.

Contents

1 Introduction **1**
1.1 Framework of the Thesis 1
1.2 Objectives 8
1.3 Methodology 9
1.4 Document organization 10
References 12

2 Thesis summary **15**
2.1 Dielectric charging in contacless MEMS 16
2.1.1 The dielectric charging problem in MEMS 16
2.1.2 Dielectric charging dynamics 22
2.2 Mitigation techniques 31
2.2.1 Actuation strategies 31
2.2.2 Mechanical improvements 36
2.2.3 Fabrication process approaches 38
2.3 Charge control strategies 40
2.4 Ionizing radiation 58
2.5 Main contributions of the Thesis 65
References 67

3 Compendium publications **75**
3.1 Dielectric charge control in electrostatic MEMS 79
3.2 Characterization method of the dynamics of the trapped charge . 95
3.3 $\Delta - \Sigma$ control of dielectric charge 101
3.4 Real-time characterization of dielectric charging 115
3.5 Second order $\Delta - \Sigma$ control of dielectric charge 127
3.6 Closed-loop compensation of dielectric charge induced by radiation 131

3.7 Charge induced by ionizing radiation 135
3.8 Simultaneous control of dielectric charge and device capacitance . 141

4 Conclusions and future work 145
4.1 Conclusions 145
4.2 Future work 146

Appendices 149

A Other Thesis-related journal publications 151
A.1 Sliding Mode Analysis of the dielectric charge dynamics 153
A.2 $\Sigma - \Delta$ effects and charge locking under dielectric charge control . 163
A.3 Characterization of dielectric charging with diffusive representation 169

B Thesis-related patents 175
B.1 A method and a controller for a MEMS device 177

C Other Thesis-related conference publications 203
C.1 Modelling of a charge control method for capacitive MEMS 207
C.2 Sigma-Delta control for the improvement of MEMS reliability . . 211
C.3 Understanding complexity in multiphysics systems-on-a-chip . . . 215
C.4 Sigma-Delta closed loop control of multiexponential systems . . . 219
C.5 Circuit considerations and design for MEMS measurements 225
C.6 Circuit modeling of a MEMS varactor 229

D PDO-related journal publications 235
D.1 Control of MEMS vibration modes with Pulsed Digital Oscillators 237
D.2 Pulsed Digital Oscillators for electrostatic MEMS 249
D.3 A CubeSAT payload for monitoring pentacene degradation 261

Chapter 1

Introduction

1.1 Framework of the Thesis

Micro-Electro-Mechanical Systems, henceforth referred to as MEMS, is a relatively new technology based on the miniaturization of different electro-mechanical integrated components where the feature size and the actuating range are within (and even below) the micro-scale. Several specific techniques of microfabrication have been developed during the last decades with the aim of reaching critical physical dimensions. Nowadays, MEMS structures can be fabricated with dimensions ranging from well below one micron (NEMS) to several millimetres. One of the main objectives behind MEMS miniaturization is to provide integrability with CMOS IC technologies, which can allow these devices to be batch-fabricated and thus making them less expensive and increasing their reliability. Furthermore, these tiny devices offer solutions which cannot be attained by classical macro-machined products. For example, capacitive pressure sensors are able to sense pressure ranges of the order of 1 mTorr, an unreachable magnitude for macro-machined capacitive diaphragms. In the case of switches working as parts of communications circuitry, this technology allows phase shifting and signal switching at speeds that are not possible to achieve by macro-scale switches.

However, although most MEMS are fabricated using Si-based processes related to conventional IC technologies, its integrability is not as easy as thought to be [1]. Different aspects that can be present in MEMS fabrication processes that are different from typical IC fabrication are summarized in Table 1.2 [2].

Likewise, a MEMS can be seen as a transducer which converts a measurable mechanical signal into an electrical or optical one or vice-versa. This term can

Feature	Differences
Unconventional Materials	More kinds of materials are present in the MEMS fabrication process such as quartz, ceramics, or polymide.
Lack of Standard Processes	MEMS fabrication is much more customized and diversified among different applications and different foundries.
Feature Size	Cheaper mask cost in MEMS fabrication due to its large feature size compared with IC components.
Mechanical Properties	MEMS fabrication needs more care with mechanical properties such as Young's modulus, yield strength, density, residual stress..
Unique Unit Processes	Some unit processes such as plating, molding, and wafer bonding, are more common in MEMS. Also thicker deposition of materials and the use of DRIE process to create deep penetration, steep-sided holes and trenches.
Release Process	This is needed in MEMS to release the movable parts of the device from the substrate.
Stiction	Stiction caused by strong adhesion forces between movable structures and the substrate must be avoided by the use of special layers.
Doping	the doping of materials is not as critical process as in the case of IC. This could cause compatibility problems.
Wafer Bonding	MEMS fabrication usually need wafer bonding to form protective caps/cavities, or wafer level packaging, or implement the integration of ASIC and MEMS transducers.
Less Layers	The number of layers/masks in MEMS fabrication is usually less than IC fabrication.
Front/Back Side Processing	Some MEMS devices need to be processed on both front and back sides of the wafer in contrast with IC fabrication.
MEMS Package Stress	The package stress can cause deflection and stress MEMS structures and thus change the device behaviour.

Table 1.1: Differences in MEMS fabrication processes from those used in IC fabrication.

therefore be used to include both sensors and actuators. In this regard, a large number of MEMS micro-sensors for almost every possible sensing modality have been developed, including temperature, pressure, inertial forces, chemical species, magnetic fields, radiation, etc. As a consequence, different MEMS-based solutions have been proposed and they can be found today in many real applications and multiple markets. Some examples of these applications are shown in Table 1.2, [3].

Product	Examples
Pressure sensor	Manifold pressure (MAP), tire pressure, blood pressure...
Inertia sensor	Accelerometer, gyroscope, crash sensor...
Microfluidics, BioMEMS	Inkjet printer nozzle, micro-bio-analysis systems, DNA chips...
Optical MEMS, MOEMS	Micro-mirror array for projection (DLP), micro-grating array for projection (GLV), optical fiber switch, adaptive optics...
RF MEMS	High Q-inductors, switches, antenna, filters...
Others	Oscillators, Relays, microphone, data storage...

Table 1.2: MEMS products example.

2015-2021 MEMS market forecast in US$B
(Source: Status of the MEMS Industry report, Yole Développement, May 2016)

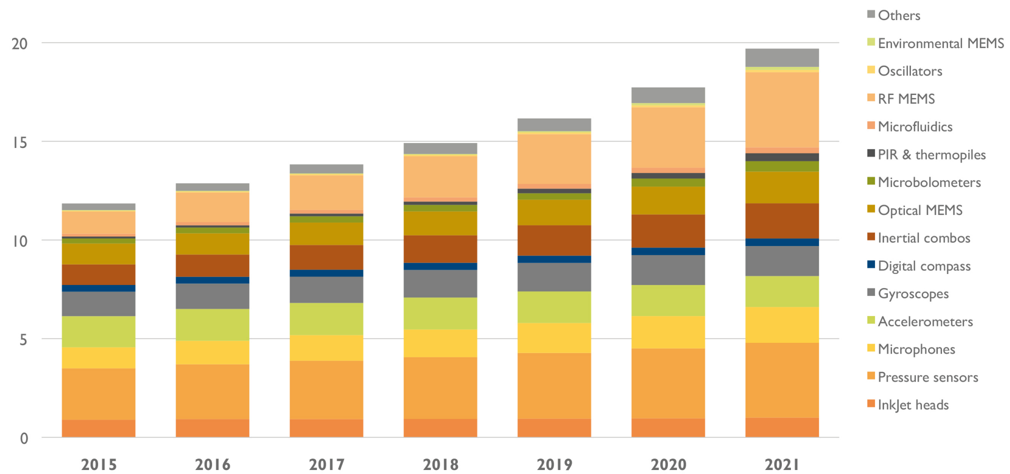

Figure 1.1: MEMS market forecast, from [4].

The MEMS market is continuously growing due to improvements in key factors like size, weight, reliability or cost. These improvements allow to implement this technology in numerous industrial applications such as automotive, consumer, defence, medical, and communications, among others. Figure 1.1 summarizes the results of a study carried out by Yole Development, an important market research and strategy consulting company [4]. This study reflects the market increase of MEMS switches, MEMS pressure sensors and MEMS microphones. This can be associated with the use of this components in current hand-held devices such as smartphones or tablets.

On the other hand, from the point of view of the actuation strategy, MEMS

can be classified into four main categories: electrostatic , magnetic , thermal-bimetallic and piezoelectric [5]. These different methods are associated with the type of energy transduction mechanism that generates mechanical movements in the device. They can be briefly summarized as follows:

- Electrostatic actuation: force generated when an applied electric field acts on induced or permanent charges.
- Magnetic actuation: moment and force due to interaction of magnetic domains with external magnetic field lines.
- Thermal bimetallic actuation: force due to differential volume expansion of at least two different materials when temperature changes.
- Piezoelectric actuation: force due to change of material dimensions when an electric field is applied.

The Thesis work related in this document is focused on the analysis and compensation of dielectric charging in electrostatically actuated MEMS. In accordance with this, electrostatic MEMS devices will be explained in more detail in the next section. On the other hand, a side project that used electrostatic and thermoelectric MEMS in Pulsed Digital Oscillators (PDO) [6–8] applications was also done during Thesis time.

Electrostatic MEMS

The typical configuration to analyse electrostatic MEMS is the two-parallel plate structure depicted in Fig 1.2. It consists in two conducting plates, one moveable and the other fixed, separated by an air gap. In this kind of structures, the movement of the top plate is due to the electrostatic force generated when the device is biased with a voltage $V(t)$. Additionally, a dielectric layer is usually deposited on top of the fixed plate to avoid short-circuiting of the electrodes. However, let us consider a first approximation in which the effect of the dielectric layer is not contemplated. In this case, the relationship between the bias voltage V and the electrostatic force exerted on the movable plate F_{el} can be modelled as [9],

$$F_{el}(x) = \frac{\varepsilon A V^2}{2(g-x)^2} \tag{1.1}$$

where x is the deflection of the moveable plate, ε is the dielectric constant of the

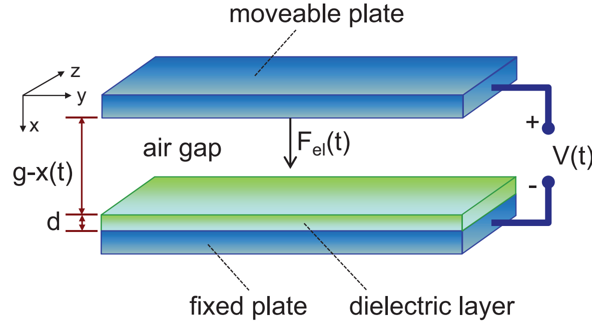

Figure 1.2: Typical structure of an electrostatic MEMS.

air, A the plate area and g the air gap when V =0 is applied.

Equation (1.1) implies that the electrostatic force increases when increasing the bias voltage. This leads to distance reduction between both electrodes and thus an increase of the device capacitance. Under this operating principle the electrostatic force is countered by the restoring mechanical force of the top electrode and then an equilibrium point is reached. However, when a certain voltage value, pull-in voltage $V_{pull-in}$, is reached the electrostatic force becomes greater than the mechanical force and causes the collapse of the plates. That is, the pull-in phenomenon produces sudden switching from the OFF (or open) to the ON (or closed) states of the device. For a device with no dielectric between the plates, the pull-in value corresponds to a displacement of 1/3 of the gap $x = g/3$ [10].

On the other hand, when decreasing the bias voltage from the ON-closed state, the transition to the OFF-open state occurs at the pull-out $V_{pull-out}$, or release, voltage, which is usually smaller than $V_{pull-in}$. Since the electrostatic force is a non-linear function of the gap, the device reveals an hysteresis-like behaviour, in which the voltage that allows closing the gap is different to that needed to release the plate from the ON state.

Furthermore, it must be noted that the electrostatic force is always attractive, and thus it does not depend on the polarity of the voltage applied. Then, pull-in and pull-out voltages exist for both positive and negative bias. Figure 1.3 [11] shows the typical capacitance-voltage (C-V) characteristic of an electrostatic MEMS. There, the two possible working states (ON and OFF) that exhibit these devices are clearly seen. Many applications take advantage of these two states to implement actuating devices such as RF-MEMS switches or tunable antennas. In these applications, switching between the ON and OFF states is often used to

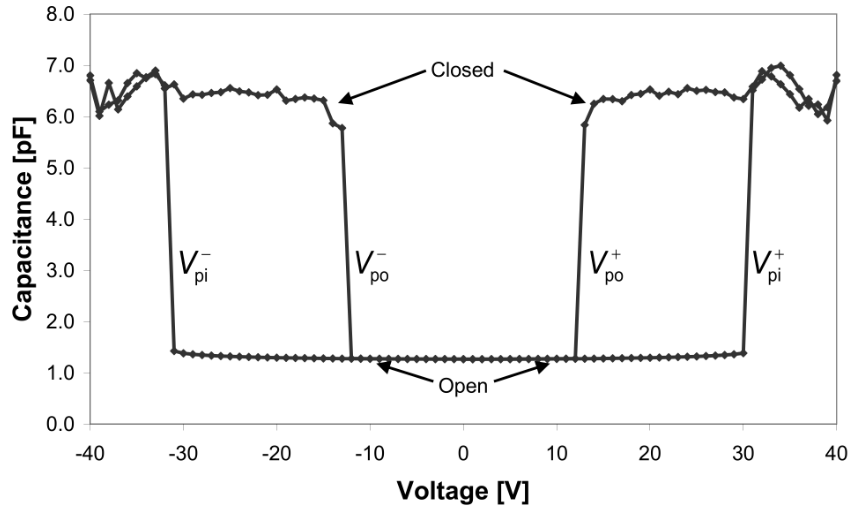

Figure 1.3: Typical C-V curve of an electrostatic MEMS. Reproduced from [11], ©IEEE.

cause significant changes in the impedance of the circuit. On the other hand, in other applications MEMS are only used in the OFF, or contactless, state. For instance, changes in a sensing variable are detected as small variations of the device capacitance. This is the case of MEMS microphones [12] or accelerometers [13].

Figure 1.4 shows the contactless zone of a C-V curve of a MEMS microphone [12]. In this application, the device works as a variable capacitor in which the transduction principle is the coupled capacitance change between the fixed and movable plates caused by the incoming sound waves. This movement is then detected by an integrated circuit which converts these capacitance changes into a digital or analog signal output.

As it has been previously commented, in electrostatic MEMS, a dielectric layer is usually present between both electrodes. The main objective for the use of this layer is to avoid short-circuiting in the ON state, but also to increase the capacitance ratio C_{ON}/C_{OFF}, a key factor in applications such as RF-MEMS components. However, the presence of dielectric layers is responsible of a major reliability problem in electrostatic MEMS: *dielectric charging*. This phenomenon occurs due to the accumulation of charge induced by device polarization. The charge accumulated in the dielectric layer alters the electric field distribution in the gap and it can cause significant changes on the behaviour of the device, such as shifts in the C-V characteristic. This charge can be seen as a built-up voltage present in the dielectric that varies slowly with use. As a consequence,

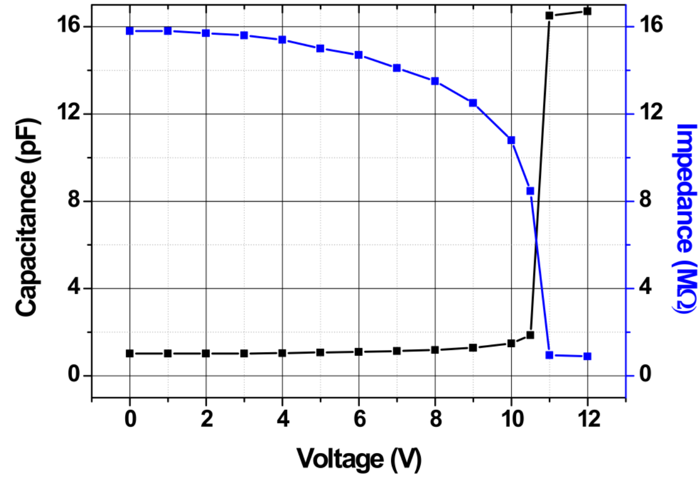

Figure 1.4: C-V curve of a MEMS microphone. Reproduced from [12], ©IEEE.

the effective voltage "seen" by the device varies with time and is different than the external bias applied. This effective voltage can exceed $V_{pull-in}$, causing unwanted switching events, or, moreover, it can increase enough to provoke the permanent stiction of the plates [14–17]. In this case, the device will remain in ON state even when the bias voltage is set to zero. Dielectric charging also causes reliability problems in MEMS working only in the contactless state. For example, in MEMS oscillators dielectric charges can change the resonant frequency [18–20], whereas in the case of MEMS microphones they can cause drifts in the sensitivity of the device. This is a big issue since the performance algorithms used in functions such as noise cancellation usually assume sensitivity matching between different devices working in an array configuration [21]. In this specific application this can also make difficult to know the direction of the arrival sound, since it is inferred from the variation of the sensitivity response between different devices [22].

However, and unfortunately, charge accumulation is not the only mechanism that can affect the C-V characteristic of an electrostatic MEMS. There are some mechanical factors that can also reduce the reliability of these devices. Figure 1.5 depicts up to four possible evolutions of the C-V, which can be explained as follows:

a) Typical C-V characteristic in the discharged (zero dielectric charge) case.

b) *Shifting:* Horizontal shift of the C-V caused by trapped charge. In this ideal case, the lifetime of a device could be determined by analizing dielectric charging dynamics. It will be explained in Section 2.1.2.

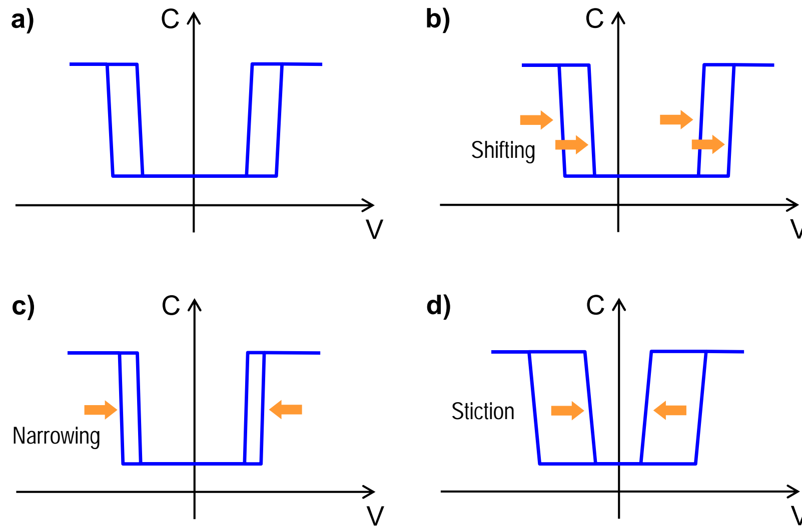

Figure 1.5: Possible C-V evolutions.

c) *Narrowing:* This is a complex phenomenon, the causes of which are more speculative. On one side, it has been reported to be due to non-uniform charge distribution along the dielectric layer [23]. Also, mechanical creep has been indicated to be the cause of this effect, since it reduces the effective stiffness of MEMS mechanical structures and thus both pull-in and pull-out voltages are also reduced [24].

d) *Stiction:* It is associated with MEMS switches where the device is relatively stable when working in the ON-closed state, but the contact becomes sticky and reduces the release voltage.

1.2 Objectives

Accordingly to the discussion above, the main objective of this Thesis is to contribute to the improvement of the reliability of electrostatic MEMS, by proposing and demonstrating effective strategies for dielectric charging control. As it will be discussed in Chapter 2, different methods for both analyzing and mitigating this undesired phenomenon have been proposed in the literature. These techniques usually focus on mitigation by either improving the design of the device, or using specific-proprietary fabrication processes, or implementing smart voltage waveforms to actuate the device (in open-loop). Although these mitigation strategies

are able to enlarge the lifetime of the devices in some applications, none of them has demonstrated to completely solve this key issue at long term. This Thesis proposes, analyzes and verifies experimentally closed-loop control strategies to set and keep the dielectric charge, and thus its effects on device performance, to a previously given value. The devices used to this purpose are electrostatic MEMS working in the contactless state.

To achieve this goal, the following steps have been performed:

- *Dielectric charge sensing*: the method proposed must be able to continuously monitor the net trapped charge of devices working in the contactless state. In this situation the typical methods based in measuring the displacement of the pull-in voltage must be avoided.

- *Dielectric charge analysis and modelling*: characterization of the charge dynamics by applying an approach based on state-variables analysis. The previous step is needed to obtain this evolution under different bias voltages.

- *Dielectric charge controls*: from the results obtained in the previous step, new closed-loop control strategies must be implemented. In this phase it is important to demonstrate the viability of controlling dielectric charging by applying smart strategies, based on sigma-delta modulation, in which bipolar voltage waveforms are used.

- *Capacitance control*: As a final challenge, in this phase it is proposed to implement a new method able to compensate dielectric charge while maintaining a desired value of device capacitance. This last step is focused on solving dielectric charging issues in those applications in which the capacitance value is a key factor. For example: positioners, varactors, MEMS microphone, etc.

1.3 Methodology

This Thesis had the objective to analize dielectric charging in electrostatic MEMS working in the contactless state and propose new control techniques. As a first stage, the research done included the analysis of this phenomenon under different bias voltages. For this analysis, the device was stressed at positive and negative

voltages while monitoring the charge evolution. The results obtained were analized by applying an approach based on state-variables analysis, consisting in a set of first-order differential equations describing the evolution of multiple positive and negative charge contributions to model charge injection and detrapping at constant stress. This work was carried out using a multi-exponential model (one of the most common models used in the literature to describe dielectric charging dynamics) which allowed to determine the evolution of the dielectric charge depending on the specific sequence of applied voltages. Extensive experimental measurements were made to extract dynamical models. In order to process all these measurements MATLAB and C programming were used. The same tools were used for simulation and model extraction (i.e. fittings from measurements).

On the other hand, the experimental set-up to implement charge control experiments consisted in a Keysight E4980a precision LCR meter that was in charge of making capacitance measurements and applying smart device actuation. The apparatus was connected to a computer, which implemented the control feedback loops. Since the capacitance measurements carried out needed to be as precise as possible, i.e. in the range of femto Farads, the use of the commercial LCR meter was the option chosen against of other possible solutions, such as discrete or integrated electronic designs. Furthermore, a high versatility of the measurement set-up was needed to implement different control strategies, then the use of programmable instrumentation was incredibly useful. The equipment used in this Thesis to carry out the experiments includes other laboratory stuff, such as a probe station for on-waver measurements, an impedance anayzer Agilent 4294A, vacuum and climate (ambient control) chambers, etc. Additionally, other experimental work made outside the UPC implied using X-Ray and Gamma irradiation equipment.

As it has been commented above, different control strategies were tried during the Thesis. As a consequence, a set of specific software programs to control the laboratory equipment cited above and to perform data post-processing has been developed using Visual Basic, Java and MatLab environments.

1.4 Document organization

The research work done along this Thesis is presented in this report as a compendium of publications. After this chapter, which contains an introduction to

MEMS technology with special emphasis in the electrostatic actuated devices and their most typical reliability issues, the remaining of this document is organized as follows.

- Chapter 2 describes the state of the art preceding this Thesis and links it with the work performed within the Thesis. In this chapter it can be found the most significant contributions regarding the analysis and mitigation techniques proposed to solve dielectric charging phenomenon in electrostatic MEMS. For all of them, it will be briefly presented the methods proposed in this Thesis to face this key problem, which are explained in detail in Chapter 3.
- Chapter 3 contains the full text of the publications conforming the compendium. It is composed of seven publications in JCR-indexed scientific journals plus one publication in an international research conference. All these papers are presented in chronological order, in agreement with how the related tasks were done.
- Chapter 4, and last, draws the main conclusions derived from the results of the Thesis work. It also includes a future work section, which highlights potential research lines stemming from this work.
- Finally, the appendixes include a selection of other Thesis-related publications not included in the compendium. They are organized as follows:
  - Appendix A includes three journal publications related either to works performed or to methods proposed in this Thesis.
  - Appendix B includes an European Union patent of one of the dielectric charge controls proposed, the first-order sigma-delta control that can be found in Section 3.3.
  - Appendix C includes several conference publications related to methods proposed in this Thesis.
  - Appendix D presents three journal publications derived from the results obtained in a side project of this Thesis in which thermoelectric and electrostatic MEMS were used to implement Pulsed Digital Oscillators.

References

[1] R. Vemal et al. "MEMS vs. IC manufacturing: Is integration between processes possible". In: *2009 1st Asia Symposium on Quality Electronic Design.* 2009, pp. 39–43.

[2] *MEMS fabrication versus IC fabrication.* Sept. 2015. URL: `http://memsfoundry.wikia.com/wiki/MEMS_fabrication_versus_IC_fabrication`.

[3] F. Chollet and H. Liu. *A (not so) short introduction to Micro Electromechanical Systems.* June 2016. URL: `http://memscyclopedia.org/introMEMS.html`.

[4] E Mounier et al. *Status of the MEMS industry 2016.* Tech. rep. Yole Developpment, 2016.

[5] C. Liu. *Foundations of MEMS.* Pearson, 2013.

[6] M. Dominguez et al. "Analysis of the Sigma-Delta; pulsed digital oscillator for MEMS". In: *IEEE Transactions on Circuits and Systems I: Regular Papers* 52.11 (2005), pp. 2286–2297.

[7] M. Dominguez, J. Pons-Nin, and J. Ricart. "General Dynamics of Pulsed Digital Oscillators". In: *IEEE Transactions on Circuits and Systems I: Regular Papers* 55.7 (2008), pp. 2038–2050.

[8] S. Gorreta et al. "Pulsed Digital Oscillators for Electrostatic MEMS". In: *IEEE Transactions on Circuits and Systems I: Regular Papers* 59.12 (2012), pp. 2835–2845.

[9] L. Castaner. *Understanding MEMS, Principles and Applications.* Wiley, 2016.

[10] G. M. Rebeiz. *RF MEMS theory, design and technology.* Wiley, 2003.

[11] R. W. Herfst et al. "Characterization of dielectric charging in RF MEMS capacitive switches". In: *2006 IEEE International Conference on Microelectronic Test Structures.* 2006, pp. 133–136.

[12] C. H. Je et al. "A surface micromachined MEMS capacitive microphone with back-plate supporting pillars". In: *2013 IEEE Sensors.* 2013, pp. 1–4.

[13] S. Tez and T. Akin. "Fabrication of a sandwich type three axis capacitive MEMS accelerometer". In: *2013 IEEE Sensors.* 2013, pp. 1–4.

[14] J. Wibbeler, G. Pfeifer, and M. Hietschold. “Parasitic charging of dielectric surfaces in capacitive microelectromechanical systems (MEMS)”. In: *Sensors and Actuators A* 71 (1997), pp. 74–80.

[15] C. Goldsmith et al. “Lifetime characterization of capacitive RF MEMS switches”. In: *2001 IEEE MTT-S International Microwave Symp. Digest.* Phoenix, AZ, 2001, pp. 227–230.

[16] J. Webster et al. “Process-induced trapping of charge in PECVD dielectrics for RF MEMS capacitive switches”. In: *Proc. of 43rd (2005) Annual IEEE International Reliability Physics Symposium.* 2005, pp. 330–336.

[17] D. Molinero, R. Comulada, and L. Castaner. “Dielectric charge measurements in capacitive microelectromechanical switches”. In: *Applied Physics Letters* 89 (2006), p. 103506.

[18] S. Kalicinski, M. Wevers, and I. De Wolf. “Charging and discharging phenomena in electrostatically-driven single-crystal-silicon MEM resonators: DC bias dependence and influence on the series resonance frequency”. In: *Microelectronics Reliability* 48 (2008), pp. 1221–1226.

[19] G. Bahl et al. “Model and Observations of Dielectric Charge in Thermally Oxidized Silicon Resonators”. In: *IEEE JMEMS* 19 (2010), pp. 162–174.

[20] G. Bahl et al. “AC Polarization for Charge-Drift Elimination in Resonant Electrostatic MEMS and Oscillators”. In: *IEEE JMEMS* 20 (2011), pp. 355–364.

[21] J Widder and A Morcelli. *Basic principles of MEMS microphones.* Tech. rep. EDN Network, 2014.

[22] *MEMS Microphone - a breakthrough innovation in sound sensing.* Feb. 2017. URL: `http://www.eeherald.com/section/design-guide/mems-microphone.html`.

[23] X. Rottenberg et al. “Analytical Model of the DC Actuation of Electrostatic MEMS Devices with Distributed Dielectric Charging and Nonplanar Electrodes”. In: *IEEE JMEMS* 16 (2007), pp. 1243–1253.

[24] M. van Gils, J. Bielen, and G. McDonald. “Evaluation of Creep in RF MEMS Devices”. In: *2007 International Conference on Thermal, Mechanical and Multi-Physics Simulation Experiments in Microelectronics and Micro-Systems. EuroSime 2007.* 2007, pp. 1–6.

Chapter 2

Thesis summary

As commented in the previous chapter, dielectric charging is still an open issue which limits the use of electrostatic MEMS in a large set of applications. As a consequence, dielectric charge-related phenomena and their effects on device performance have been the objective of many research works. Additionally, there exist two different-separate scenarios in which this phenomena can be studied: in the closed-ON and the open-OFF states of the device. In the ON state, the voltage applied is large enough to close the device, that is both electrodes are contacting the dielectric layer. In this case the amount of net charge injected into the dielectric can be very large and its dynamics more hard to predict. In this state, undesirable effects such like non-uniform charge distribution along the dielectric layer are more noticeable and thus they can cause permanent stiction of the device. For instance, this is a major problem in an RF-MEMS switch since, after some actuation cycles, the device it is not able to recover its open state.

On the other hand, in the OFF state the bias applied is below the pull-in voltage and therefore the electrodes are separated by the air gap and the dielectric layer. In this case the dielectric charge is injected from the fixed electrode and it is less than in ON state. Moreover, in this situation the sign of the net charge injected becomes easy to know, and as a consequence, the movement of the C-V curve when a certain voltage is applied is determined by the sign of this voltage. In this state, the net charge in the dielectric generates drifts in the capacitance of the device for a given voltage and, in the end, it could also lead to undesired pull-in and thus to the ON state. This capacitance drift poses a big problem in those applications in which the capacitance of the device or the position of the moveable electrode must be well known and stable when the MEMS is being

actuated, like in the case of MEMS varactors or even MEMS microphones.

The objective of this Thesis was to analyze the dielectric charge dynamics while different voltages were being applied to the device, and to propose new control strategies to mitigate the undesirable effects of this phenomenon in different electrostatic MEMS working in the contactless or OFF state.

2.1 Dielectric charging in contacless MEMS

2.1.1 The dielectric charging problem in MEMS

Although the physics behind dielectric charging phenomena are not a matter of this Thesis, research data accumulated over recent years indicates that two processes can contribute to external charge injection: trap-assisted tunnelling and Schottky emission from the conductor directly into the dielectric [1–5]. In order to deepen in the analysis of dielectric charging, one should keep in mind two things. Firstly, the dielectric can accumulate charges of both polarities, positive and negative, depending on the applied voltage. Secondly, as in [6], in the specific devices used in this Thesis, the source of charge is the bottom electrode when high electric fields are applied, and that the trapped charge is negative for $V > 0$ and positive otherwise.

Let us build a first model of the influence of the trapped charge in the performance of an electrostatic MEMS. An schematic view of a voltage driven MEMS with movable-top and fixed-bottom electrodes is depicted in Figure 2.1. It can be analyzed as follows. Using a typical mass-spring-damper ordinary differential equation, the dynamics of the deflection of the upper electrode $x(t)$ can be easily described as:

$$m\ddot{x}(t) + b\dot{x}(t) + kx(t) = F_{el}(x, t) \tag{2.1}$$

where F_{el} is the electrostatic force applied to the movable electrode, m its mass, b the damping factor and k the effective spring constant.

In order to obtain a simple model of the electrostatic force F_{el} for devices with homogeneous charge distribution of one sign, $Q_1(t)$, $Q_2(t)$ and $Q_d(t)$ are assigned to the instantaneous charges of the top and bottom electrodes and the top of the dielectric layer respectively. This approach follows [7].

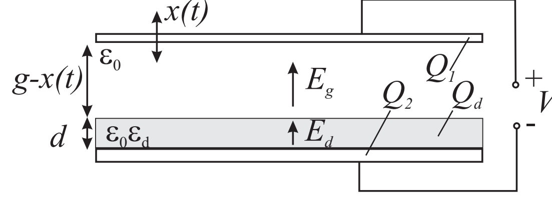

Figure 2.1: Schematic view of an electrostatic MEMS with a movable-top electrode and a dielectric layer on the fixed-bottom electrode.

For an electrically neutral system, one can write that

$$Q_1 + Q_2 + Q_d = 0 \tag{2.2}$$

Then, by applying Gauss' Law, the electric fields in the air gap and in the dielectric (see Fig. 2.1) are found to be

$$E_g(t) = -\frac{Q_1}{A\varepsilon_0} \qquad E_d(t) = \frac{Q_2}{A\varepsilon_0\varepsilon_d} = -\frac{Q_1 + Q_d}{A\varepsilon_0\varepsilon_d} \tag{2.3}$$

where ε_0 is the air permittivity, ε_d is the relative permittivity of the dielectric, A is the area of the electrodes and g is the equilibrium gap.

The voltage drop $V(t)$ can be calculated by integrating the electric field across the device, from the bottom electrode (at $z = 0$) to the top (at $z = d + g - x$, where d is the thickness of the dielectric layer).

$$V(t) = -\int_0^d E_d\, dz - \int_d^{d+g-x} E_g\, dz = -E_d d - E_g(g - x) = \frac{Q_1 + Q_d}{C_d} + \frac{Q_1}{C_g(t)} \tag{2.4}$$

Here the capacitance of the gap is $C_g(t) = A\varepsilon_0/(g - x)$ and the constant capacitance of the dielectric layer is $C_d = A\varepsilon_0\varepsilon_d/d$. Thus, the total MEMS capacitance is

$$C(t) = C_g||C_d = \frac{A\varepsilon_0\varepsilon_d}{d + \varepsilon_d(g - x)} \tag{2.5}$$

and the charge at the top electrode Q_1 can be written as

$$Q_1 = \left(V - \frac{Q_d}{C_d}\right) C \tag{2.6}$$

Finally, the electrostatic force applied to the top electrode can be expressed as

$$F_{el} = -\frac{Q_1 E_g}{2} = \frac{Q_1^2}{2A\varepsilon_0} = \frac{C^2}{2A\varepsilon_0}(V - \frac{Q_d}{C_d})^2 \tag{2.7}$$

From the last expression, one can observe that the electrostatic force F_{el} for a certain bias voltage depends on the amount of dielectric charge Q_d. The term substracted in eq. (2.7) is often referred to as the voltage shift due to Q_d

$$V_{shift} = \frac{Q_d}{C_d} \tag{2.8}$$

making $V - V_{shift}$ the effective voltage applied to the electrode. Measuring V_{shift} is one of the most common techniques carried out in experiments, since this simple relation allows one to determine the net dielectric charge (well almost, as it will be discussed later in this chapter).

In order to measure the value of V_{shift} some different strategies have been reported in the literature. The most typical one consists in measuring the shift of the pull-in voltage in the capacitance-voltage (C-V) characteristic of the device. Then, an initial measurement of the pull-in is required $V_{pull-in}(t = 0)$ to measure the amount and type of charge generated as $V_{shift} = V_{pull-in}(t) - V_{pull-in}(t = 0)$. This method allows to see easily the horizontal shift of the C-V due to dielectric charging, since at $V = V_{shift}$ the capacitance of the device changes abruptly. The same procedure has been used to measure the shift of the pull-out, or release, voltage but in this case the voltage sweep of the C-V measurement must start at a high voltage, ensuring the ON state of the device and go down to switch the device state to the OFF one. One can obtain the net dielectric charge as $V_{shift} = V_{pull-out}(t) - V_{pull-out}(t = 0)$. These techniques have been studied and compared in [8].

In the right side of Fig 2.2, extracted from [8], the authors show the evolution of V_{shift} during 100 min while applying different stress voltages at different temperatures. These $V_{shift}(t)$ curves have been obtained and compared using both the pull-in and pull-out methods. In the left side of the figure, it is shown an example of the C-V measurements carried out to obtain $V_{pull-in}$ and $V_{pull-out}$ during the test. The results obtained reveal strong influence of the voltage value in the accumulated charge, being such influence greater for higher voltage values.

The pull-in and pull-out based methods to study dielectric charging have been demonstrated to be effective in some applications and, in fact, the pull-in method

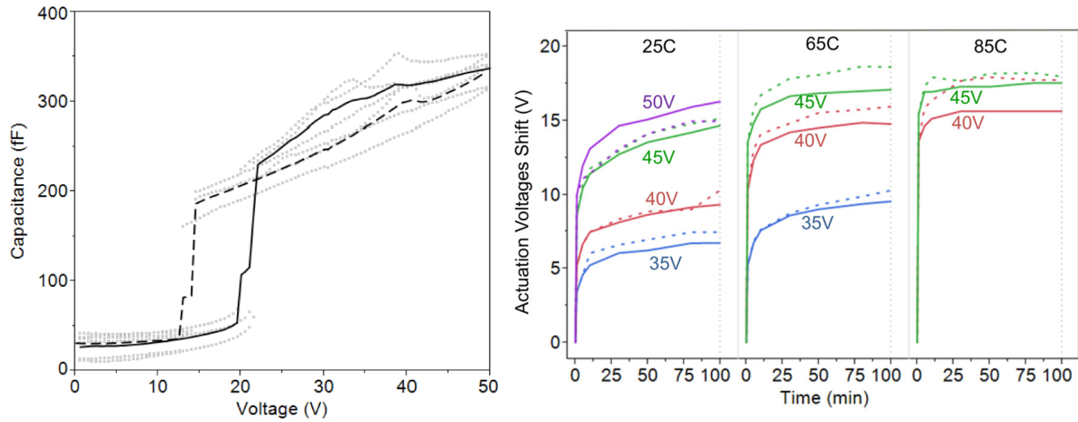

Figure 2.2: C-V curve of a cantilever test structure with pull-in and pull-out voltages around 20V and 13V respectively (left). Pull-in (solid) and pull-out (dashed) voltage shift caused by different stress voltages at different temperatures (right). Reproduced from [8], ©IEEE.

was used at the beginning of this Thesis. However, two important issues for the use of these methods in the case of contactless MEMS are found:

- Pull-in and pull-out methods imply switching from OFF to ON state, or vice-versa. Then, since the charge injection in the ON state is much higher than in the OFF one, a complete C-V measurement leads to a big change in the dielectric charge state. This does not allow to obtain the evolution of V_{shift} during a stress time.

- These methods are not compatible with the normal operation of the device, since one must remove the stress voltage to make the periodical C-V measurements.

To overcome the first issue, the authors of [9, 10] propose a new method that, although in this reference the method is used to study the dynamics of dielectric charging in the ON state, it is really suitable in the contactless scenario. This is the center-shift method. From the typical shape of a C-V in the OFF state zone shown in Fig 2.3, they propose to measure the V_{shift} by calculating the voltage at which the capacitance value is minimum. This value is obtained by fitting the parabola (2.9) through the center of the C-V characteristic.

$$C(V) = \alpha(V - V_{shift}) + C_0 \tag{2.9}$$

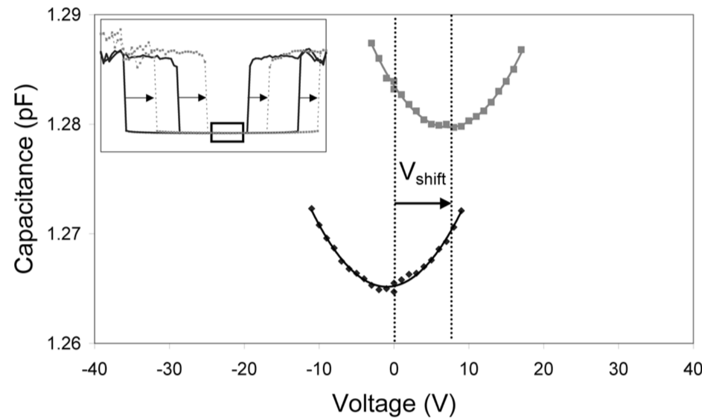

Figure 2.3: Center of the C-V characteristic before (black) and after (grey) a MEMS switch has been stressed at 65V for 272 seconds. Reproduced from [9], ©IEEE.

This technique to infer the net dielectric charge agrees with what has been discussed above. Assuming an uniform charge distribution, $V = V_{shift}$ will correspond to the minimum value of the electrostatic force applied $F_{el} = 0$ (see eq. (2.7)) and thus, it will also correspond to the minimum capacitance value in a C-V measurement. Note that the position of the moveable electrode and therefore the MEMS capacitance, depend on the electrostatic force applied.

Finally, in [9] there is a comparison between the center-shift method and two alternatives of the typical pull-in method. A first alternative is the typical DC voltage sweep. In the second one, the authors search the value of $V_{pull-in}$ by applying an algorithm based on successive approximation. It can be seen in Fig 2.4 from [9] that with the use of the center-shift method the state of the dielectric charge is practically not altered by the technique used to find the V_{shift} compared with the other two methods. To do this experiment, no stress voltage was applied between consecutive measurements of V_{shift} with the three different methods.

The center-shift method has been used in this Thesis to make the needed C-V measurements to corroborate the effectiveness of the different control methods proposed. However, although this allows to precisely measure the voltage shift without much alteration of the state of the charge, it still poses an inconvenience:

- The method is not compatible with the normal operation of the device, since one must remove the stress voltage and make a C-V measurement to know the current V_{shift}.

A new strategy based on the center-shift method to monitor $V_{shift}(t)$ is intro-

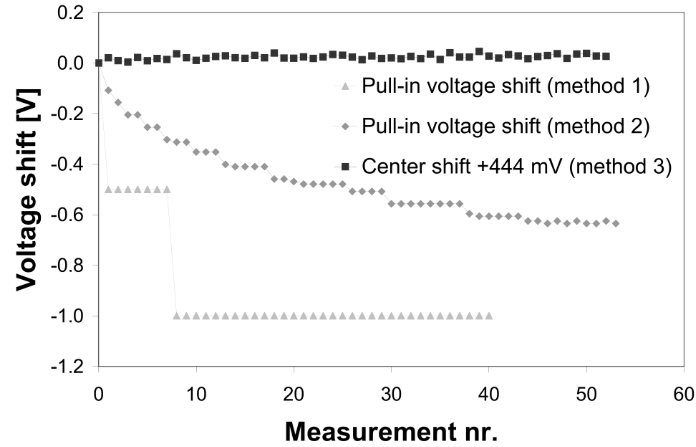

Figure 2.4: Effect of measurements on the V_{shift} determined by measuring the change in the pull-in and by determining the center of the C-V curve when applying zero voltage stress. Reproduced from [9], ©IEEE.

duced in this Thesis. This method has been thought to be minimally invasive. Taking equation (2.9), where the α parameter must be fitted for each device and C_0 is the minimum capacitance value of the C-V curve, the dynamics of the trapped charge could be studied by applying a stress voltage during a certain time and monitoring the capacitance between the plates of the device. This way, it would be possible to extract the $Q_d(t)$ values from the measured $C(t)$. However, changes in temperature or humidity, or changes in the uniformity of charge distribution, among other processes, can also generate vertical displacements in the C-V curve [10–12]. This means that the constant term in eq.(2.9) may easily present a slow time dependence $C_0(t)$, as shown in Figure 2.4. It is observed there that both V_{shift} and C_0 exhibit noticeable variations after a voltage stress has been applied.

To avoid the effect of vertical drifts when measuring V_{shift}, in the method proposed the device capacitance is measured at two voltages of different sign, $V^+ > 0$ and $V^- < 0$. These two measurements are made in close instants of time t and $t + \Delta t$. For instance, let us suppose that $C^+ = C(V^+)$ is obtained at t and that $C^- = C(V^-)$ is obtained at $t + \Delta t$. Assuming, as commented above, that α is constant and that there is a slow drift in the charge dynamics, that is $V_{shift}(t) \approx V_{shift}(t + \Delta t)$ and $C_0(t) \approx C_0(t + \Delta t)$, then V_{shift} can be extracted

from the following equation:

$$\begin{aligned}\Delta C(t) &= C^{+}(t) - C^{-}(t+\Delta t) = \\ &= \alpha[(V^{+})^{2} - (V^{-})^{2}] - 2\alpha V_{shift}(t)[V^{+} - V^{-}]\end{aligned} \tag{2.10}$$

Under the above assumptions, namely that $C_0(t)$ and $V_{shift}(t)$ change slowly when compared with the time between two consecutive measurements, we have that $\Delta C(t)$ is fairly independent of $C_0(t)$. From equation (2.10) it becomes obvious that $\Delta C(t)$ is an affine function of dielectric charge $Q_{\mathrm{d}}(t)$. For instance, note that for $V = V^{+} = -V^{-}$ it yields,

$$Q_{\mathrm{d}}(t) \approx C_{\mathrm{d}} V_{\mathrm{sh}}(t) = \frac{-C_{\mathrm{d}}}{4\alpha V}\Delta C(t) \tag{2.11}$$

The application of this method to measure the evolution of V_{shift} in the characterization of the dielectric charge dynamics will be seen in more detail in the next section.

2.1.2 Dielectric charging dynamics

Although the study of the dielectric charging effects on device performance and the proposal of mitigation techniques have received considerable attention in the literature, there is still a lack suitable physical models for the prediction of long-term behavior of electrostatic MEMS [5]. This section introduces and discusses three different phenomenological models that describe the dynamics of the trapped charge. It is important to note that the dynamics of charge strongly depends on the fabrication process of the device and thus, this study in the literature is usually linked to specific MEMS topologies.

Both charging and discharging dynamics are usually analized. The typical methodology used to analyze the dynamics of the charging process consists in measuring the evolution of Q_d or V_{shift} while applying a specific stress voltage to a previously discharged device. It is the step voltage response. After a certain time, the bias voltage is switched to $0V$ to analyze the discharging process.

Although in the previous section it has been presented different techniques to monitor the displacement of $V_{shift}(t)$ and thus, the evolution of $Q_d(t)$, in some works [13, 14] the transient charging/discharging currents are used to calculate the steady-state charge density and the time constants involving these two processes.

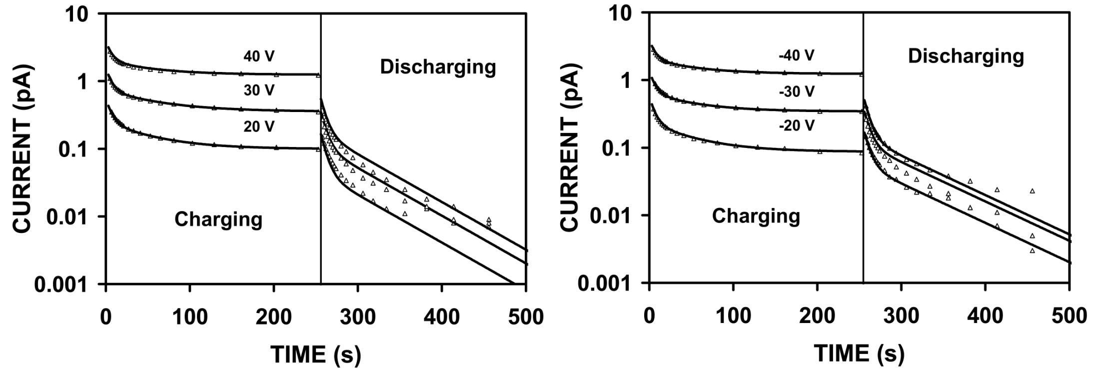

Figure 2.5: Absolute values of (symbols) measured and (lines) calculated charging and discharging current transients under (left) positive and (right) negative stress voltages. Reproduced from [14], ©IEEE.

As an example, in Figure 2.5, taken from [14], charging and discharging current transients under different positive (left) and negative (right) voltages are shown.

The objective behind these different techniques to study the charge evolution is to obtain a good model able to predict the charge state over time. Below, it is described the three more extended models of the dielectric charge dynamics [15] to evaluate the charge evolution. To formulate the models two sets of expressions are used: charging with negative Q_d^n and discharging of the positive Q_d^p charge at $V > 0$, and, vice versa, discharging of the negative and charging with the positive charge at $V < 0$. Thus, the total accumulated charge is a superposition of such charges as:

$$Q_d(t) = Q_d^n(t) + Q_d^p(t) \tag{2.12}$$

Model A — Exponential Dynamics

The dynamics of the charge of one sign resembles an exponential function of the form $Q(t) = A_0 + A_1 \exp(-t/\tau)$, where the constants A_0 and A_1 are found from experimental data fitting and time constant τ represents the characteristic time scale of the process.

In order to take into account both polarities of the voltage and their influence on charge dynamics, A_0 and A_1 are redefined. The saturation levels Q_{max}^n and Q_{max}^p are those eventually reached by negative and positive charges. In this representation of the model, the initial conditions such that the charging processes start from zero $Q^{n,p}(0) = 0$ and the discharging processes start from the maximum value $Q^{n,p}(0) = Q_{max}^{n,p}$. In the most general case, there may be any arbitrary

negative and positive charges accumulated in the dielectric by the time t_0: $Q_0 = Q^n(t_0) + Q^p(t_0)$, $t_0 > 0$. Therefore, we obtain the equations

$$Q_d^n = \begin{cases} Q_{max}^n(1 - e^{-t/\tau_C^n}) & V > 0 \\ Q_{max}^n e^{-t/\tau_D^n} & V < 0 \end{cases} \tag{2.13}$$

$$Q_d^p = \begin{cases} Q_{max}^p e^{-t/\tau_D^p} & V > 0 \\ Q_{max}^p(1 - e^{-t/\tau_C^p}) & V < 0 \end{cases} \tag{2.14}$$

where $\tau_C^{n,p}$ and $\tau_D^{n,p}$ are the charging and discharging constants for negative and positive charges.

Model B — Multi-exponential Dynamics

The "natural" extension of Model A is a superposition of exponentials with different time constants τ_i: $Q = A_0 + A_1 e^{-t/\tau_1} + A_2 e^{-t/\tau_2} + ...$ Here, it will be taken the form of the model from [16], with maximum levels $Q_{max,i}^{n,p}$ for each ith component of negative and positive charges, such that the total maximums are $Q_{max}^{n,p} = \sum_i Q_{max,i}^{n,p}$. Being $\zeta_i^{n,p} = Q_{max,i}^{n,p}/Q_{max}^{n,p}$ the charging and discharging dynamics for Model B can be described as

$$Q_d^n = \begin{cases} Q_{max}^n - \sum_i \zeta_i^n Q_{max}^n e^{-t/\tau_{Ci}^n} & V > 0 \\ \sum_i \zeta_i^n Q_{max}^n e^{-t/\tau_{Di}^n} & V < 0 \end{cases} \tag{2.15}$$

$$Q_d^p = \begin{cases} \sum_i \zeta_i^p Q_{max}^p e^{-t/\tau_{Di}^p} & V > 0 \\ Q_{max}^p - \sum_i \zeta_i^p Q_{max}^p e^{-t/\tau_{Ci}^p} & V < 0 \end{cases} \tag{2.16}$$

Note that, according to the definition, $\sum_i \zeta_i^{n,p} = 1$.

The superposition model is extensively developed in [14, 16, 17]. It is based on measurements of the transient charging and discharging currents of MEMS switches in the ON state. In these works, the superposition model with only two time constants τ_1 and τ_2 shows a good agreement with experiments. Model B with two time constants has been also successfully employed to fit experimental results in other works [18, 19]. In Fig 2.6 there is a comparison between the application of Model A and Model B with two time constants to fit an experimental data. It can be observed a strong difference between them, being the second fit much

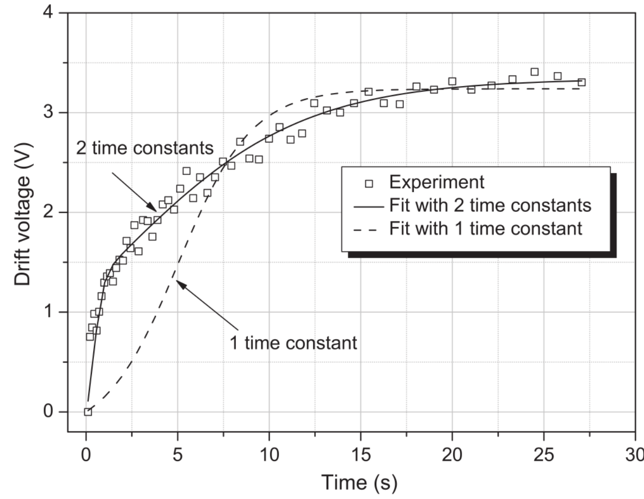

Figure 2.6: Example of one and two time constant fit of the V_{shift} drift in a device stressed at 50V. Reproduced from [19], ©Elsevier.

better than the first.

Model C — Stretched Exponential Dynamics

The charge dynamics is described as: $Q(t) = A_0 + A_1 e^{-(t/\tau)^\beta}$, where $0 < \beta < 1$. In contrast with Models A and B, this law involves non-linear time t^β. The conventional form often found in literature as *Model C* is then:

$$Q_d^n = \begin{cases} Q_{max}^n \left(1 - e^{-(t/\tau_C^n)^{\beta_C^n}}\right) & V > 0 \\ Q_{max}^n e^{-(t/\tau_D^n)^{\beta_D^n}} & V < 0 \end{cases} \tag{2.17}$$

$$Q_d^p = \begin{cases} Q_{max}^p \left(1 - e^{-(t/\tau_C^p)^{\beta_C^p}}\right) & V > 0 \\ Q_{max}^p e^{-(t/\tau_D^p)^{\beta_D^p}} & V < 0 \end{cases} \tag{2.18}$$

In [20], the stretched exponential law appears from the assumption that traps in a dielectric layer have a continuous distribution in the time scale $\int_0^\infty \rho(\tau) e^{-t/\tau} d\tau$.

The transient capacitance in the ON and OFF states of a MEMS was well fitted by the stretched exponential law in [21–23]. It can be noted that non-saturation models are suggested in the literature. For example, in [24] the voltage drift as a function of time does not saturate. In addition, Herfst et al [9, 15], while applying the exponential, stretch exponential and square root models to fit experimental data, note that $\sqrt{t}$ accurately describes the voltage shift versus time.

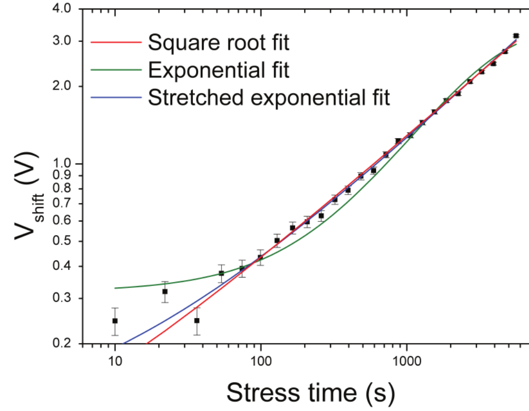

Figure 2.7: Comparison of three different fit functions of the V_{shift} evolution in a device stressed at 40V. Reproduced from [15], ©IEEE.

The square root itself is a non-saturation function, however, these works note that it might appear as a Taylor expansion of the stretched exponential with $\beta \approx 0.5$. Note that this is also the typical response of a fractionary systems. An example of this can be seen in Figure 2.7, from [15], where the authors show a comparison between an square root and stretch exponential fittings. In the figure, the result of the same experiment is also fitted using the simple exponential model, which exhibits a worse adjustment than the other two.

Regarding this Thesis

Model B, or multi-exponential, was chosen in this Thesis to characterize the dynamics of dielectric charging in the MEMS used in the experiments. From the method explained in the previous section to monitor the evolution of V_{shift}, let us now consider a sampled-time system, where the "quasi-differential" capacitance measurement, eq. (2.10) is performed at each sampling time. This means that it is necessary to execute the voltage switching within each sampling period. On the other hand, it is needed to have two predetermined waveforms such that while conserving the capability of monitoring the charge, by doing the voltage switching, would serve to increase (or decrease) the amount of charge in the dielectric. To this effect, two bipolar voltage waveforms, or symbols, have been proposed and extensively used in this Thesis. These waveforms, shown in Figure 2.8, have been called BIT0 and BIT1. In BIT0, V^- is applied during most of the sampling period, whereas in BIT1 V^+ is applied most of the time.

As it has been explained in the previous section, the application of a positive

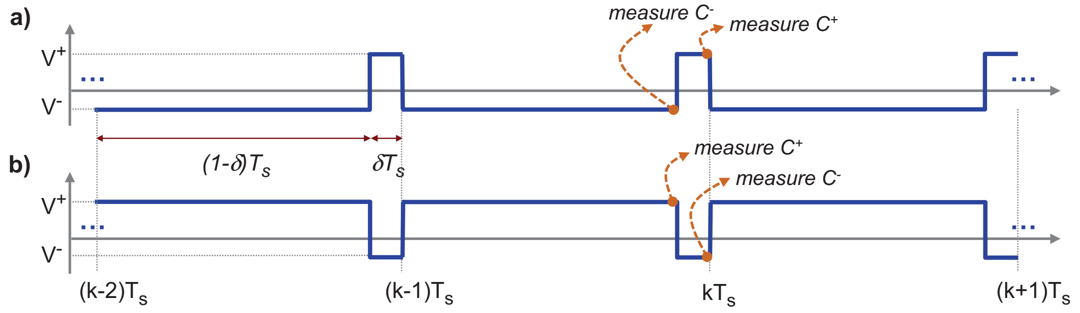

Figure 2.8: Bipolar voltage symbols BIT0 and BIT1 applied to the MEMS. In BIT0[BIT1], $V^+ > 0[V^- < 0]$ is applied during $(1-\delta)T_S$, then $V^- < 0[V^+ < 0]$ for a short time δT_S. Capacitances $C^+ = C(V^+)$ and $C^- = C(V^-)$ are measured at symbol instants $(1-\delta)T_S$ and T_S, and $\Delta C_n = \Delta C(nT_S)$ is obtained as $C^+ - C^-$.

stress voltage V^+ increases negative charge Q_d^n while decreasing positive charge Q_d^p. The effect is opposite when applying a negative voltage V^-. Then, from eq. (2.12) it can be observed that, for appropriate values of V^+, V^- and δ, the application of BIT0 to the device, in the contactless case, increases the positive charge and reduces the negative charge stored in the dielectric. On the other hand, the application of BIT1 the has opposite effect on the charge injected into the dielectric. This means that by applying these two symbols, it is possible to monitor the charge in the dielectric while at the same time deciding between an increase or decrease of the net amount of charge by the application of BIT0 or BIT1.

Note that in each symbol both voltage polarities are applied. Then, a certain increase and decrease of both positive and negative charges are present when stressing the device with one of them. For example, when the MEMS is actuated with BIT0s, positive charge Q_d^p increases during most of the symbol time $(1-\delta)T_s$, while decreasing negative charge Q_d^n. After this time of positive voltage application, the bias voltage is switched to a negative voltage and Q_d^p start to decrease while increasing Q_d^n.

To take into account the dynamics involving this characterization method, equations (2.15) and (2.16) must be reformulated. Then, Model B must be discretized to obtain the charge evolution in the dielectric for the decision instants kT_s and it must contemplate the effect of both voltage polarities in each voltage waveform. The discretized equations extracted for the ith charge component of

each sign are the following:

$$Q^{p,i}(k+1) = \begin{cases} BIT0: & Q^{p,i}_{\max}(1-\alpha^{p,i}_{C_{1-\delta}})\alpha^{p,i}_{D_\delta} + Q^{p,i}(k)\alpha^{p,i}_{C_{1-\delta}}\alpha^{p,i}_{D_\delta} \\ BIT1: & Q^{p,i}_{\max}(1-\alpha^{p,i}_{C_\delta}) + Q^{p,i}(k)\alpha^{p,i}_{C_\delta}\alpha^{p,i}_{D_{1-\delta}} \end{cases} \tag{2.19}$$

and

$$Q^{n,i}(k+1) = \begin{cases} BIT0: & Q^{n,i}_{\max}(1-\alpha^{n,i}_{C_\delta}) + Q^{n,i}(k)\alpha^{n,i}_{C_\delta}\alpha^{n,i}_{D_{1-\delta}} \\ BIT1: & Q^{n,i}_{\max}(1-\alpha^{n,i}_{C_{1-\delta}})\alpha^{n,i}_{D_\delta} + Q^{n,i}(k)\alpha^{n,i}_{C_{1-\delta}}\alpha^{n,i}_{D_\delta} \end{cases} \tag{2.20}$$

where the following parameters are introduced:

$$\begin{array}{ll} \alpha^{p,i}_{C_\delta} = e^{-\delta T_s/\tau^{p,i}_C} & \alpha^{p,i}_{D_\delta} = e^{-\delta T_s/\tau^{p,i}_D} \\ \alpha^{p,i}_{C_{1-\delta}} = e^{-(1-\delta)T_s/\tau^{p,i}_C} & \alpha^{p,i}_{D_{1-\delta}} = e^{-(1-\delta)T_s/\tau^{p,i}_D} \\ \alpha^{n,i}_{C_\delta} = e^{-\delta T_s/\tau^{n,i}_C} & \alpha^{n,i}_{D_\delta} = e^{-\delta T_s/\tau^{n,i}_D} \\ \alpha^{n,i}_{C_{1-\delta}} = e^{-(1-\delta)T_s/\tau^{n,i}_C} & \alpha^{n,i}_{D_{1-\delta}} = e^{-(1-\delta)T_s/\tau^{n,i}_D} \end{array} \tag{2.21}$$

Equations (2.19) and (2.20) imply that, given a set of parameters of the multi exponential model describing the dielectric charging process, $\{Q^p_{\max}, \zeta^p_i, Q^n_{\max}, \zeta^n_i, \tau^{p,i}_C, \tau^{p,i}_D, \tau^{n,i}_C, \tau^{n,i}_D\}$, then it is possible to calculate the time evolution of the net dielectric charge when a known sequence of symbols BIT0 and BIT1 is applied to the device. Then, the characterization method consists in finding the set of model parameters that minimize the mean square error between the predicted time evolution and the one experimentally obtained. In the case of this Thesis, these fittings have been carried out using the well known unconstrained non-linear minimization Nelder-Mead algorithm.

An example of the use of the BITs proposed to analyze the charging dynamics of a specific device is presented now. The aim of the measurement carried out in this example was to find the dynamical model for a MEMS stressed with positive $V^+ = 4V$ and negative $V^- = -4V$ voltages. To do this, BIT0 and BIT1 waveforms, with a sampling time $T_s = 250\,ms$ and $\delta = 1/5$ were applied successively to the MEMS in 48-hour lapses. The time length of each BIT is n clock periods, therefore $T_s = nT_{\text{clk}}$. During each symbol, the device capacitance was measured at both $(n-1)T_{\text{clk}}$ and nT_{clk} instants, see Fig 2.8, so that a new value of the "quasi-differential" capacitance ΔC ($\Delta C = C^+ - C^-$) is provided at the end of each symbol.

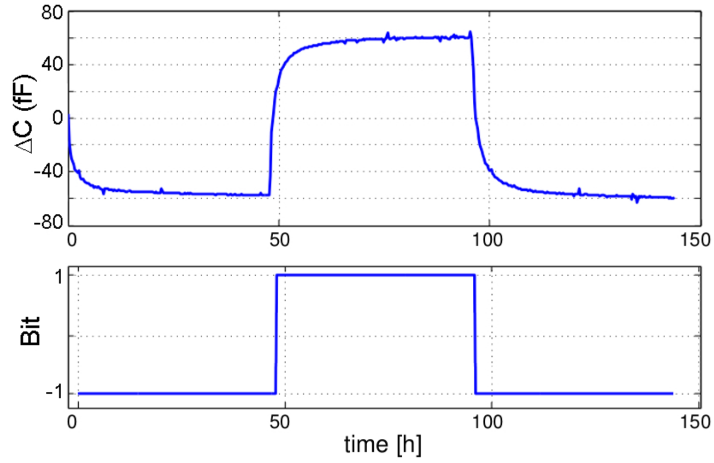

Figure 2.9: Evolution of the "quasi-differential" capacitance $\Delta C(t)$ (top) and sequence of applied symbols (bottom). In this experiment, BIT0's were applied first to the MEMS, then BIT1's and, again, BIT0's. Each step was for 48 h. BIT parameters: $V^{+} = -V^{-} = 4\,V$, $T_s = 250\,ms$, $\delta = 1/5$.

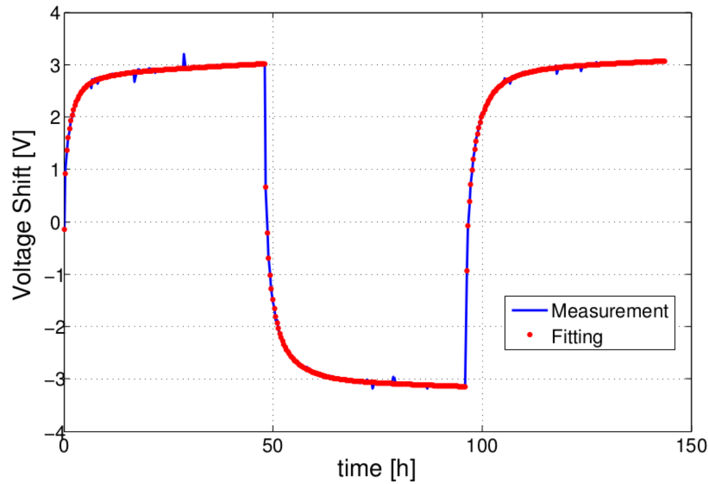

Figure 2.10: Evolution of the voltage shift during the experiment shown in Figure 2.9 (solid line) and fitting of the experimental data (in red) by 1D model simulations based on eqs. (2.19) and (2.20).

Figure 2.9 shows the evolution of $\Delta C(t)$ obtained in the experiment. To obtain $V_{shift}(t)$ from $\Delta C(t)$, it is necessary to know the α parameter in eq. (2.10). This parameter can be obtained from a single C-V measurement. In this example, it yields $\alpha = 1.4\,fF/V^2$. The evolution of the voltage shift obtained during this measurement is shown in Fig 2.10.

In Figure 2.10 one can also observe the fitting of the model given by equations (2.19) and (2.20) with the experimental data. As a result of this fitting with a two-exponential model, the set of parameters of the charge dynamics shown in Table 2.1 has been obtained. Note that all the time constants reported in Table 2.1 are far above the sampling period $T_s = 2.5s$. It should be noted that the charging and discharging time constants of the second exponential associated to positive charge are very large. This means that in this case it is only possible to infer the slope of the curve, i.e., only the amplitude divided by the corresponding time constant will be accurate. This is something to be expected since, as can be observed in the transients, the charge does not reach a strictly stable value after the application of the excitation waveforms.

Table 2.1: Parameters for the negative and positive components of the two-exponential charge dynamics model, obtained from the fittings shown in Fig 2.10.

Parameter	n	p
$Q_{\max}/C_d$ [V]	-5.3	5.3
$\tau_{C,1}$ [min]	13	113
$\tau_{C,2}$ [min]	509	2369
$\tau_{D,1}$ [min]	11	87
$\tau_{D,2}$ [min]	483	5567
ζ_1	0.68	0.94
ζ_2	0.32	0.06

In contrast with the other methods present in the literature discussed above, this characterization strategy offers three advantages:

- The state of the dielectric charge trapped is monitored at each sampling time. This is really useful to find a good fitting of the dynamical model with the measurement, since there are several measurements of $V_{shift}(t)$ in the data obtained.

- All contributions of the stress voltages applied V^+ and V^- are taken into account in the fitting. In other methods, each time the C-V is measured to obtain V_{shift}, the current state of the charge is distorted. This usually implies to make C-V measurements enough separated in time. In this case, it can be not possible to find fast time constants.

- This method allows to characterize charge dynamics of alternating bias voltages. This is really useful when predicting the evolution of $Q_d(t)$ in a

bipolar voltage actuation technique. These techniques will be presented in the next section.

2.2 Mitigation techniques

Although the effects of charging on MEMS performance have been extensively studied, obtaining solution or mitigation strategies to the reliability issues due to this phenomenon is still an open challenge which often limits an extensive use of these devices in some applications. To face this problem, several different approaches have been proposed in the literature. These approaches range from the improvement of mechanical design to smart actuation strategies.

The methods proposed in this Thesis to compensate dielectric charging effects have been thought to be compatible with typical MEMS structures and fabrication processes. Because of this, the studies carried out have been made from the electrical point of view. The objective was to propose new methods that could be applied to the vast majority of devices and no proprietary technologies were needed. In this regard, methods trying to solve the problem from the mechanical or fabrication points of view have not been matter of this Thesis. This section tries to provide an overview of different techniques found in the literature, but putting more emphasis in those related with the context of this Thesis.

The different charge mitigation strategies available in the literature can be divided in three different approaches: actuation strategies, mechanical improvements and specific fabrication processes.

2.2.1 Actuation strategies

As it has been explained above, the application of bias voltages of different polarities has opposite effects on charge injection/depletion into/from the dielectric. For instance, negative charges trapped in the dielectric can be removed by applying negative voltages or injected by applying positive voltages. Indeed, since the electrostatic force is always attractive, MEMS devices can be actuated by either positive or negative voltages. According to all this, unipolar-switched voltage waveforms [25] and periodical bipolar-switched voltage waveforms[16, 26] have been demonstrated as promising ways to reduce the effects of dielectric charging.

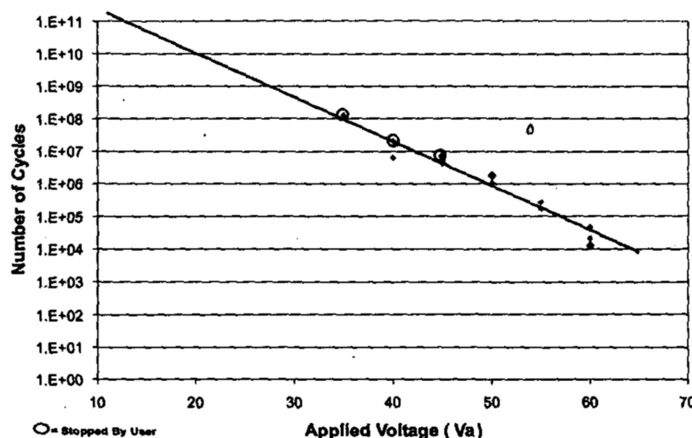

Figure 2.11: MEMS lifetime characterization. Reproduced from [27], ©IEEE.

Dual-pulse actuation

In [27], the authors state that an exponential relationship exists between the value of the stress voltage and the lifetime of a RF-MEMS switch, measured as the number of switching cycles (between OFF and ON state) until device collapse. According to this, the device lifetime increases when reducing the bias voltage (Fig 2.11). Following this principle, the authors proposed and implemented a dual-pulse actuation waveform to stress the device. This method, which has been also used in [25, 28, 29], consists in applying firstly a high-voltage pulse during a short time to close the device and then switching downto a lower voltage that is enough to maintain the device in the ON-closed state while keeps dielectric charging to a minimum, see Figure 2.12, taken from [16]. Of course, this "hold" voltage must be between the $V_{pull-in}$ and $V_{pull-out}$ values. As seen in the left side of the figure, three different waveforms were applied to the device continuously. In these waveforms three different voltages are present: $0V$, $-15V$ and $-30V$. The experiment shows that dielectric charging effects can be accelerated or reduced by changing the duty factor and peak voltage of the dual-pulse actuation waveform. A variation of this technique was used later in bipolar actuation voltage methods [29].

Smart bipolar waveforms

Bipolar actuation methods consist in alternating voltage polarity following a predetermined pattern [30–32]. Since the effect of bipolar voltages on the charge dynamics is not symmetrical and strongly depends on the device structure and

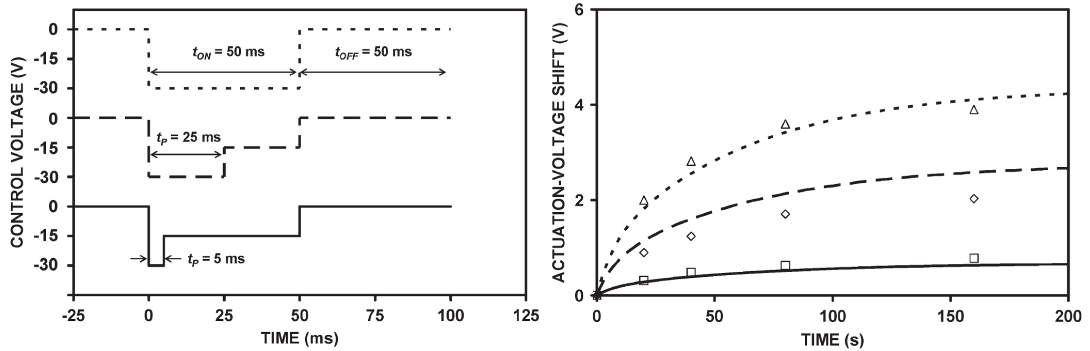

Figure 2.12: Different dual-pulse voltage waveforms (left) and the V_{shift} evolution when applying them to a RF-MEMS (right). Reproduced from [16], ©IEEE.

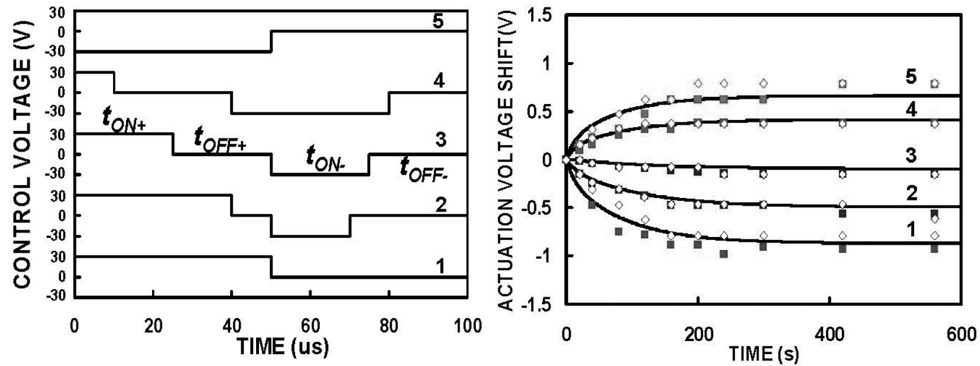

Figure 2.13: Modeled (line) vs. measured (symbol) V_{shift} evolution (right) under different stress voltage waveforms (left). Reproduced from [32], ©IEEE.

materials used [21], a study of charge dynamics is needed to conform the appropriate voltage waveforms to actuate the device. An example of this can be found in [31] and [32]. As one can see in left side of Fig 2.13 [32], the authors configured several different actuation waveforms to study the dielectric charge dynamics of a RF-MEMS under these excitations. As a result, the right plot shows that the evolution of $V_{shift}(t)$ strongly depends on the waveform pattern used. Moreover, the authors linked the evolution of charge injection due to the application of the waveforms shown in the figure with a bipolar charging model based on superposition of unipolar charging models.

Other bipolar actuation waveforms have been proposed in the literature, as those shown in Figure 2.14 from [33]. According to this work, voltage polarities can be alternated on a switching cycle-to-cycle basis or the polarity can be swept during the ON-closed state of the MEMS. In the first approach, the sign of the voltage is changed each time the device is opened. In the second one, the device

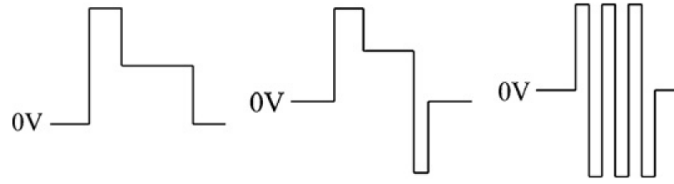

Figure 2.14: Example of different actuation waveforms applied on capacitive RF-MEMS switches to increase the lifetime of the device. Reproduced from [33], ©IOP Publishing Ltd.

can be in the closed state continuously. It is important to note that in the last situation, the capacitor constituting the MEMS, is charged and discharged more often than when using a single pulse. This implies higher power consumption.

Second order effects

Although bipolar techniques usually applied to RF MEMS have been reported to be a partial solution for the dielectric charging issue, they only contemplate the effects of net dielectric charge. It is, due to the fact that positive and negative voltages have opposite effects on dielectric charging, these solutions try to minimize the displacement of $V_{shift}(t)$ by alternating both polarities in order to enlarge the lifetime of devices. However, this assumption does not contemplate second order effects of dielectric charging, such as the C-V narrowing effect and they can still fail.

As explained in [34], dielectric charging can produce rigid vertical or horizontals shifts of the C-V curve but it can also cause a distortion of the curve, consisting in a narrowing of the pull-in and pull-out windows. This phenomenon, which can be seen in Figure 2.15 [35], has been extensively linked to inhomogeneous distribution of charge in the dielectric layer [12, 34, 35]. In this figure, the displacement of the C-V curve cannot be determined from a unique shift of the pull-in and pull-out voltages. That is, even being the C-V curve centred at $V_{shift} = 0V$ different shifts in the pull-in and pull-out voltages can appear. These pull-in to pull-out shifts can lead to stiction, hence to device failure, when the pull-out voltage crosses the $0V$ threshold. In this situation, the device cannot go back to the OFF-open state by switching down the stress voltage.

In [34], the authors propose an analytical model to explain the causes of the C-V narrowing due to voltage stresses. Concretely, they state that defects and traps

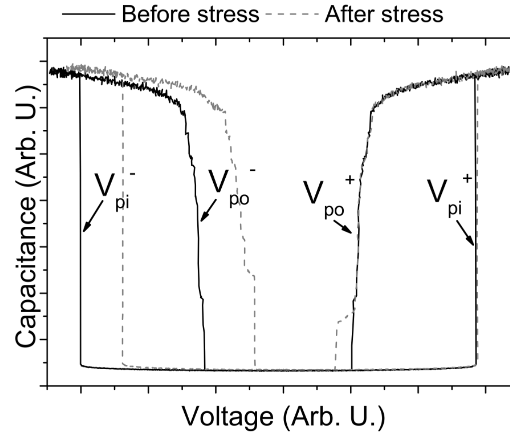

Figure 2.15: C-V measurement of a MEMS switch before and after applying a DC stress voltage. Reproduced from [35], ©IEEE.

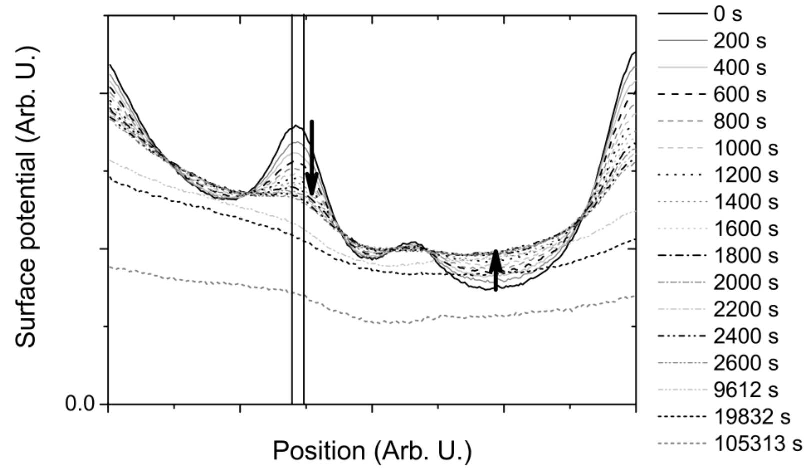

Figure 2.16: Diffusing and decaying surface potential measured across a surface line of a MEMS. Reproduced from [35], ©IEEE.

imprinted in the dielectric layer during the fabrication process cause non-uniform charge injection. This induces an asymmetry of the charging effect. In [35], the authors comment that charges are trapped in a laterally inhomogeneous way and that these charges are confined in the vertical direction. They also define the non-uniform charge distribution as a diffusive process which slowly reduces this inhomogeneity. Figure 2.16 shows the diffusing and decaying surface potential of a stressed device along a single line, obtained with a Scanning Kelvin Probe Microscopy. This measurement is used to calculate a diffusion coefficient.

On the other hand, in the contactless, or OFF state, case considered in this Thesis non-uniform charge distributions produce vertical movements of the C-V

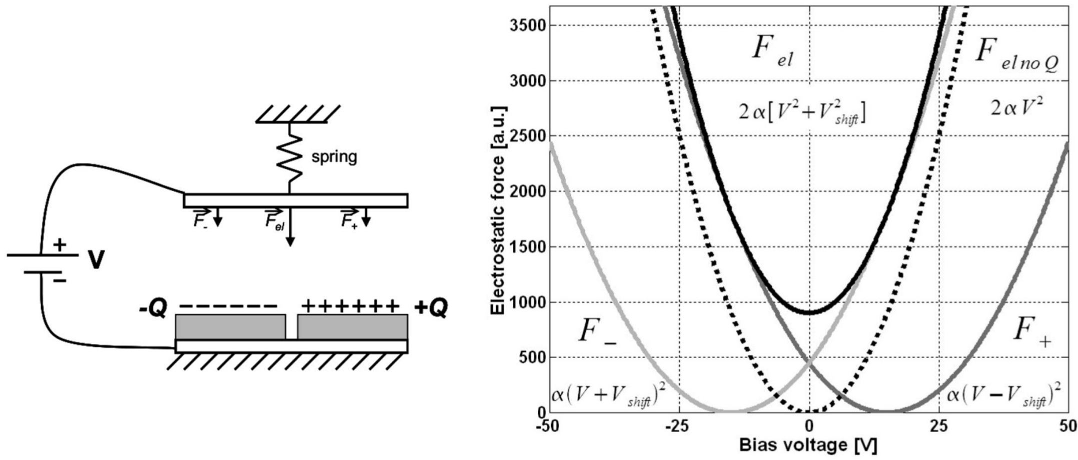

Figure 2.17: Example of a simple non-uniform dielectric charge distribution (left) and description of its effect on the electrostatic force the effect exerted on the moving plate (right). Reproduced from [12], ©IEEE.

curve. In [12], the authors provide an explanation for this effect without assuming any trapping/de-trapping model. In the schematic shown in the left part of Figure 2.17 two separated dielectric islands have constant surface charges of opposite sign ($\pm Q$), which implies zero net charge $Q_d = 0$. When a bias voltage is applied between the electrodes, the ($\pm Q$) charges shift the local voltage-forces, following equation (2.7). As a result, opposite voltage shifts appear in the two dielectric islands, leading to the situation shown in the right part of Figure 2.17. There, the electrostatic forces caused by bias voltage and dielectric charge are represented for both islands, concluding that even in the case of $V = 0V$ the total electrostatic force exerted on the moveable plate/electrode is not zero (black line). Therefore non-uniform charge distributions can produce vertical shifts of the C-V characteristic.

Although it has been reported that non-uniform charge distributions generate vertical displacements of the C-V characteristics, these movements have also been extensively attributed to changes of the environmental conditions, such as temperature and humidity [22, 36].

2.2.2 Mechanical improvements

As commented above, permanent stiction due to dielectric charging is the most important reliability issue for the use of MEMS as ON/OFF switches. This phenomenon can be observed in the C-V characteristics of the device: it corresponds

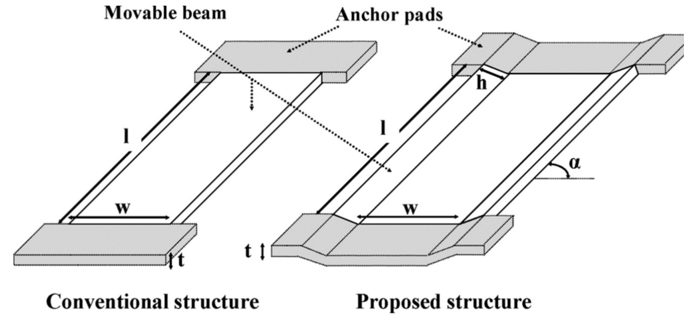

Figure 2.18: Geometry of a conventional bridge and a boat-like bridge where l; w; t; and h represents the planar beam length, width, thickness, and the bent side additional width, respectively. Reproduced from [37], ©IEEE.

to the situation in which the pull-out, or release, voltage shifts beyond the $V = 0V$ threshold. In this regard, since it can be seen as an insufficient restoring force of the device, some proposed techniques try to increase this force with the aim of enlarge the lifetime of the device in presence of dielectric charge injection.

In [33], it is noted that by increasing the thickness of the movable plate and shortening its length one can obtain a higher restoring force. However, this solution implies an increase of the actuation voltage, since a higher voltage will be needed to close the device. However, the higher voltage is applied the more charge is injected in the dielectric.

Another method, proposed in [37], is an improved design of the shape of the movable electrode. In this work, the authors present a new MEMS structure with U-beam profile for better stiffness than classical beams. Figure 2.18 shows a comparison between the new-proposed structure with a typical one. It is stated that with the use of U-shaped devices, the mechanical resonance frequency increases, and, consequently, devices with faster switching properties are obtained. In this case, switching times under $400\,ns$.

In [38], the authors go to the roots of the dielectric charging problem, the presence of dielectric layers in the device, and propose significant reduction of the dielectric area. As can be expected, this strategy has become extensively used by MEMS designers. In the design presented in [38], the authors used dielectric studs instead of a continuous film, resulting in a fill factor of 25%, thereby reducing dielectric charging by 75%. However, although reliability problems caused by charge injection can be significantly reduced using this technique, it implies a reduction in the C_{ON}/C_{OFF} ratio. his poses a problem in RF-MEMS devices,

since a large C_{ON}/C_{OFF} ratio is important to have a large impedance change and make the device work as a switch rather than a variable capacitor with a limited range.

2.2.3 Fabrication process approaches

Dielectric charging has been extensively studied from the point of view of the fabrication process. The aim of these studies is to find new MEMS topologies which do not suffer from charge injection. In this direction, many works have focused on removing dielectric materials from the structures or implementing dedicated actuation electrodes while maintaining the same geometry as in typical capacitive switches. In this last case, the actuation electrodes are placed at a lower position than the dielectric contacting the top electrode when the MEMS is in the closed state. Then, there is still an air gap between the bottom and top electrodes and only the RF signal, much smaller in amplitude than actuation voltages, can be responsible of charge injection. Furthermore, separating the electrodes also allows the device to be operated with a relatively low electric field applied across the dielectric. An example of this is shown in Figure 2.19 [18]. This work experimentally demonstrates good response of the proposed device after some hours of switching test.

In [39], the authors present a new capacitive switch with no dielectric. There, in order to avoid the contact between both electrodes in the ON-closed state, the bridge is shaped such that it does not touch the bottom contact, see Fig 2.20. This configuration has the advantage that RF and actuation electrodes can still be combined, reducing the total area of the device, i.e. compared with that shown in Figure 2.19. The main drawbacks of this design is a poor C_{ON}/C_{OFF} ratio. In this MEMS topology, the charge injection issue is significantly reduced but not completely solved, as commented in [40, 41]. The presence of charge in these devices is associated by the authors with charge injection from the wafer substrate.

As an alternative of the previous design strategy, in [42], Van Spengen *et al* present a capacitive switch without dielectric in which stopper dimples are placed in the bottom electrode. These dimples avoid contact between both electrodes in the ON state. Figure 2.21 shows the structure of this MEMS prototype. In the experiments carried out in this work, the authors tested the device by operating it in a switching regime for more than 10^8 cycles without any measurable

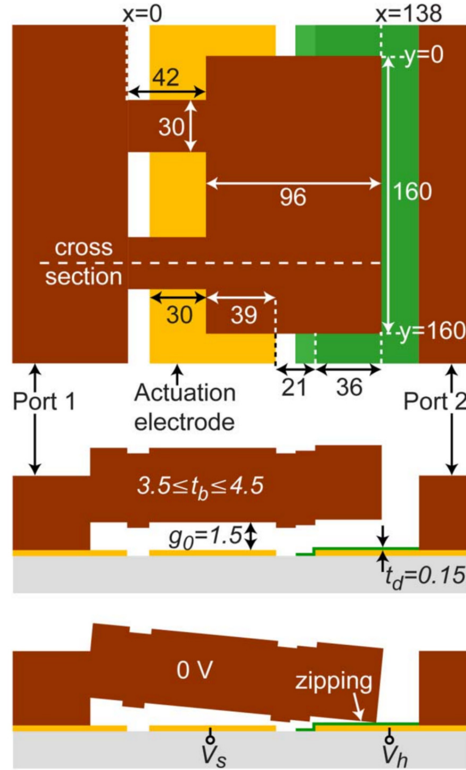

Figure 2.19: Dielectric-less actuation switch with dielectric on the signal line for high C_{ON}/C_{OFF}. All dimensions are in μm. V_s is the voltage on the actuation electrode, while an extra holding voltage V_h can be applied under the dielectric; g_0 is the initial gap height, t_b is the bridge thickness, and t_d is the dielectric thickness. Ports 1 and 2 are the two RF signal lines. Reproduced from [18], ©IEEE.

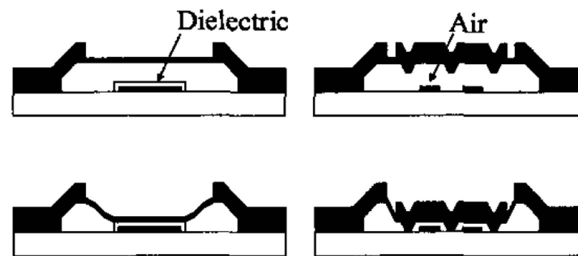

Figure 2.20: Example of a device which contains no dielectric. Figure (a) shows a conventional shunt switch cross-section, and (b) the device without dielectric. Reproduced from [39], ©IEEE.

degradation or drift.

Finally, it is important to note that although dielectric-less strategies used in some fabrication processes are clearly a promising option to minimize dielectric charging, they present poor C_{ON}/C_{OFF} ratios, which poses a fundamental

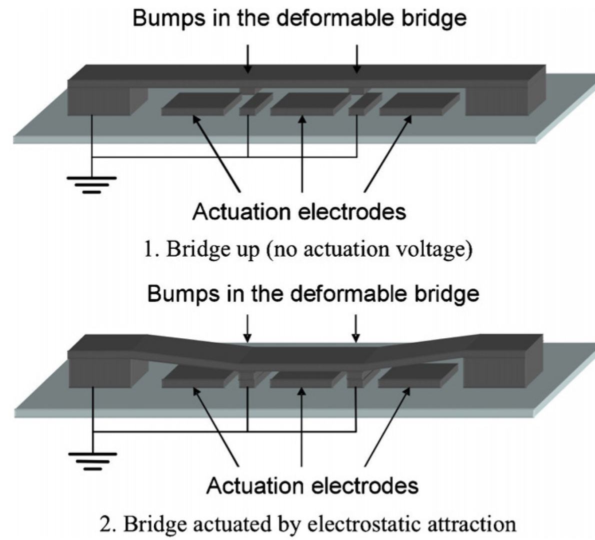

Figure 2.21: Example of a MEMS bridge with stoppers on a grounded electrode, preventing charge build-up at the landing site. Reproduced from [42], ©IOP Publishing Ltd.

limitation in many applications [33, 42].

2.3 Charge control strategies

The main effects of dielectric charging have been presented in Section 2.1. It has been explained the influence of voltage polarity on the sign of charge trapped. This well-known phenomenon has been extensively used to design open-loop mitigation techniques which mainly focus on improving lifetime of capacitive MEMS devices, as those summarized in Section 2.2. Although the use of these techniques has been demonstrated to be a good approach to face this reliability issue, the effect of bipolar voltages on the charge dynamics is not symmetrical and strongly depends on the device structure and the materials used [21]. As a consequence, open-loop control methods based on bipolar actuation are not effective in the long term, since they may not adapt to the drift in the characteristics of the materials involved or even in the environmental variables. This means that some amount of charge will still be accumulating and generating drifts in the device response [26, 29]. In [26], the authors agree with the fact that "it is difficult to fine tune the waveform to completely eliminate charging".

Within this context, closed-loop control methods arise as a promising way to

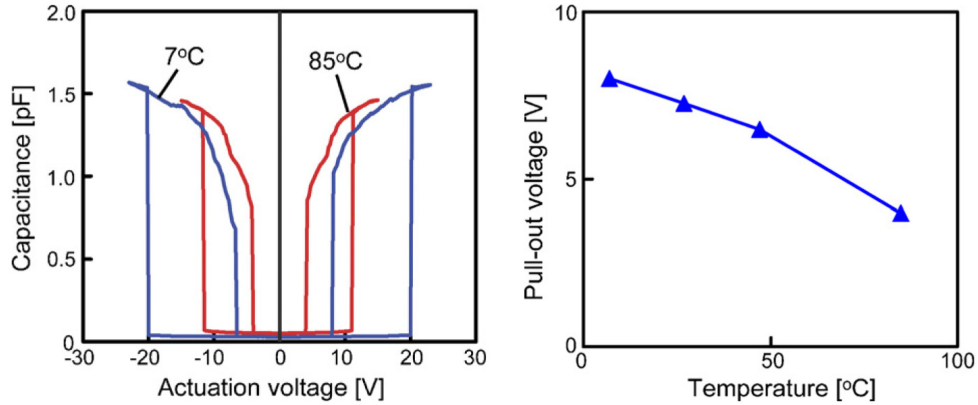

Figure 2.22: Temperature dependence of C-V hysteresis curve (left). Pull-out voltage as function of temperature (right). Reproduced from [47], ©Elsevier.

reduce the long-term effects of dielectric charging. The main advantage of this approach is the fact that charge or its effects can be continuously compensated, even when its dynamics changes due to external factors such as environmental variables. In this regard, some closed-loop strategies have been proposed to date both for ON-closed and OFF-open states of MEMS. In switching applications, these techniques usually focus on avoiding device stiction. Instead, in the contactless scenario, control methods have been thought to offer fine tuning of dielectric charge and device capacitance [43–46].

Examples of methods employing closed-loop elements of control and bipolar actuation for MEMS working at given ON/OFF regimes can be found in [29, 47]. These methods monitor the pull-out voltage shift of the device in order to decide the sign of the voltage to be applied the next time it is pulled down. In [47] the influence of temperature on the pull-out voltage is first shown, since this voltage is necessary to release the device after a certain stress time. As it can be seen in Figure 2.22, the pull-out voltage decreases when the temperature increases. This is an important conclusion which demonstrates that dielectric charging cannot be the only responsible of C-V shifts.

The method introduced in [47] consists in stressing the device to close it with the necessary voltage polarity in order to continuously compensate the induced charge. To do it, the authors define an increment of pull-out voltage ΔV_o. This is the shift experimented by the release voltage, which is inferred by measuring the V_{shift} of the device in the OFF state, as explained in Section 2.1. Figure 2.23 shows an example of the measurements carried out to find ΔV_o and thus, V_{shift}.

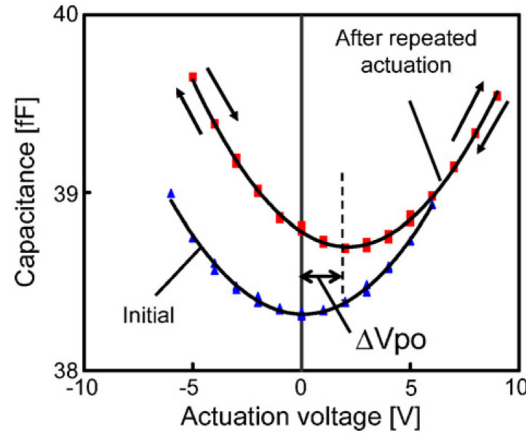

Figure 2.23: C-V hysteresis curve of the contactless state of the device. V_{shift} is defined by the shift of the minimum point of the fitted curves. Reproduced from [47], ©Elsevier.

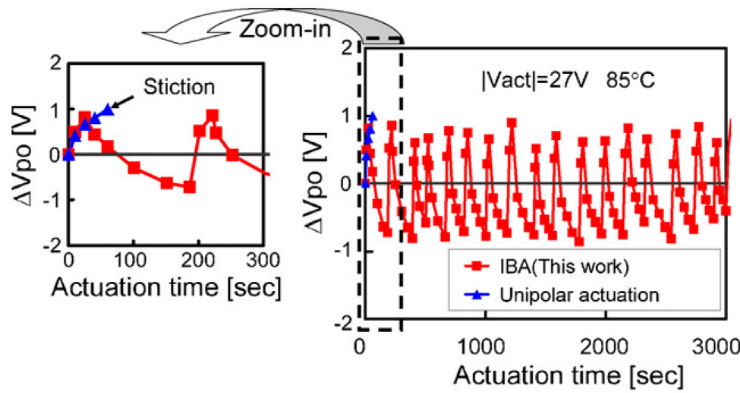

Figure 2.24: Pull-out voltage shifts of unipolar actuation and IBA method. Reproduced from [47], ©Elsevier.

This shift is detected after the actuation voltage is turned off and then, depending on the obtained value, the polarity of the succeeding actuation voltage is, or not, reversed. To take this decision, a threshold voltage shift V_{th} is defined and continuously compared with the obtained V_{shift}.

In Figure 2.24, the authors show the result of applying this method. They compare a measurement in which only unipolar actuation is used with the proposed method. While, in the first case, the capacitive switch suffers from stiction in just 60 sec., with the use of this control the device is still working after 3000 sec. As one can easily see, the lifetime of the device becomes really improved, thus demonstrating the goodness of this approach.

A more complex control method is the IBA (intelligent bipolar actuation),

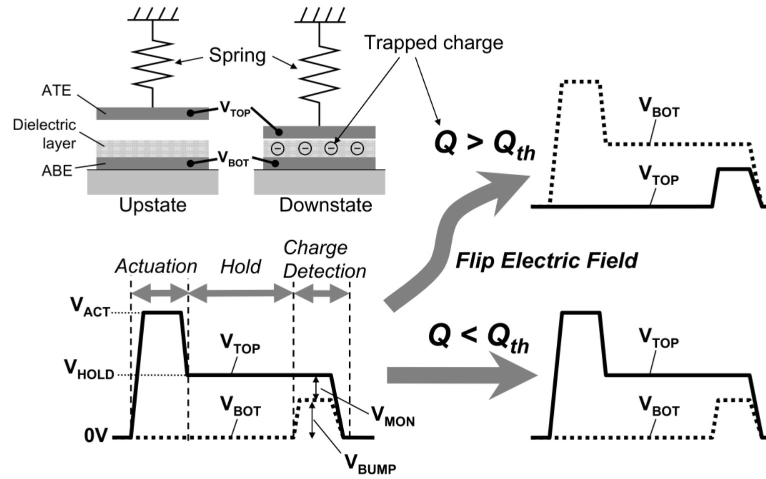

Figure 2.25: Concept of intelligent bipolar actuation (IBA). V_{ACT} and V_{HOLD} are actuation and hold voltages, respectively. Reproduced from [29], ©IEEE.

introduced in [29]; there, a dual-pulse voltage waveform, from [27], is used to actuate the device. In this strategy, the device is actuated with a different voltage voltage waveform on each electrode, in such a manner that applying negative voltages is not needed. This approach makes easier the circuital implementation of the method. Figure 2.25 describes the two voltage waveforms that can be applied to the electrodes: depending on whether the measured dielectric charge is above or below a prefixed charge threshold Q_{th}, each voltage waveform will actuate the top or bottom electrode.

For example, if in the previous sampling time it was detected that $Q_d < Q_{th}$, then a certain voltage V_{ACT} and $0V$ will be applied to the top and bottom electrodes respectively. This first stage ensures that the device goes into the ON-closed state. Next, V_{ACT} is dropped to a value $V_{HOLD} < V_{ACT}$ to maintain the device in the closed state while reducing voltage stress, thus charge injection. As previously discussed, V_{ACT} must be over the pull-out voltage but below the pull-in voltage (hysteresis zone of the C-V characteristic). These voltages will be maintained until the detection stage starts. In this stage, the bottom voltage is raised to V_{BUMP} to reduce the voltage drop across the device. In this situation the switch state (ON or OFF) will depend on the position of pull-out voltage. Finally, this bottom voltage is turned off again and the top voltage is cut-off from V_{HOLD}. At this moment, the voltage on the top electrode also drops, because of the capacitive coupling between the electrodes. Since the actuator capacitance is dependent on the actuator being in ON or OFF state, the trapped charge can be

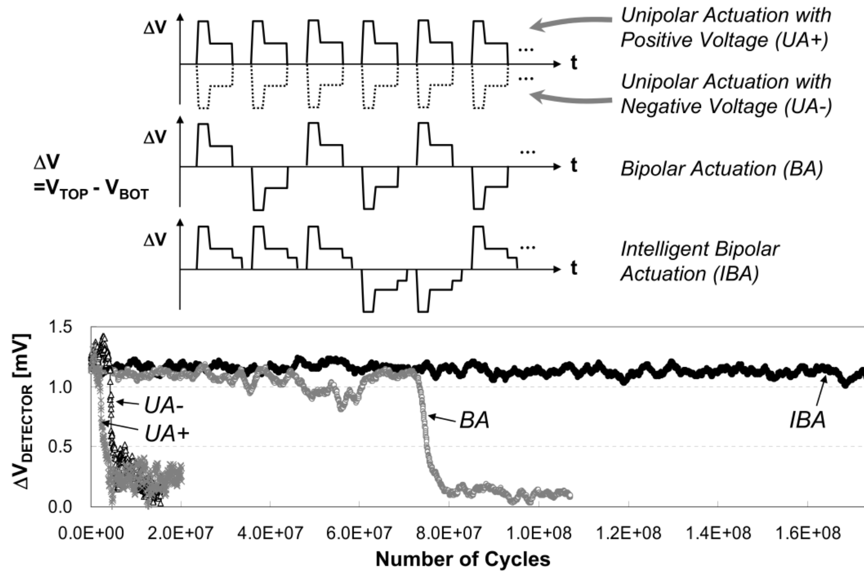

Figure 2.26: Comparison of measured lifetimes between foru different methods: positive and negative unipolar actuation, bipolar actuation and IBA. Reproduced from [29], ©IEEE.

detected by comparing the dropped voltage with a certain reference value V_{REF}. The result of this comparison is then used to decide the next actuation waveform.

In this work, the authors compare the result of applying the IBA method with the use of both open-loop unipolar and bipolar actuations. As it can be seen in Fig 2.26, in this comparison the device is being actuated while the RF output power is measured at each sampling time in the holding phase $\Delta V = V_{HOLD}$. As a result, the use of unipolar excitations limits the use of the device to less than $5x10^6$ cycles, while the lifetime is considerably increased by implementing an open-loop strategy with polarity alternation of dual-pulse waveforms. Finally, the authors show a great increase of the lifetime of the device with the use of the IBA method. After $1.6x10^8$ switching cycles the device keeps working fine with no noticeable damage.

IBA method was implemented in a specific integrated circuit [29] and patented by Toshiba with the title "Semiconductor device and method of controlling electrostatic actuator" [48].

Regarding this Thesis: First control approach

Several different closed-loop strategies for dielectric charge control in contactless MEMS are proposed in this Thesis. The first approach [43, 49] was based

in bipolar actuation and indirect charge sensing from absolute capacitance measurements. That is, the capacitance of the device was measured at each sampling time and then compared with a given threshold value C_{th}. If the measured capacitance was below the threshold, then a positive or 'charge' voltage V_{ch} (which produces charge injection into the dielectric layer) is to be applied during the next sampling period. Otherwise, if the measured capacitance is above the threshold value, then a negative or 'discharge' voltage V_{disch} is to be applied, thus removing charge from the dielectric.

Then, defining V_n as the voltage applied after each sampling time nT_s, one can write

$$V_n = \begin{cases} V_{ch} & \text{if} \quad C_n < C_{th} \\ V_{dis} & \text{if} \quad C_n > C_{th} \end{cases} \tag{2.22}$$

where $C_n = C(nT_s)$ is the total MEMS capacitance (see eq. (2.5)), directly related to the net dielectric charge Q_d (2.6) if only horizontal shifting of C-V is contemplated.

This method was extensively simulated in order to check if it was able to keep the net dielectric charge under control, avoiding undesired effects such as time drifts or device collapse after large working periods. Figure 2.27 shows the simulation results when the charge control method is implemented to a reference device with $V_{ch} = 13.5\,V$, $V_{disch} = -5.5\,V$, $C_{th} = 0.6\,pF$ and using Model A for the charging dynamics, see Section 2.1. Let us note that both V_{ch} and V_{disch} are far below the pull-in values. In this case, both the device capacitance and the parasitic charge increase when V_{ch} is applied until C_{th} is reached. At this moment, the control method applies the negative voltage V_{disch}, forcing the capacitance to decrease to a new steady-state position due to charge removal. At the next sampling time, the capacitance is under the threshold value, so V_{ch} is reapplied and the cycle restarts. Note that the device capacitance is kept predominantly under C_{th}, but with oscillations of about $0.15\,pF$. However, this amplitude decreases for higher values of the sampling frequency.

In order to experimentally validate the feasibility of this first control method, an extensive set of measurements with and without applying the control method to different MEMS devices was performed. Figure 2.28a shows the capacitance transients obtained by applying or not the control method. The plot marked as '1' is the capacitance transient obtained when a constant voltage $V_{ch} = 13.5\ V$ is applied to the MEMS for 55 hours. The measurement starts with an initial

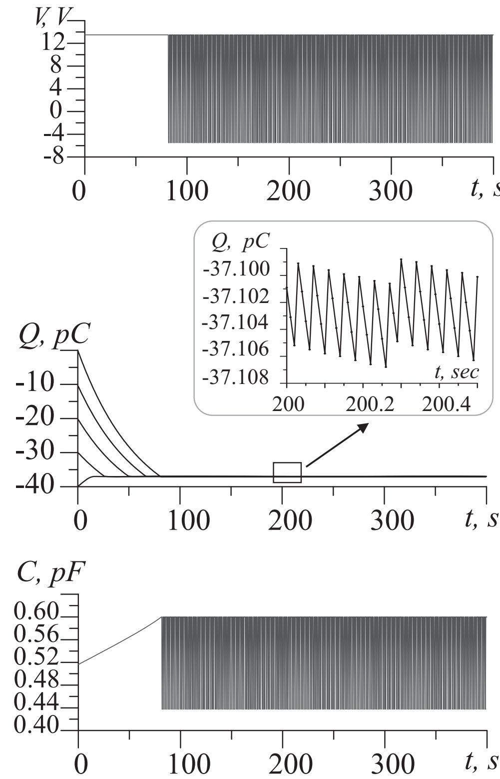

Figure 2.27: Simulated capacitance and dielectric charge transients applying the charge control method. Model A was used for charging dynamics.

time lapse of 300 s, in which zero voltage is applied to set the device to its initial or 'discharged' state. After that, the measurement time line clearly exhibits two different behaviours. In the first one, which lasts until the 38th hour, The capacitance increases about 260 fF due to charge accumulation. From t=38h on, the measured capacitance remains around its maximum value, since the device is closed. Note that the change in behaviour seen at $t = 38$ h is due to the fact that the injected charge during the previous phase produces an additional and slowly-increasing electrostatic force that leads to a pull-in event, forcing the device to collapse despite the fact that the applied voltage V_{ch} is below the initial pull-in value.

The plot marked as '2' in Fig. 2.28a shows the capacitance transient when applying the control method with $C_{th} = 1.1pF$, which is in strong contrast with plot '1'. V_{ch} is applied until the capacitance reaches C_{th}. At this point, a V_{disch} pulse is applied for the first time. From then on, voltage switches to V_{ch} or V_{disch} accordingly to the value of the current capacitance samples. After the first hour some "steady-state" behaviour is reached, with capacitance values closer to

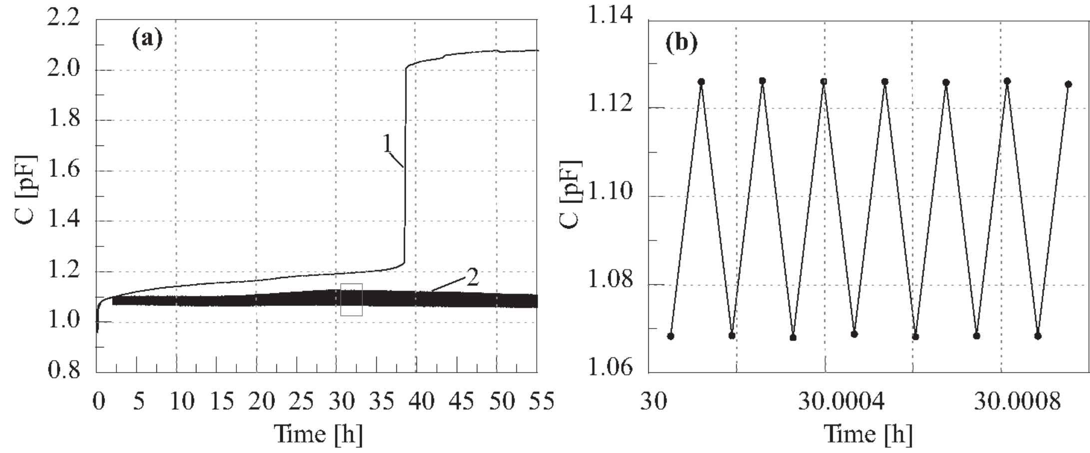

Figure 2.28: (a) Plot '1': Experimental capacitance transient obtained applying a constant voltage $V_{ch} = 13.5V$, i.e. with no control method; plot '2': experimental capacitance transient obtained applying the charge control method with $V_{ch} = 13.5V$ and $V_{dis} = -5.5V$. (b) Zoom-in of the "steady-state" section of plot '2'.

C_{th} (see magnification in Fig. 2.28b), implying that the dielectric charge is kept around a certain value.

In order to contrast the effects of the charge stored in the dielectric layer between applying and not the charge control method in terms of charge, C-V characteristics of the MEMS device have been obtained before and after the experiments. The comparison of the C-V curves obtained after each measurement with the one measured in the discharged state, allows one to extract the shift of the pull-in voltage value. Thus, the expression for the pull-in voltage is

$$V_{pull-in} = V_{pull-in}(Q_d = 0) + V_{shift} \tag{2.23}$$

being $V_{pull-in}(Q_d = 0)$ the pull-in voltage with no trapped charge and V_{shift} the voltage shift due to the dielectric charge from eq. (2.8). As one can see in Fig 2.29, the pull-in voltage of the C-V curve obtained after the application of $V_{ch} = 13.5\ V$ for 55 hours, is below this voltage value and thus, it matches with the collapse of the device after the first 38 hours of stress in Fig. 2.28a.

This control method was later adopted by Ding *et al* [50], who designed and tested an ASIC implementation of this technique.

Although this control method was demonstrated to be useful to improve the lifetime of the devices, it was negatively affected by eventual vertical displacements of the C-V. These displacements have the effect of disconnecting the capac-

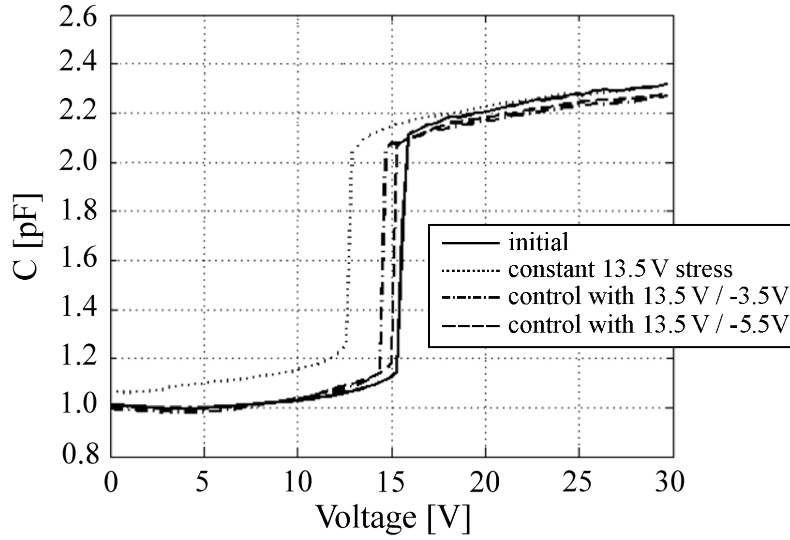

Figure 2.29: Experimental C-V characteristics of a MEMS device after applying several voltage stresses and controls for 55 hours.

itance measure performed at each sampling time from the real voltage shift. That is, a unique capacitance measurement device may be not enough to obtain a good estimation of the voltage shift and of the net dielectric charge. As a consequence, the new-improved charge control strategies discussed below were investigated.

First order $\Sigma\Delta$ control

In [44], it was introduced a new closed-loop control strategy. This control method allows one to sustain a desired amount of net dielectric charge even in the case of vertical movements of the C-V characteristics. As it will be shown, with the use of this method, it is possible to switch on real-time between positive and negative target values of net charge by adjusting the threshold parameter used in the control loop.

The proposed method senses in real time the capacitance difference, which is directly linked with the amount of charge in the dielectric, see eq. (2.10), and it dynamically selects the actuation voltage. This control scheme is inspired by sigma-delta modulation, see Fig. 2.30. Sigma-delta modulators [51] have been used for decades as analog to digital converters and also as closed-loop control circuit topologies for inertial or thermal sensors and actuators [52–54]. The control method presented here can be described, under some conditions, by the equation of a first-order sigma-delta modulator. The behavior of this type of circuits is

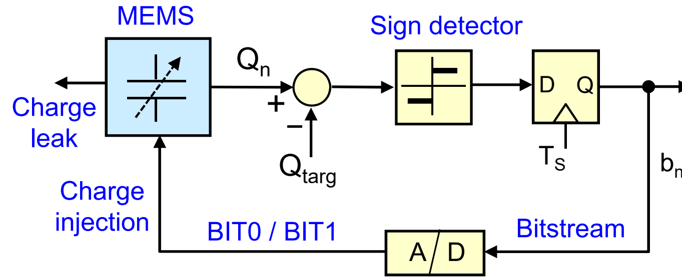

Figure 2.30: Block diagram of the 1st order control method.

well known, and therefore this will allow one to extract real-time information on the state of the device, from the point of view of dielectric charging, directly from the generated digital output.

Equation (2.10) was used to establish the desired actuation parameters of the control method. The aim of the control method was to fix the capacitance difference $\Delta C(t)$ around a threshold value specified beforehand, ΔC_{th}. To accomplish this, the system applies different sequences of positive and negative voltages, V^+ and V^-. Since it is needed to make a quasi-differential capacitance measurement at each sampling time, it is necessary to switch voltages during the sampling period. Then, the voltage waveforms or BITs introduced in Section 2.1, see Fig 2.8, are used. As it has been also explained in Section 2.1, for appropriate values of V^+ and V^- and δ applying BIT0 to the device increases the positive charge and reduces the negative charge in the dielectric. Applying BIT1 has opposite effects on the charge components of each sign.

Following this principle, the closed-loop algorithm proposed was:

1. Choose a suitable set of values for V^+, V^- and a threshold value ΔC_{th} which, from equation (2.10), will lead to a target voltage shift $V_{\text{shift}} = V_{th}$ and a target net charge $Q_d = Q_{\text{target}}$.

2. Actuate the device with any of the symbols shown in Fig. 2.8, BIT0 or BIT1.

3. Perform capacitance measurements at symbol times $(n-1)T_s + (1-\delta)T_s$ and nT_s. Since different voltages V^+ and V^- are applied in these times, values of C^+ and C^- are obtained and, for T_s far below the time constants of the charge dynamics, ΔC is obtained as $C^+ - C^-$.

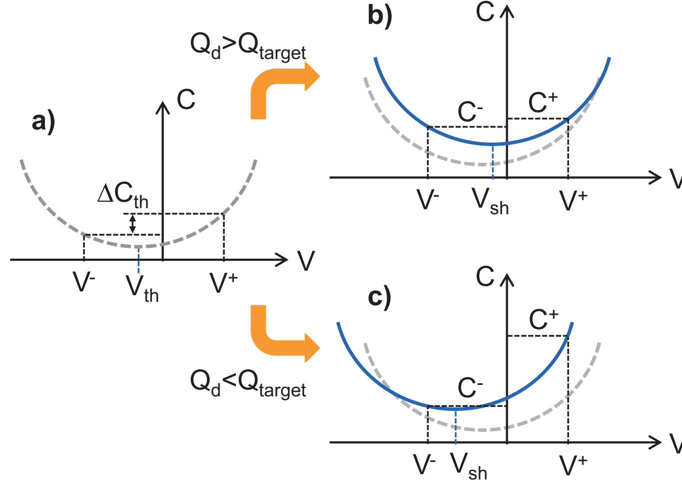

Figure 2.31: Illustration of the decision law (2.24). Curve (a) is a target C-V with $V_{th} = Q_{\text{target}}/C_d < 0$. In curve (b) the net amount of charge is not enough negative ($V_{\text{sh}} > V_{th}$, so $Q_d > Q_{\text{target}}$), then $\Delta C = C^+ - C^- < \Delta C_{\text{th}}$ and, according to (2.24), the next actuation symbol is BIT1. In curve (c) the net charge is too negative ($V_{\text{sh}} < V_{th}$ so $Q_d < Q_{\text{target}}$), then $\Delta C > \Delta C_{\text{th}}$ and the next symbol is BIT0.

4. The next symbol to be applied to the device comes from the comparison between ΔC and the threshold ΔC_{th}, according to the following decision law:

$$\text{Next Symbol} = \begin{cases} BIT0 & \text{if } \Delta C > \Delta C_{\text{th}} \\ BIT1 & \text{otherwise} \end{cases} \tag{2.24}$$

5. Apply the next symbol and go back to step 3.

Figure 2.31 shows an example of how the decision law works: a target C-V is shown in Fig. 2.31(a). Figure 2.31(b) corresponds to the case $Q_d > Q_{\text{target}}$, in which the next symbol to apply is BIT1. This will shift the C-V to the left, that is to decreasing values of Q_d. Symmetrically, in Fig. 2.31(c) $Q_d < Q_{\text{target}}$ and the next symbol, BIT0, would increase Q_d.

Long time experiments were performed to demonstrate that the voltage shift V_{shift} (and thus the net dielectric charge Q_d) can be fixed at arbitrary desired levels using the proposed control method. To this effect, a set of six increasing values of V_{shift} was programmed in the experimental set-up. The device was initially discharged and each target value, or step, has a time length of 48 hours. The threshold values of the control method applied at each step are listed in Table 2.2.

Table 2.2: Parameters of the control method used in the experiment shown in Figure 2.32

Step	1	2	3	4	5	6
V_{th} [V]	0.25	-0.5	0.75	-1	1.25	-1.5
ΔC_{th} [fF]	-5.6	11.2	-16.8	22.4	-28	33.6

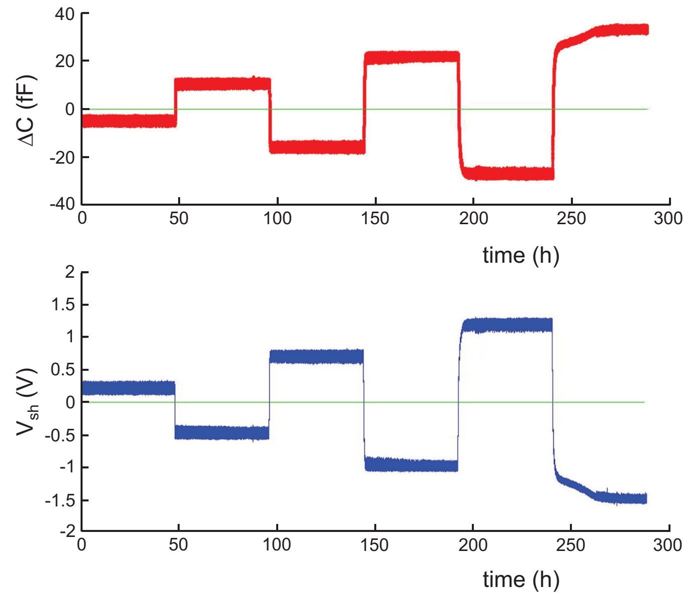

Figure 2.32: Experimental results on which the sigma-delta control is applied to obtain the desired set of V_{shift} values of Table 2.2. Plots (a) and (b) are, respectively, the evolution of the "quasi-differential" capacitance and of the voltage shift with time. BIT parameters: $V^{+} = -V^{-} = 4V$, $T_s = 2.5s$, $\delta = 0.2$.

It can be seen in Figure 2.32 that the values of the "quasi-differential" capacitance ΔC and of the voltage shift V_{shift} fairly match with the desired ones at the steady-state phase of each step. That is, the charge is kept almost constant once stable regimes are achieved.

Figure 2.33 shows the evolution with time of the average of the control bit stream, extracted from the experiment. Let us note that some steady-state behaviour is reached at the end of each stage, with bit stream averages denoting the values of Q_{target}.

In this method, based on 1st order sigma-delta ($\Sigma\Delta$) modulation, the MEMS dielectric works as a leaky charge integrator under two competing mechanisms: charge being injected by the actuation symbols and charge escaping the traps in

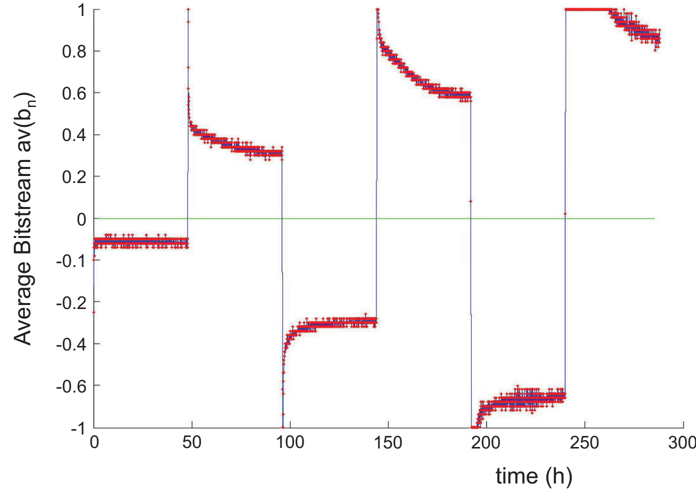

Figure 2.33: Average of the control bit stream av(b_n) as function of time, extracted from the experiment reported in Fig. 2.32.

the material. The $\Sigma\Delta$ modulator generates an actuation bit stream that compensates in average the charge being leaked out of the dielectric so that $Q_d = Q_{target}$. However, well known issues of first order $\Sigma\Delta$ modulators limit the effectiveness of this method. One is the presence of tones in the spectrum of the bit stream (see Fig.18 in [44]), which poses a problem for retrieving real-time information about the charge status. Another issue is the presence of a Devil's Staircase fractal (see Figs.11 to 13 in [55]), a typical effect when leaky integrators are used. The fractal plateaus are "dead zones" that cannot be observed or controlled, thus hindering the possibility of having a good charge control in certain cases.

In order to solve these two typical issues, a second-order $\Sigma\Delta$ charge control is proposed in this Thesis. This new approach is explained in the next section.

Second order $\Sigma\Delta$ control

The 2nd order charge control method improves the previous 1st order one. In this new approach, an error signal integrator is introduced before the comparison stage. Let us note that in the 1st order method the error signal $\Delta C - \Delta C_{th}$ is used to decide the next BIT symbol to apply. In the 2nd order method, this error signal is integrated over time, and the sign of this integrated error signal decides which BIT symbol is to be applied in the next sampling period. As a consequence, in this method two-cascaded charge integrators are present. The first is the MEMS

dielectric itself, which acts as a low-pass filter with typical 1st order noise shaping [7], while the second integrator improves noise rejection at low frequencies, thus providing 2nd order noise shaping. Figure 2.34 shows schematic views of the 2nd order control circuit.

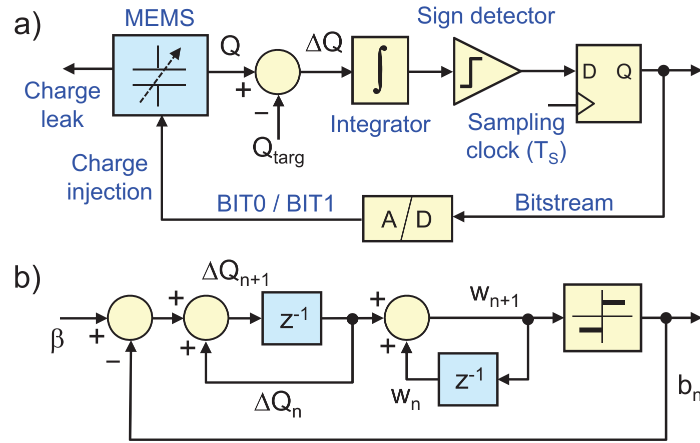

Figure 2.34: Block diagram (a) and equivalent sampled-time circuit (b) of the 2nd order control method. In practice the sensing variable is the quasi-differential capacitance, but equivalent dielectric charge is used here instead.

The aim of the first experiments carried out is to perform a comparison on the feasibility of both control methods (1st and 2nd order) to obtain a given sequence of target values of V_{sh}, thus of Q_d. Figure 2.35 shows the results obtained when each method is applied to successively obtain $V_{shift} = 0.5\,V, -0.75\,V$ and $0\,V$ in 48-hour intervals. Note that the values of V_{shift} fairly match with the desired ones for both methods. Moreover, once steady-state regimes are reached, the values of V_{shift} are always kept constant.

Another important comparison carried out is between the obtained average of the bit stream in this experiment. The bottom plots in Figure 2.35 compare these experimental bit stream averages with their simulated counterparts, explained in [56]. Note that all bit streams, measured and simulated, reach the same values once in steady-state, but they also exhibit the same behaviour in the transients.

Figure 2.36 compares the spectral power densities of the bit streams obtained from an experiment in which a device was set to $V_{shift} = -0.5\,V$ using both control methods. The presence of the additional integrator in the 2nd order method produces noticeable differences. Firstly, the tones around 0.1 Hz found in the 1st order method are no longer present in the 2nd order one. Furthermore, the noise

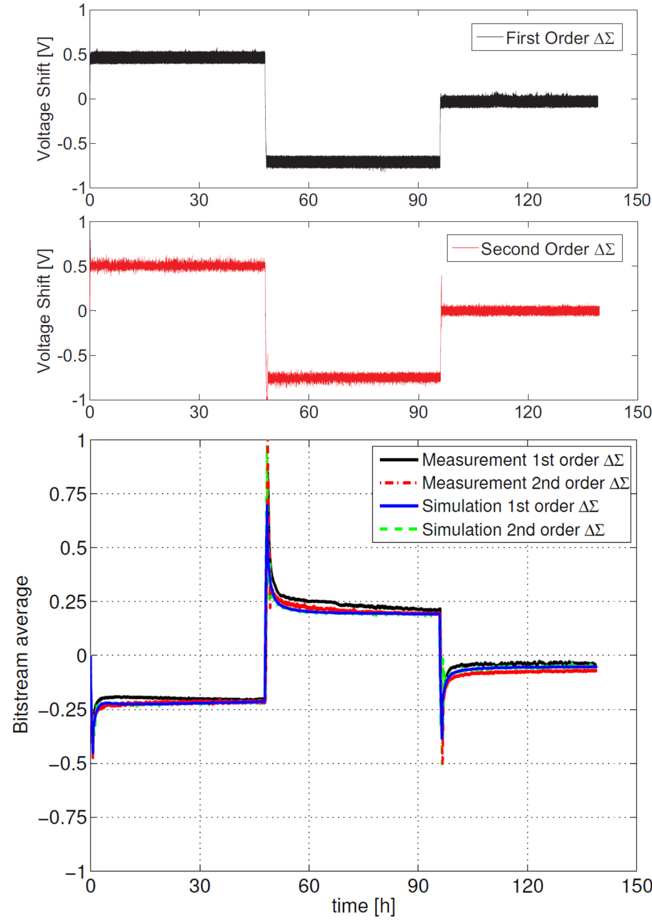

Figure 2.35: Comparison of first and second order sigma-delta control methods to the same device to obtain same sequence of three different values of V_{shift}. The bottom plot compares the experimental average bit streams with those obtained from simulations. BIT parameters: $V^+ = -V^- = 4V$, $T_s = 2.5s$, $\delta = 0.2$.

at low frequencies becomes considerably reduced and the slope of the quantization noise rolled out of the band of interest clearly increases in the 2nd order case. Let us note that these results strongly resemble those obtained in [57], where 1st and 2nd order thermal $\Delta\Sigma$ modulators for flow sensing applications are compared.

The fractal sensitivity of both methods was also checked using a device which exhibits faster charging dynamics. The experiment consisted in applying real-time charge control to obtain stepped values of ΔC_{th}, thus of Q_{target}. Each step lasted for 30 minutes, time enough to achieve stable regimes with the devices used. The bit stream average obtained in each step is shown in Figure 2.37. Both simulation and experimental results for the 1st order control show fractal behaviour: the same bit stream average is observed for four different values of

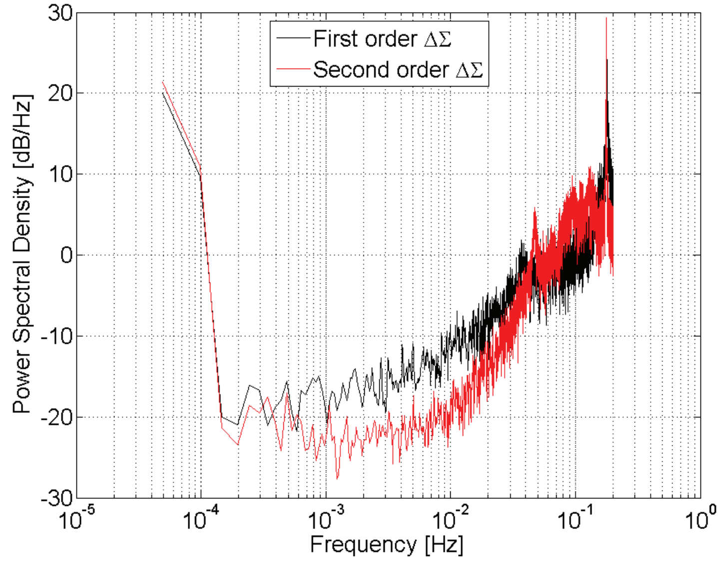

Figure 2.36: Power spectrum densities (P-Welch estimation) obtained the control bit streams of an experiment in which 1st and 2nd order methods were applied to the same device to set $V_{shift} - 0.5V$.

ΔC_{th} around zero, then fair control leading to a discharged state was not possible in this case. On the other hand, the fractal behaviour is no longer seen and thus the relationship between the output bit stream and the total dielectric charge becomes univoque when using the 2nd order control method.

Although the two methods based on $\Sigma\Delta$ modulation introduced here have demonstrated to be useful to maintain a certain net charge in contactless electrostatic MEMS, they do not allow to compensate vertical movements of the C-V characteristics due to non-uniform distributions of charge and environmental variations. This may imply that although the net dielectric charge is being controlled, a constant device capacitance or position is not guaranteed. In this regard, a simultaneous control of net charge and device capacitance has been also proposed in this Thesis.

Double-loop control

This section introduces a double-loop control strategy which allows to maintain both a target level of net dielectric charge and a target capacitance value. The first loop, based on $\Sigma\Delta$ modulation, indirectly monitors the total charge and actuates the device with appropriate BIT waveforms. The second loop implements a method that dynamically varies the value of V^+ and V^- conforming BIT0 and

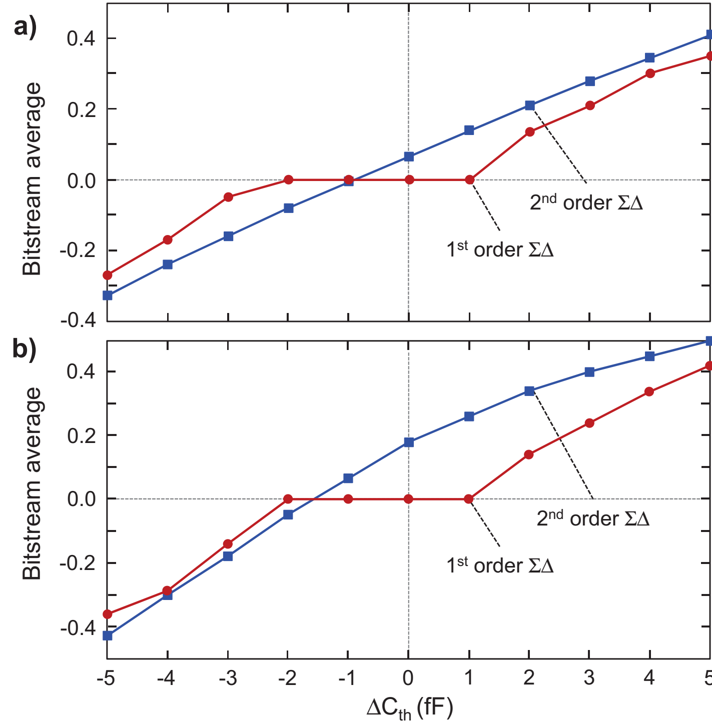

Figure 2.37: Simulated (a) and measured (b) bit stream average values obtained with the same device and several values of ΔC_{th}. Each point of the graphs is taken from a 30-minute experiment. BIT parameters: $V^+ = -V^- = 10V$, $T_s = 1.7s$, $\delta = 0.15$.

BIT1 to keep constant the device capacitance.

The block diagram of Fig 2.38 describes the double-loop control proposed. It allows to set the device capacitance to a target value C_{th}, against potential vertical displacements of the C-V, while the net dielectric charge is simultaneously being controlled. It works as follows: once the charge control loop decides which symbol, BIT0 or BIT1, must be applied during the next sampling period, the values of V^+ and V^- are adapted to maintain the target capacitance. That is, at each sampling time, depending on whether C^+ and C^- are above or below C_{th}, V^+ and V^- are increased or decreased in a small predetermined step ΔV .

Figure 2.39 illustrates qualitatively how this double-loop control works. Two different situations are shown. In the first-initial one (curve 1), BIT0s and BIT1s are applied to set the bottom of the C-V at $V = V_{shift1} < 0$, being V_1^+ and V_1^- the voltages needed to obtain the target capacitance C_{th}. In the second case (curve 2), a majority of BIT0s has been applied to shift the curve to $V_{shift2} > 0$. However, since the C-V has also suffered some vertical shift, the applied voltages must be set to V_2^+ and V_2^- to keep the same device capacitance C_{th}. This means that

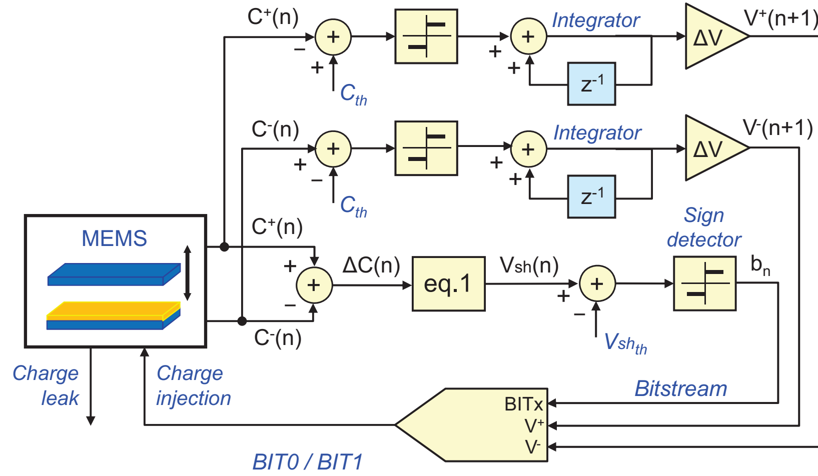

Figure 2.38: Block diagram of the double-loop control method.

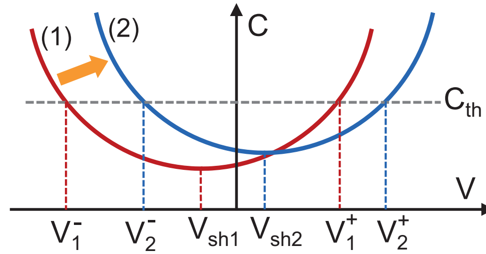

Figure 2.39: Illustration of hypothetical C-V displacements generated by the application of the double-loop control method.

horizontal displacements produced by net charge injection can be compensated by applying appropriate sequences of BIT0 and BIT1, while vertical displacements of the C-V can be compensated through V^+ and V^- variations.

This method has been validated through experiments, as the one shown in Fig. 2.40. In this experiment, three target capacitances, C_{th} = 6.34, 6.36 and 6.35 pF, were set in 5-hour steps, while $V_{th} = 0\ V$ (thus zero net dielectric charge) was also set. The time parameters of BIT0 and BIT1 are $\delta = 1/7$ and $T_S = 816\ ms$. The initial voltages are $V^+ = -V^- = 7\ V$ and the voltage step is $\Delta V = 10\ mV$. The results show that the double-loop control works successfully, allowing to reach and maintain the three different device capacitance values, while the net dielectric charge is kept constant during the whole experiment. The bit stream generated by the first control loop sets the net dielectric charge while the additional control loops adapt the actuation voltages, $V^+(t)$ and

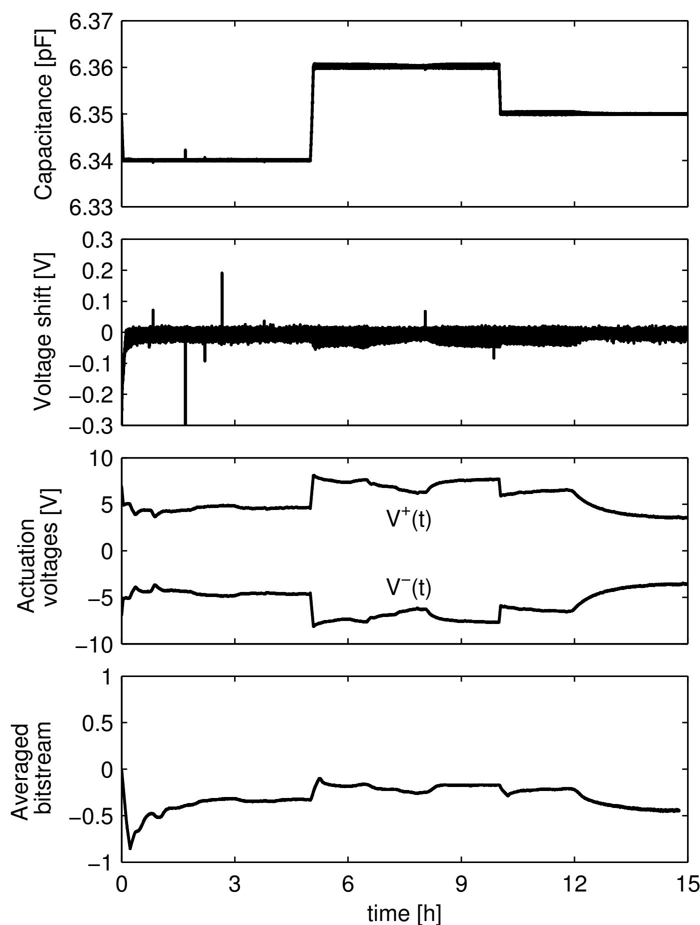

Figure 2.40: Results of an experiment in which the double-loop control is applied to set zero net charge and three different consecutive target capacitances. BIT timing parameters are $\delta = 1/7$ and $T_S = 816\ ms$, the initial voltages are $V^+ = -V^- = 7\ V$ and the voltage step is $\Delta V = 10\ mV$

$V^-(t)$, to keep constant the device capacitance at the predefined thresholds. The time evolution of the averaged bit stream is clearly affected by the evolution of the actuation voltages. This reflects the fact that the dynamics of these three actuation variables are clearly intertwined.

2.4 Ionizing radiation

It has been commented above the influence of bias polarization on reliability issues due to dielectric charging in electrostatic MEMS. Different methodologies to characterize the dynamics of this phenomenon and some proposed closed-loop methods to compensate this charge have also been introduced and discussed. This

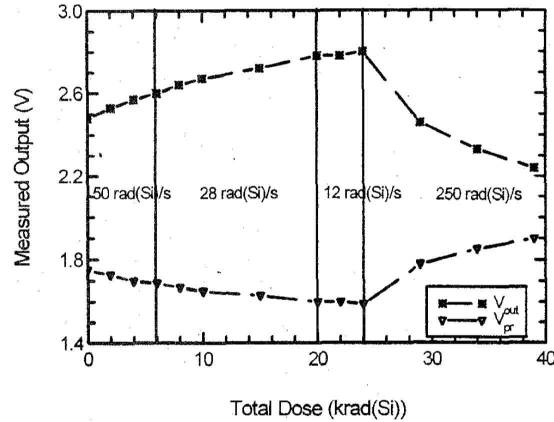

Figure 2.41: Output voltage (V_{out}) and pre-amplified voltage (V_{pr}) of an accelerometer as a function of fluence for different dose rates of 65 MeV protons. Reproduced from [63], ©IEEE.

section introduces the use of the dielectric charge control methods proposed in this Thesis to MEMS devices under ionizing radiation such as Gamma or X-Ray.

MEMS technology is nowadays widely used in space applications [58–61], covering the same range of applications as MEMS working on Earth. However, in this kind of applications, devices work at different environmental conditions, such as temperature, vacuum, vibration or ionizing radiation. Regarding electrostatic MEMS, the influence of charge trapping due to ionizing radiation can be seen as a continuous electric field which actuates the device, even when the bias applied is 0 V [62]. This electric field, as in the case of voltage bias, causes some dielectric charging, which can produce changes in the calibration of MEMS sensors, such as accelerometers, or even permanent stiction in MEMS switches.

In the case of MEMS accelerometers, Knudson *et al* [63], observed the influence of radiation on the accelerometer sensitivity. Although this influence was expected by the authors due to the presence of other electronic components, they found that the change in the output voltage was caused by charge build up in dielectric layers beneath the moving mass. In Fig 2.41, the authors show the evolution of the sensor output voltage under radiation test. The device was irradiated with 65-MeV protons under a static force of 1g. Being V_{pr} the output of the internal pre-amplifier and V_{out} the output of an internal buffer (V_{pr} is inverted and amplified by a factor of 2), one can see that V_{pr} decreases at low dose rates ($<$ 50 rad(Si)/s) up to total dose of 24 krad(Si) and increases for high dose rates (20 rad(Si)/s).

In MEMS optical mirrors [64, 65], Miyahira *et al* in [65] compare the influ-

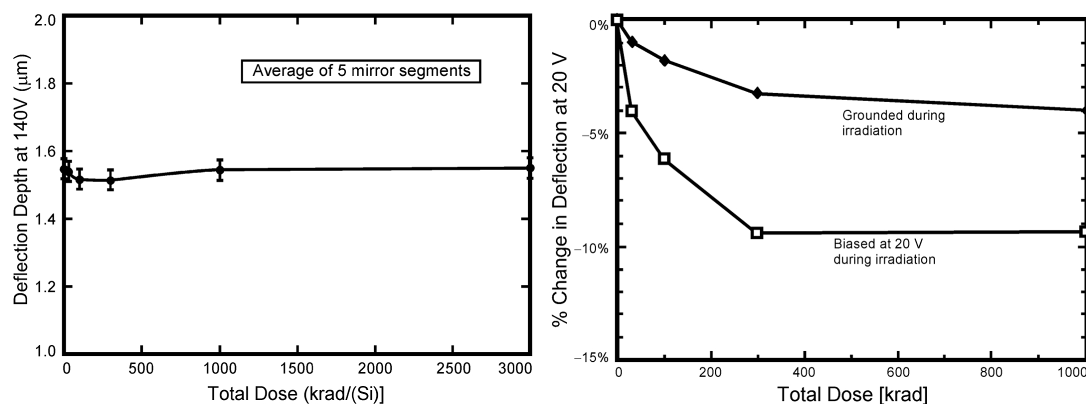

Figure 2.42: Change in mirror deflection due to radiation for biased segments of the BMC mirror array (left). Change in mirror deflection due to radiation for a typical piezoelectric mirror (right). Reproduced from [65], ©IEEE.

ence of ionizing radiation on two different types of devices. The first one was a commercial MEMS mirror manufactured by Boston Micromachines Corporation (BMC), which does not contain any dielectric layer in the regions between the top and bottom electrodes. The second device tested was a deformable mirror activated by a piezoelectric thin-film, developed in the Jet Propulsion Laboratory (JPL) in conjunction with the Pennsylvania State University. In this work, the radiation tests were done with ^{60}Co Gamma rays at the JPL irradiation facility and the deflection of the MEMS mirror was measured at different total irradiation doses for both devices under test. The results of this comparison showed the influence of dielectric layers under ionizing radiation. In Figure 2.42 it can be seen that the first device was practically not affected by radiation, since no appreciable changes in the device deflection are observed. However, as it could be expected, the results of the second device evidence that ionizing radiation can potentially affect device operation when dielectric layers are used. In this case, two devices were irradiated: one biased at 20 V and the other with zero bias. Although in the case of 20 V bias the device suffered more from ionizing radiation, shifts in deflection sensitivity were also observed in the zero-biased device.

Different studies about the effects of ionizing radiation on RF-MEMS switches have been carried out to determine the influence of this phenomenon on the device lifetime [66–70]. In [69] the authors demonstrate the reliability issues due to the total irradiation dose on the characteristics of a RF-MEMS and propose a new device design to mitigate these effects. In the experiments carried out in this work, two different MEMS designs were used: the standard and the alternate

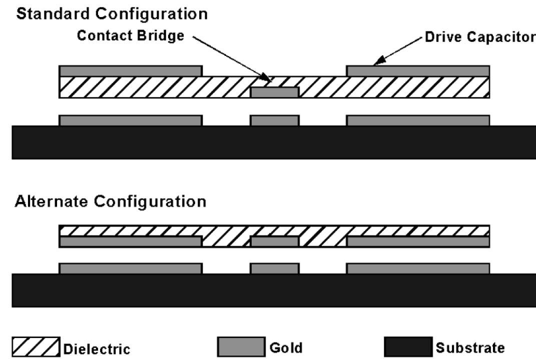

Figure 2.43: Cross section of standard and alternate configurations of the RSC RF MEMS Switch. Reproduced from [69], ©IEEE.

configurations, depicted in Fig. 2.43. As it can be observed there, in the standard topology the dielectric layer is located between both electrodes, as usual configurations. However, in the second design, the dielectric is above the top plate. This alternate configuration was developed primarily to reduce dielectric charging due to polarization. Electrical performance of the two configurations is nearly identical.

Gamma radiation tests were made at ^{60}Co facility in the JPL with a 50 rad(GaAs)/s dose rate. In the experiment, both MEMS structures were irradiated while applying positive and negative bias voltages. Also the case of zero bias was tested with no measurable degradation with total dose. Both positive and negative pull-in voltages were monitored during the experiment to observe the radiation effects in each configuration and bias polarization. In Fig. 2.44, it can be seen the results of a radiation test while applying positive (left) and negative bias (right) in the standard device configuration. For the case of positive bias, the device was irradiated until the positive pull-in voltage reached $+90\ V$. Then, both radiation and positive bias were switched off to study device recovery. Although no changes in the pull-in voltages were observed after 3 days at $25°C$, the device was totally recovered after an unbiased anneal at $125°C$ for 24 hours. As it can be also observed in the right side of Fig. 2.44, degradation was faster when a negative bias of $-90\ V$ was applied in the same experiment.

Figure 2.45 shows the result of applying positive bias under radiation with the use of the alternate configuration. As it can be seen, no significant degradation was found after a total dose of 150 krad.

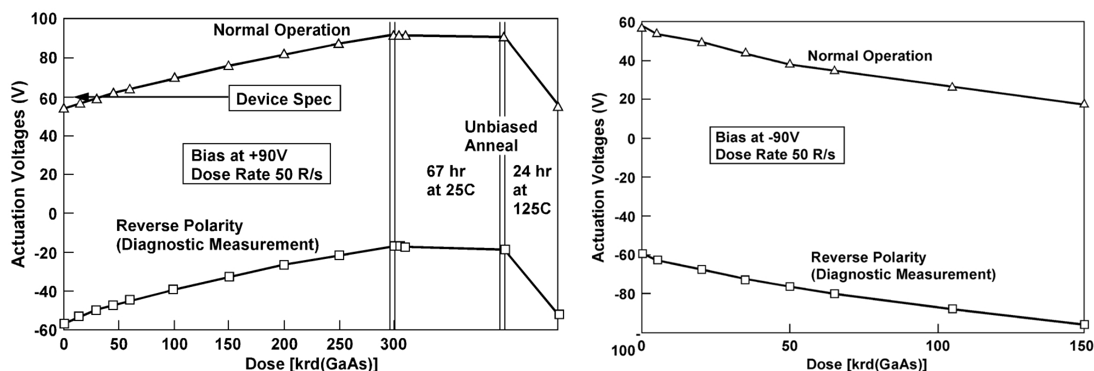

Figure 2.44: Actuation voltage vs. dose for the standard configuration biased positively during irradiation (left). Actuation voltage vs. dose for the standard configuration biased negatively during irradiation (right). Reproduced from [69], ©IEEE.

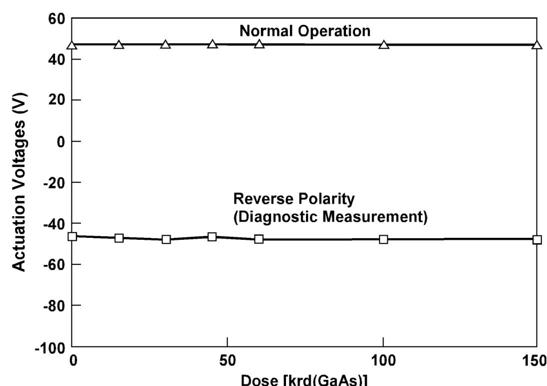

Figure 2.45: Actuation voltage vs. dose for alternate configuration biased positively during irradiation. No measurable change in actuation voltage was observed. Reproduced from [69], ©IEEE.

Regarding this Thesis

In this Thesis, the second-order sigma-delta dielectric charge control has been used to compensate charge injection produced by Gamma and X-Ray radiation sources. As it has been previously commented, the control is always trying to compensate any deviations from the desired target charge by generating an adequate sequence of actuation symbols, BIT0 and BIT1. Then, in presence of charge induced by radiation, the control loop must provide the changes in the actuation sequence necessary to take into account this additional charge generation. Globally, there is a balance between the charge being continuously leaked out of the dielectric, that being injected by the control actuation and that being generated by ionizing radiation. The presence of this new charging source will imply a variation of the averaged output bit stream provided by the control.

The X-Ray experiments were performed at the Radiation Physics Laboratory of the University of Santiago de Compostela. The die containing the device under test (DUT) was placed on an uncovered 84-pin package facing the radiation source. The DUT was irradiated by a 50 kV X-Ray beam. The first test investigated whether radiation induces noticeable dielectric charging. The DUT, initially discharged, was irradiated with a dose rate of 0.65 Gy/s for 1.5 h and not irradiated for the next 2 h. To ensure that no charge was induced by mechanisms other than radiation, the voltage between the MEMS electrodes/plates was set to zero. Furthermore, in order to monitor the charge evolution, the value of V_{shift} was periodically obtained by measuring the C-V characteristics.

The results, plotted in Fig 2.46a, clearly show an increasing amount of negative charge during irradiation. When radiation ceases, the zero bias tends to remove the charge. However, such charge removal is slow and only partial at the end of the experiment. In this measurement campaign, also the effect of using a bipolar open-loop mitigation strategy for actuation-induced charge was investigated. A zero-average sequence of alternate BIT0 and BIT1 symbols actuated the DUT during a second experiment, which included a dose rate of 1.3 Gy/s irradiation for 1 h. The evolution of V_{shift} in this case, Fig. 2.46b, indicates an increase of negative charge during the irradiation phase. After irradiation, the DUT slowly returns to the initial state. It is concluded that the same behavior is observed in both experiments of Fig. 2.46.

Finally, a closed-loop control was used to compensate the radiation effects seen in the previous experiments. The loop was configured to set $V_{shift} = 0\ V$ (zero net charge), while a series of irradiation steps was applied to the DUT, see Fig 2.47. The figure shows that V_{shift} is kept around zero during all the experiment, thus demonstrating the effectiveness of the control to partially compensate the charge induced by radiation. Furthermore, the averaged bit stream clearly correlates with the sequence of dose rates applied. Irradiation phases increase the amount of negative charge to be compensated by the control, thus extra positive charge must be injected by the control loop. Then, as it can be seen, the average bit stream tends to -1 (BIT0 or V^- dominant). In the rest phases the average tends to zero, indicating that net charge is being removed.

An experiment for investigating the effect of applying the charge control method under Gamma radiation was performed at the ESA-ESTEC ^{60}Co facility. In the experiment, charge control with target $V_{shift} = 0\ V$ was continuously

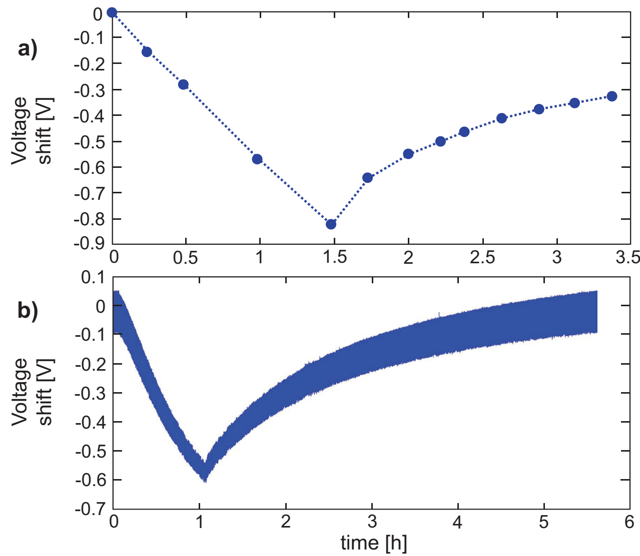

Figure 2.46: Results of two X-Ray irradiation experiments. (a) Evolution of V_{shift} when the MEMS is first irradiated with 1.3 Gy/s for 1.5 h, then not irradiated for the next 2 h. The actuation voltage was V=0 during all this time. (b) Evolution of V_{shift} when alternate BIT0 and BIT1 symbols are applied to the MEMS. The device is initially discharged, then irradiated with 1.3 Gy/s for 1 h. BIT parameters: $V^+ = -V^-$=10V, δ=1/3, T_S=1.2 s.

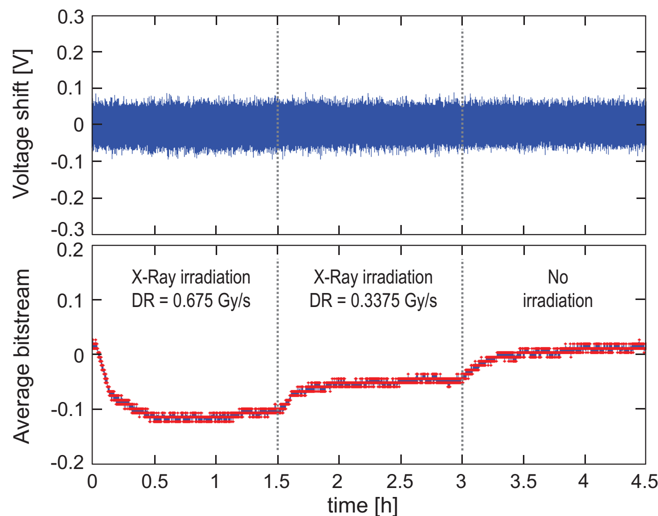

Figure 2.47: Results of a X-Ray irradiation experiment. Evolution of V_{shift} and of the average bit stream when second-order sigma-delta control is applied to obtain $V_{shift} = 0$ (zero charge). Two different dose rates are delivered to the MEMS.

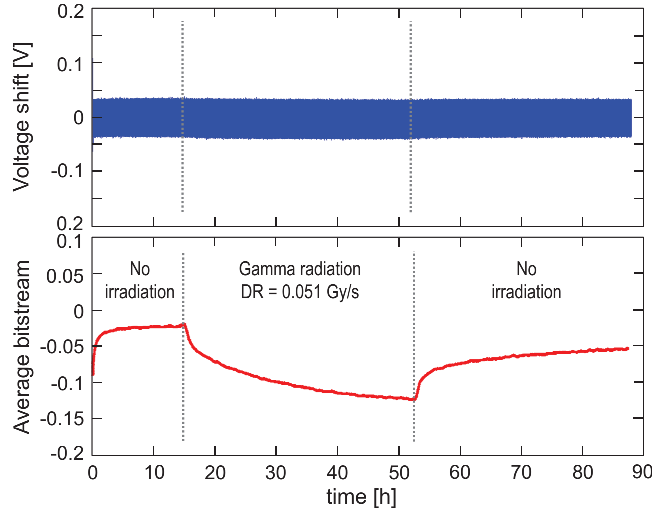

Figure 2.48: Results of a Gamma irradiation experiment. Evolution of V_{shift} and of the averaged bit stream when second-order sigma-delta control is applied to obtain V_{shift}=0 (zero charge). A dose rate of 0.051 Gy/s is delivered to the MEMS, preceded and succeeded by zero radiation steps.

applied to the DUT, under successive steps with no radiation for $15h$, irradiation with dose rate of 0.051 Gy/s for 37 h and, again, no radiation for 35 h. The results in Figure 2.48 show that V_{shift} is kept around zero during the experiment. Furthermore, also in this case a clear correlation exists between the behavior of the average bit stream and the irradiation sequence.

It can be noted that with the use of this control method, real-time information about the charge being induced by radiation is obtained by monitoring the average bit stream. This may allow to use this technique in radiation detection applications.

2.5 Main contributions of the Thesis

This section summarizes the most significant contributions of this Thesis to the MEMS research community. To give more insight about how these results have been obtained, they are presented chronologically. These highlighted contributions, always from a subjective point of view, are reported in detail in the next chapter.

- First dielectric charge closed-loop control which actuates the device accordingly to periodical capacitance measurements [43, 49]. This method, based

on bipolar voltage actuation was thought to compensate horizontal displacements of the pull-in voltage as a first approach to mitigate undesired effects of the net trapped charge. Later, in [50], Ding *et al* designed an ASIC to implement this proposal. The method description can be found in Section 3.1.

- New methodology to characterize dielectric charging in contactless electrostatic MEMS [45, 55]. From the analysis of the shape of C-V characteristics introduced by [9], new voltage waveforms, named BIT0 and BIT1 were proposed. These symbols allow to inject charge of both signs while monitoring the evolution of the net charge without distorting the measurement. To infer this net charge at each sampling time, a quasi-differential capacitance measurement was proposed and used. This technique is explained in detail in Sections 3.2 and 3.4.

- First and second order sigma-delta based controls have been proposed to compensate dielectric charging [44, 56]. Both controls use a feedback loop to maintain the net dielectric charge at the desired level by using the same voltage waveforms, or symbols, used to characterize charge dynamics. Since they are able to monitor the current net charge, a comparison with a desired charge value is used to decide the specific symbol to be applied in the next sampling time. This decision is taken accordingly with the corresponding control law. Because of the technique used to infer dielectric charge, these two methods still work properly in front of vertical displacements of the C-V characteristics. The second order topology was proposed with the aim of improving the first one, by avoiding typical plateaus of first-order strategies and providing second-order quantization noise shaping. First and second sigma-delta charge controls are explained in Sections 3.3 and 3.5, respectively.

- Charge controls proposed have been tested under external charge source provided by ionizing radiation [71, 72]. The aim of this study was to check whether these techniques could be used to compensate not only dielectric charging induced by polarization, but also by radiation. In this regard, several experiments have been carried out under Gamma and X-Ray radiation sources. Due to the charging process induced by ionizing radiation, changes in the output bit stream of the control have been detected. This

fact provides an opportunity to examine whether these methods or even a modification of them could be used in radiation detection applications. The radiation tests carried out in this Thesis can be found in Sections 3.6 and 3.7.

- Finally, in order to address the proposed charge control techniques to those applications in which the capacitance value is a key factor, a simultaneous control of both charge and capacitance has been provided [46].

References

[1] S. Sze and K. Ng. *Physics of Semiconductor Devices. Third Edition.* Wiley, 2007.

[2] M. Razeghi. *Fundamentals of Solid State Engineering. Sec. Edition.* Springer, 2006.

[3] A. Gehring and S. Selberherr. “Modeling of tunneling current and gate dielectric reliability for nonvolatile memory devices”. In: *Device and Materials Reliability, IEEE Trans. on* 4.3 (2004), pp. 306–319.

[4] A. Jain, S. Palit, and M. A. Alam. “A Physics-Based Predictive Modeling Framework for Dielectric Charging and Creep in RF MEMS Capacitive Switches and Varactors”. In: *Microelectromechanical Systems, Journal of* 21.2 (2012), pp. 420–430.

[5] A. Koszewski et al. “Physical model of dielectric charging in MEMS”. In: *Journal of Micromechanics and Microengineering* 23.4 (2013), p. 045019.

[6] D Molinero and L. Castaner. “Comparison of airgap breakdown and substrate injection as mechanisms to induce charging in microelectromechanical switches”. In: *Applied Physics Letters* 92 (2008), p. 43502.

[7] J. Wibbeler, G. Pfeifer, and M. Hietschold. “Parasitic charging of dielectric surfaces in capacitive microelectromechanical systems (MEMS)”. In: *Sensors and Actuators A* 71 (1997), pp. 74–80.

[8] D. Molinero et al. “Dielectric charging characterization in MEMS switches with insulator-insulator contact”. In: *2014 IEEE International Reliability Physics Symposium.* 2014, pp. 5C.3.1–5C.3.4.

[9] R. W. Herfst et al. “Characterization of dielectric charging in RF MEMS capacitive switches”. In: *2006 IEEE International Conference on Microelectronic Test Structures*. 2006, pp. 133–136.

[10] R. Herfst et al. “Center-Shift Method for the Characterization of Dielectric Charging in RF MEMS Capacitive Switches”. In: *IEEE Trans. on Semiconductor Manufacturing* 21 (2008), pp. 148–153.

[11] M. Kouteoureli and G. Papaioannou. “The Discharge Current Through the Dielectric Film in MEMS Capacitive Switches”. In: *Proc. of the 6th European Microwave Integrated Circuits Conf.* 2011, pp. 133–136.

[12] X. Rottenberg et al. “Analytical Model of the DC Actuation of Electrostatic MEMS Devices With Distributed Dielectric Charging and Nonplanar Electrodes”. In: *IEEE JMEMS* 16 (2007), pp. 1243–1253.

[13] J. C. M. Hwang and C. L. Goldsmith. “Reliability of MEMS capacitive switches”. In: *2013 IEEE International Wireless Symposium (IWS)*. 2013, pp. 1–4.

[14] X. Yuan et al. “Modeling and Characterization of Dielectric-Charging Effects in RF MEMS Capacitive Switches”. In: *Digest of IEEE MTT-S 2005 Microwave Symposium Digest*. 2005, pp. 753–756.

[15] R. Herfst, P. Steeneken, and J. Schmitz. “Time and voltage dependence of dielectric charging in RF MEMS capacitive switches”. In: *IEEE 45th Annual Int. Reliability Physics Symp., Phoenix*. 2007, pp. 417–421.

[16] X. Yuan et al. “A Transient SPICE Model for Dielectric-Charging Effects in RF MEMS Capacitive Switches”. In: *IEEE J ED* 53 (2006), pp. 2640–2648.

[17] X. Yuan et al. “Initial observation and analysis of dielectric-charging effects on RF MEMS capacitive switches”. In: *Digest of 2004 IEEE MTT-S International Microwave Symposium*. 2004, pp. 1943 –1946.

[18] A. Grichener and G. Rebeiz. “Effects of dielectric charging on fundamental forces and reliability in capacitive microelectromechanical systems radio frequency switch contacts”. In: *IEEE JMTT* 58 (2010), pp. 2692–2701.

[19] M. Matmat et al. “Life expectancy and characterization of capacitive RF MEMS switches”. In: *Microelectronics Reliability* 50 (2010), pp. 1692–1696.

[20] S. Zafar et al. “Charge trapping in high k gate dielectric stacks”. In: *Digest of International Electron Devices Meeting (IEDM 2002)*. 2002, pp. 517–520.

[21] U. Zaghloul et al. “Dielectric charging in silicon nitride films for MEMS capacitive switches: Effect of film thickness and deposition conditions”. In: *Microelectronics Reliability* 49 (2009), pp. 1309–1314.

[22] G. Papaioannou et al. “Temperature Study of the Dielectric Polarization Effects of Capacitive RF MEMS Switches”. In: *IEEE JMTT* 53 (2005), pp. 3467–3473.

[23] G. J. Papaioannou et al. “Contactless Dielectric Charging Mechanisms in RF-MEMS Capacitive Switches”. In: *Proc. of The First European Microwave Integrated Circuits Conference*. 2006, pp. 513–516.

[24] A. Koszewski et al. “Modeling of dielectric charging in electrostatic MEMS switches”. In: *Microelectronics Reliability* 50 (2010), pp. 1609–1614.

[25] D. Czaplewski et al. “A soft-landing waveform for actuation of a single-pole single-throw ohmic RF MEMS switch”. In: *IEEE JMEMS* 15 (2006), pp. 1586–1594.

[26] Z. Peng et al. “Superposition Model for Dielectric Charging of RF MEMS Capacitive Switches Under Bipolar Control-Voltage Waveforms”. In: *IEEE JMTT* 55 (2007), pp. 2911–2918.

[27] C. Goldsmith et al. “Lifetime characterization of capacitive RF MEMS switches”. In: *2001 IEEE MTT-S International Microwave Symposium Digest*. Phoenix, AZ, 2001, pp. 227–230.

[28] X. Yuan et al. “Acceleration of Dielectric Charging in RF MEMS Capacitive Switches”. In: *IEEE J DMR* 6 (2006), pp. 556–563.

[29] T. Ikehashi et al. “An RF MEMS Variable Capacitor with Intelligent Bipolar Actuation”. In: *IEEE International Solid-State Circuits Conference (ISSCC 2008)*. Feb 3-7, 2008, pp. 581–583.

[30] G. Rebeiz. *RF MEMS theory, design and technology*. Wiley, 2003.

[31] X. Yuan et al. “A transient SPICE model for dielectric-charging effects in RF MEMS capacitive switches”. In: *IEEE Transactions on Electron Devices* 53.10 (2006), pp. 2640–2648.

[32] Z. Peng et al. “Dielectric Charging of RF MEMS Capacitive Switches under Bipolar Control-Voltage Waveforms”. In: *IEEE/MTT-S International Microwave Symposium*. 2007, pp. 1943 –1946.

[33] W. Spengen. "Capacitive RF MEMS switch dielectric charging and reliability: a critical review with recommendations". In: *Journal of Micromechanics and Microengineering* 22 (2012).

[34] X. Rottenberg et al. "Distributed dielectric charging and its impact on RF MEMS devices". In: *34th European Microwave Conference, 2004*. Vol. 1. 2004, pp. 77–80.

[35] R. W. Herfst et al. "Kelvin probe study of laterally inhomogeneous dielectric charging and charge diffusion in RF MEMS capacitive switches". In: *2008 IEEE International Reliability Physics Symposium*. 2008, pp. 492–495.

[36] Z. Olszewski, R. Duane, and C. O'Mahony. "Effect of environment humidity on the C-V characteristics of RF MEMS capacitive switch". In: *9th Int. Symp. on RF MEMS and Microsystems (MEMSWAVE)*. 2008.

[37] B. Lacroix et al. "Sub-Microsecond RF MEMS Switched Capacitors". In: *IEEE Transactions on Microwave Theory and Techniques* 55.6 (2007), pp. 1314–1321.

[38] C. Goldsmith et al. "Understanding and improving longevity in RF MEMS capacitive switches". In: *Reliability, Packaging, Testing, and Characterization of MEMS/MOEMS VII*. Vol. 6884. 2008, p. 688403.

[39] P. Blondy et al. "Dielectric less capacitive MEMS switches". In: *2004 IEEE MTT-S International Microwave Symposium Digest*. Vol. 2. 2004, 573–576 Vol.2.

[40] D. Mardivirin et al. "Study of Residual charing in dielectric less capacitive MEMS switches". In: *2008 IEEE MTT-S International Microwave Symposium Digest*. 2008, pp. 33–36.

[41] D. Mardivirin et al. "Charging in Dielectricless Capacitive RF-MEMS Switches". In: *IEEE Transactions on Microwave Theory and Techniques* 57.1 (2009), pp. 231–236.

[42] W. M. van Spengen et al. "The MEMSamp: using (RF-)MEMS switches for the micromechanical amplification of electronic signals". In: *Journal of Micromechanics and Microengineering* 20.12 (2010.), p. 125011.

[43] E. Blokhina et al. "Dielectric charge control in electrostatic MEMS positioners / varactors". In: *IEEE JMEMS* 21 (2012), pp. 559–573.

[44] S. Gorreta et al. "Delta-Sigma Control of Dielectric Charge for Contactless Capacitive MEMS". In: *Microelectromechanical Systems, Journal of* 23.4 (2014), pp. 829–841.

[45] S. Gorreta et al. "Characterization method of the dynamics of the trapped charge in contactless capacitive MEMS". In: *2014 Symposium on Design, Test, Integration and Packaging of MEMS/MOEMS (DTIP)*. 2014, pp. 1–6.

[46] S. Gorreta, J. Pons-Nin, and M. Dominguez-Pumar. "Simultaneous Control of Dielectric Charge and Device Capacitance in Electrostatic MEMS". In: *Journal of Microelectromechanical Systems* 24.6 (2015), pp. 1684–1686.

[47] H. Yamazaki et al. "An intelligent bipolar actuation method with high stiction immunity for RF MEMS capacitive switches and variable capacitors". In: *Sensors and Acuators A* (2007), pp. 233–236.

[48] T. Miyazaki. "Semiconductor device and method of controlling electrostatic actuator". Patent US 20090072630. Mar. 2009.

[49] M. Dominguez et al. "Dielectric charging control for electrostatic MEMS switches". In: *Proc. of SPIE Conf. DSS-2010*. Vol. 7679, pp. 1-11. Orlando, 2010.

[50] G. Ding et al. "Intelligent Bipolar Control of MEMS Capacitive Switches". In: *IEEE Transactions on Microwave Theory and Techniques* 61.1 (2013), pp. 464–471.

[51] S. R. Norsworthy, R. Schreier, G. C. Temes, et al. *Delta-sigma data converters: theory, design, and simulation*. Vol. 97. IEEE press New York, 1996.

[52] M. Dominguez et al. "A hot film anemometer for the Martian atmosphere". In: *Planetary and Space Science* 56 (2008), pp. 1169–1179.

[53] E. Blokhina et al. "Control of MEMS vibration modes with pulsed digital oscillators: Part I — Theory". In: *Circuits and Systems I: Regular Papers, IEEE Trans. on* 57.8 (2010), pp. 1865–1878.

[54] J. Ricart et al. "Control of MEMS Vibration Modes With Pulsed Digital Oscillators; Part II: Simulation and Experimental Results". In: *IEEE Transactions on Circuits and Systems I: Regular Papers* 57.8 (2010), pp. 1879–1890.

[55] M. Dominguez et al. “Real-Time Characterization of Dielectric Charging in Contactless Capacitive MEMS”. In: *In Press in Analog Integrated Circuits and Signal Processing* (2014).

[56] S. Gorreta et al. “A Second-Order Delta-Sigma Control of Dielectric Charge for Contactless Capacitive MEMS”. In: *Journal of Microelectromechanical Systems* 24.2 (2015), pp. 259–261.

[57] K. Makinwa and J. Huijsing. “A 2nd order thermal sigma-delta modulator for flow sensing”. In: *IEEE Sensors 2005*. Oct, 2005.

[58] H. Shea. “MEMS for pico- to micro-satellites”. In: *Moems And Miniaturized Systems Viii*. Vol. 7208. Invited paper. San Jose, CA, USA, 2009.

[59] R. Osiander, M. Garrison-Darrin, and J. Champion. *MEMS and Microstructures in Aerospace Applications*. CRC Press, 2005.

[60] T. George. “Overview of MEMS/NEMS technology development for space applications at NASA/JPL”. In: vol. 5116. 2003, pp. 136–148.

[61] H. R. Shea. “Radiation sensitivity of microelectromechanical system devices”. In: *Journal of Micro/Nanolithography, MEMS and MOEMS* 8.3 (2009), pp. 031303–031303–11.

[62] H. R. Shea. “Effects of Radiation on MEMS”. In: *Proc. of SPIE Reliability, Packaging, Testing, and Characterization of MEMS/MOEMS and Nanodevices X*. Vol. 7928. 2011, p. 13.

[63] A. R. Knudson et al. “The effects of radiation on MEMS accelerometers”. In: *IEEE Transactions on Nuclear Science* 43.6 (1996), pp. 3122–3126.

[64] T. Fujimori and M. Watanabe. “Radiation tolerance of a MEMS mirror device”. In: *2016 International Conference on Optical MEMS and Nanophotonics (OMN)*. 2016, pp. 1–2.

[65] T. F. Miyahira et al. “Total dose degradation of MEMS optical mirrors”. In: *IEEE Transactions on Nuclear Science* 50.6 (2003), pp. 1860–1866.

[66] A. Tazzoli et al. “Accelerated testing of RF-MEMS contact degradation through radiation sources”. In: *2010 IEEE International Reliability Physics Symposium*. 2010, pp. 246–251.

[67] S. T. Patton et al. “Effect of Space Radiation on the Leakage Current of MEMS Insulators”. In: *IEEE Transactions on Nuclear Science* 60.4 (2013), pp. 3074–3083.

[68] A. Tazzoli et al. “Radiation Sensitivity of Ohmic RF-MEMS Switches for Spatial Applications”. In: *2009 IEEE 22nd International Conference on Micro Electro Mechanical Systems*. 2009, pp. 634–637.

[69] S. S. McClure et al. “Radiation effects in micro-electromechanical systems (MEMS): RF relays”. In: *IEEE Transactions on Nuclear Science* 49.6 (2002), pp. 3197–3202.

[70] A. Crunteanu et al. “Gamma radiation effects on RF MEMS capacitive switches”. In: *Microelectronics Reliability* 46.9 (2006), pp. 1741 –1746.

[71] M. Dominguez-Pumar et al. “Closed-Loop Compensation of Dielectric Charge Induced by Ionizing Radiation”. In: *Journal of Microelectromechanical Systems* 24.3 (2015), pp. 534–536.

[72] M. Dominguez-Pumar et al. “Charge induced by ionizing radiation understood as a disturbance in a sliding mode control of dielectric charge”. In: *Microelectronics Reliability* 55.9 (2015), pp. 1926–1931.

Chapter 3

Compendium publications

This chapter describes the most important part of the research work carried out during the Thesis, in the form of a compendium of publications. For the sake of readability, abstracts and links to the first page of each publication are included first and then the complete publications.

Attention¡¡
For copyright reasons, pages 79 to 144 of the thesis, containing the texts mentioned here by, should be consulted on the web pages of the respective publishers

Published:

1. **Dielectric Charge Control in Electrostatic MEMS Positioners / Varactors** on page 79.

   Abstract—A new dynamical closed-loop method is proposed to control dielectric charging in capacitive MEMS positioners/varactors for enhanced reliability and robustness. Instead of adjusting the magnitude of the control voltage to compensate the drift caused by the dielectric charge, the method uses a feedback loop to maintain it at a desired level: the device capacitance is periodically sampled and bipolar pulses of constant magnitude are applied. Specific models describing the dynamics of charge and a control map are introduced. Validation of the proposed method is accomplished both through discrete-time simulations and with experiments using MEMS devices that suffer from dielectric charging.

   Published in *IEEE - Journal of Microelectromechanical Systems*, vol. 21, no. 3, pp. 559–573, Jun. 2012.

   http://ieeexplore.ieee.org/abstract/document/6146450/

2. **Characterization method of the dynamics of the trapped charge in contactless capacitive MEMS** on page 95.

Abstract—Dielectric charging of insulating films in microelectromechanical systems (MEMS) has a crucial effect on the operation of those devices. A new method is been presented in order to characterize the dynamics of the charge trapped in the dielectric layer of MEMS devices. This allows knowing the state of the charge at each sampling time without distorting the measurement. This approach allows to model the expected behaviour of the trapped charge inside the dielectric as a response to a sigma-delta control of charge. The goodness of the proposed approach is obtained by matching the experimentally obtained closed loop response with the one predicted by the model obtained using the proposed characterization method.

Published in *Design, Test, Integration and Packaging of MEMS/MOEMS, Symposium on*, Apr. 2014.

http://ieeexplore.ieee.org/document/7056667/

3. **Delta-Sigma Control of Dielectric Charge for Contactless Capacitive MEMS** on page 101.

Abstract—In this paper, we present a new closed-loop control method of dielectric charge for contactless capacitive microelectromechanical systems (MEMS). The method uses a feedback loop to maintain the net charge in the dielectric layer at the desired level. We show that, under particular conditions, the control loop is similar to a thermal sigma-delta modulator as used in thermal sensors. In this way, the control actuation will inject an average charge into the dielectric to keep it at a desired level while applying an actuation bit stream to compensate the charge being continuously leaked out of the dielectric. The validation of the method is carried out employing numerical simulation and experimental measurements of Poly MUMPS devices.

Published in *IEEE - Journal of Microelectromechanical Systems*, vol. 23, no. 4, pp. 829–841, Aug. 2014.

http://ieeexplore.ieee.org/document/6710146/

4. **Real-Time Characterization of Dielectric Charging in Contactless Capacitive MEMS** on page 115.

Abstract—This paper presents a new method to characterize the dynamics of the charge trapped in the dielectric layer of contactless microelectromechanical systems (MEMS). For sampled-time systems, this allows knowing the state of the net charge at each sampling time without distorting the measurement. This approach allows one to model the expected behaviour of dielectric charging as a response to a sigma−delta control of charge. The goodness of the proposed approach is obtained by matching the experimentally obtained closed loop response with the one predicted using the proposed characterization method. The characterization method also provides a criterion to avoid nonlinear effects, such as fractal-like behaviour, in charge control

Published in *Journal of Analog Integrated Circuits and Signal Processing*, vol. 23, pp. 829–841, Nov. 2014.

https://link.springer.com/article/10.1007/s10470-014-0458-y

5. **A Second Order Delta-Sigma Control of Dielectric Charge for Contactless Capacitive MEMS** on page 127.

Abstract—This letter introduces a new second-order delta-sigma method for control of the dielectric charge in contactless capacitive MEMS. This method improves one previously proposed by the authors, providing second- order quantization noise shaping and allowing to avoid the plateaus typical of first-order strategies. The feasibility and the features of the new method are demonstrated both experimentally and through simulations.

Published in *IEEE - Journal of Microelectromechanical Systems*, vol. 24, no. 2, pp. 259–261, Apr. 2015.

http://ieeexplore.ieee.org/document/7050235/

6. **Closed-loop compensation of dielectric charge induced by ionizing radiation** on page 131.

Abstract—This work investigates the capability of dielectric charge control loops to cope with charge induced by ionizing radiation. To this effect, a MEMS variable capacitor has been irradiated with X-Rays and Gamma- radiation in three scenarios: without polarization, using an open-loop di- electric charge mitigation strategy and using a closed-loop control method. The results show that charge effects induced by radiation can be partially compensated using dielectric charge control.

Published in *IEEE - Journal of Microelectromechanical Systems*, vol. 24, no. 3, pp. 534–536, May 2015.

http://ieeexplore.ieee.org/document/7109101/

7. **Charge Induced by Ionizing Radiation Understood as a Disturbance in a Sliding Mode Control of Dielectric Charge** on page 135.

Abstract—The purpose of this paper is to show that the charge induced by radiation in a dielectric on which a sigma-delta control of dielectric charge is implemented, can be seen as a disturbance in a sliding mode controller. Preliminary experimental results are presented in which a MEMS device is irradiated with X-rays, while the dielectric charge control is continuously being monitored. The charge induced by radiation generates a change in the control bitstream, which is associated to the presence of an external disturbance on the governing control equations.

Published in *Elsevier - Microelectronics Reliability*, vol. 55, pp. 1926–1931, Jul. 2015.

http://www.sciencedirect.com/science/article/pii/S0026271415001766

8. **Simultaneous control of dielectric charge and device capacitance in electrostatic MEMS** on page 141.

Abstract—This work presents a double closed-loop for controlling simultaneously the net dielectric charge and the device capacitance in contactless electrostatic MEMS devices. The first loop controls the net charge trapped in the dielectric layer by continuously monitoring the horizontal displacement of the C-V characteristic and applying bipolar actuation voltages to keep such net charge at the target value. The second loop adapts the actuation voltages so that the measured capacitance matches a desired value, while maintaining the primary control of charge.

Published in *IEEE - Journal of Microelectromechanical Systems*, vol. 24, no. 6, pp. 1684–1686, Dec. 2015.

http://ieeexplore.ieee.org/abstract/document/7312878/

Chapter 4

Conclusions and future work

4.1 Conclusions

During the last years microelectromechanical systems have become a really extended technology in the microelectronics area, improving the properties of commercial devices made with more mature technologies and allowing new applications. Although MEMS is today a key technology for the mobile and connected world, commercialization efforts still encounter multiple reliability issues, delaying the availability of such devices in some specific markets. In many applications, the most significant problem which hinders the use of electrostatic MEMS is the charging trapping phenomena, which has been the framework of this Thesis. Regarding this, the ultimate goal of this Thesis was to propose and demonstrate new techniques to control dielectric charging for electrostatic MEMS. In order to achieve this challenge, several intermediate steps have been performed, which can be summarized as follows:

- A new method for charge detection has been proposed. In contrast with the methods present in the literature, its main advantage is the use of specific voltage waveforms which allow to continuously monitor the net dielectric charge. Furthermore, this has been thought to be applied in electrostatic MEMS working in the contactless state and then, it does not need to close the device to make charge measurements.

- The voltage waveforms commented above also allowed to obtain dynamical models to characterize the dielectric charge evolution under different bias voltages. The charge dynamics has been modelled by applying an approach

based on state-variables analysis. As a main contribution in this regard, all the voltages applied in the waveforms are taken into account to build the model. In contrast, in the methods found in the literature the charge status is usually being distorted each time it is measured.

- Three closed-loop control methods have been proposed. The first one was an initial approach to the following solutions, which implement sigma-delta modulations. The first control was demonstrated to be a good approach to improve the lifetime of the device. However, some second order charge effects were not contemplated in this version and thus it was not able to ensure long term stabilization. In order to face these not initially contemplated issues, two further charge control methods were proposed. These are the first and second order sigma-delta controls, which solved the previous problems and provided a complete control of the net charge trapped in the dielectric layer. The first-order sigma-delta control was patented.

- An evolution of the first-order sigma-delta control in which the device capacitance is also controlled has been proposed and demonstrated. This new method was focused on solving dielectric charging issues in those applications in which the device capacitance needs to be well controlled. This could be the case of microphone MEMS, positioners, varactors, etc.

- As a further challenge of this Thesis, both sigma-delta charge controls and the one which includes capacitance control have been successfully tested under ionizing radiation. The aim of these experiments was to prove that not only charge injected by device polarization but also that induced by ionizing radiation can be compensated. Some of these experiments were carried out at the ESA-ESTEC ^{60}Co facility.

As a result of this Thesis, 17 contributions have been sent for publication: 10 to top ranked peer reviewed journals and 7 to international conferences in the MEMS area. On the other hand, an international patent was filed with the first-order sigma-delta charge control. Finally, a book chapter was also written.

4.2 Future work

The contributions of this Thesis can be seen as first steps towards the realization of different charge control techniques which could be applied to many MEMS-

related applications but also to other devices. Concerning MEMS devices:

- Extend the dielectric charge study to obtain suitable strategies for those MEMS working in the switching regime. This implies modelling the charge dynamics and designing charge controls for MEMS working also in the ON-closed state.

- Modify some aspects of the proposed charge controls such as avoiding bias voltage switching, in order to make them compatible with the normal operation of some applications. This could be the case of microphones MEMS or RF-MEMS, in which bias switching can generate glitches in the sensing signal.

In other applications:

- Application to other devices suffering from dielectric charge related effects, such as MOS structures, Two-dimensional materials and devices (i.e. h-BN) or organic FETs.

- Increase the complexity degree, and thus the applicability to other fields, of the dynamical analysis and the resulting control strategies, including extended state observers and higher order sliding mode controls.

Appendices

Appendix A

Other Thesis-related journal publications

This appendix summarizes the journal papers related to the main subject of this Thesis which have not been included in the compendium of publications.

Works:

1. **Sliding mode analysis of the dynamics of sigma-delta Controls of dielectric charging.** on page 153.

   Published in *IEEE - Transactions on industrial electronics*, vol. 63, no. 4, pp. 2320-2329, Apr. 2016.

2. **$\Sigma - \Delta$ effects and charge locking in capacitive MEMS under di- electric charge control.** on page 163.

   Published in *IEEE - Transactions on circuits and systems II: Express Briefs*, vol. 64, no. 2, pp. 206-210, Feb. 2017.

3. **Characterization of dielectric charging in MEMS using diffusive representation.** on page 169.

   Published in *IEEE - Transactions on industrial electronics*, vol. 64, no. 2, pp. 1529-1533, Feb. 2017.

Attention¡¡

For copyright reasons, pages 152 to 174 of the thesis,
containing the texts mentioned above,
should be consulted at the editor's web

http://ieeexplore.ieee.org/document/7360169/
http://ieeexplore.ieee.org/document/7465779/
http://ieeexplore.ieee.org/document/7574316/

Appendix B

Thesis-related patents

This appendix contains the patent related to the first-order sigma-delta control for dielectric charge presented in previous sections.

(12) INTERNATIONAL APPLICATION PUBLISHED UNDER THE PATENT COOPERATION TREATY (PCT)

(19) World Intellectual Property Organization
International Bureau

(43) International Publication Date
11 June 2015 (11.06.2015)

(10) International Publication Number
WO 2015/082377 A1

(51) International Patent Classification:
B81B 7/00 (2006.01) *B81C 99/00* (2010.01)

(21) International Application Number:
PCT/EP2014/076052

(22) International Filing Date:
1 December 2014 (01.12.2014)

(25) Filing Language: English

(26) Publication Language: English

(30) Priority Data:
1321277.4 3 December 2013 (03.12.2013) GB

(71) Applicants: **UNIVERSITY COLLEGE DUBLIN NATIONAL UNIVERSITY OF IRELAND, DUBLIN** [IE/IE]; Belfield, Belfield, Dublin, 4 (IE). **UNIVERSITAT POLITÈCNICA DE CATALUNYA** [ES/ES]; Calle Jordi Girona, 31, E-08034 Barcelona (ES).

(72) Inventors: **DOMINGUEZ-PUMAR, Manuel**; Comandant Benitez 27, 4° 2ª, E-08028 Barcelona (ES). **GORRETA, Sergi**; Gran Via 102, 4° 3ª, E-08330 Premia de Mar (ES). **PONS-NIN, Joan**; Mar 25, E-43820 Calafell (ES). **FEELY, Orla**; 34 Farney Park, Sandymount, Dublin, 4 (IE). **BLOKHINA, Elena**; 30 Ailesbury Mews, Sandymount, Dublin 4 (IE). **O'CONNELL, Diarmuid**; 2 Chanterlands, Athy, Co. Kildare (IE).

(74) Agents: **BOYCE, Conor** et al.; Hanna, Moore & Curley, 13 Lower Lad Lane, Dublin, 2 (IE).

(81) Designated States *(unless otherwise indicated, for every kind of national protection available)*: AE, AG, AL, AM, AO, AT, AU, AZ, BA, BB, BG, BH, BN, BR, BW, BY, BZ, CA, CH, CL, CN, CO, CR, CU, CZ, DE, DK, DM, DO, DZ, EC, EE, EG, ES, FI, GB, GD, GE, GH, GM, GT, HN, HR, HU, ID, IL, IN, IR, IS, JP, KE, KG, KN, KP, KR, KZ, LA, LC, LK, LR, LS, LU, LY, MA, MD, ME, MG, MK, MN, MW, MX, MY, MZ, NA, NG, NI, NO, NZ, OM, PA, PE, PG, PH, PL, PT, QA, RO, RS, RU, RW, SA, SC, SD, SE, SG, SK, SL, SM, ST, SV, SY, TH, TJ, TM, TN, TR, TT, TZ, UA, UG, US, UZ, VC, VN, ZA, ZM, ZW.

(84) Designated States *(unless otherwise indicated, for every kind of regional protection available)*: ARIPO (BW, GH, GM, KE, LR, LS, MW, MZ, NA, RW, SD, SL, ST, SZ, TZ, UG, ZM, ZW), Eurasian (AM, AZ, BY, KG, KZ, RU, TJ, TM), European (AL, AT, BE, BG, CH, CY, CZ, DE, DK, EE, ES, FI, FR, GB, GR, HR, HU, IE, IS, IT, LT, LU, LV, MC, MK, MT, NL, NO, PL, PT, RO, RS, SE, SI, SK, SM, TR), OAPI (BF, BJ, CF, CG, CI, CM, GA, GN, GQ, GW, KM, ML, MR, NE, SN, TD, TG).

Published:

— *with international search report (Art. 21(3))*

(54) **Title**: A METHOD AND A CONTROLLER FOR A MICRO-ELECTROMECHANICAL SYSTEM (MEMS) DEVICE

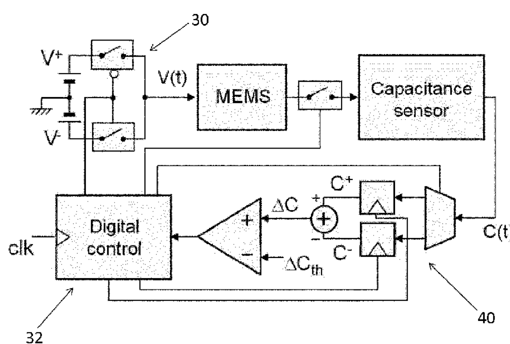

Figure 4

(57) **Abstract**: A controller for a micro-electromechanical system (MEMS) device incorporating a dielectric layer and a voltage supply contact is disclosed. The controller includes a capacitance sensor operatively connected to the MEMS device to selectively measure a capacitance of the MEMS device. An actuation controller is interposed in a feedback loop between the capacitance sensor and the device voltage supply, the actuation controller being arranged to successively select between one of two voltage waveforms during actuation of the MEMS device. A first of the waveforms comprises a voltage of a given polarity to be applied for a majority of the waveform time and a voltage of an opposite polarity to be applied for a minority of the waveform time. A second of the waveforms comprises the voltage of the opposite polarity for the majority of the waveform time and the voltage of the given polarity for the minority of the waveform time. The actuation controller is arranged to measure the capacitance during the waveform time before and after a transition between the given and the opposite polarity and to select a succeeding waveform by comparing a difference ΔC in measured capacitances C+ and C- and a threshold capacitance Cth corresponding to desired device charge.

WO 2015/082377 A1

WO 2015/082377 PCT/EP2014/076052

A method and a controller for a micro-electromechanical system (MEMS) device

Field of the Invention

5 The present invention relates to a method and a controller for a micro-electromechanical system (MEMS) device.

Background

10 Figure 1 shows a typical MEMS device comprising a parallel plate capacitor, where a voltage difference V is applied across the device to move a plate electrode relative to a fixed plate electrode. The device comprises a dielectric layer, in this case formed on the fixed plate that prevents short-circuiting between the electrodes when the device is actuated to close.

15

A variety of such micro-electromechanical systems (MEMS) including oscillators, variable capacitors (varactors) and switches are actuated electrostatically. Despite a number of advantages, this actuation technique may lead to the accumulation of charge in the dielectric layer. (It is thought that two processes primarily contribute to 20 external charge injection: trap-assisted tunnelling (TAT) and Schottky emission from the conductor directly into the dielectric.) Charge accumulation is known to be a major problem for the use of such devices in a large set of applications, since the charge trapped in the dielectric layer causes a number of reliability issues. For instance, effects such as: shift of the C-V (capacitance-voltage) characteristic, 25 explained in more detail below; permanent stiction of movable mechanical parts to actuation electrodes in varactors and RF switches; or changes of the resonant frequency in oscillators can be induced by trapped/accumulated charge.

It will be appreciated that the electrostatic force generated on the moveable plate is 30 proportional to the square of the magnitude of the applied voltage V, and so is polarity independent. Thus, the MEMS device of the type shown in Figure 1 can be actuated to close with a voltage of a given magnitude whether positive or negative.

It is known that the application of bias voltages of opposite polarities has opposite effects on charge injection/depletion into/from the dielectric: for instance, negative charges trapped in the dielectric can be removed by applying negative voltages or injected by applying positive voltages. According to this principle, several open-loop bipolar actuation methods have been proposed in order to mitigate the effects of dielectric charging, for example, as disclosed in G. Rebeiz, RF MEMS theory, design and technology. Wiley, 2003; and Z. Peng, X. Yuan, J. Hwang, D. Forehand, and C. Goldsmith, “Dielectric charging of RF MEMS capacitive switches under bipolar control-voltage waveforms,” in IEEE/MTT-S International Microwave Symposium, June 3-8 2007, pp. 1943 – 1946. However, the effect of bipolar voltages on the charge dynamics is not symmetrical and strongly depends on the device structure and material used during the fabrication process as disclosed in U. Zaghloul, G. Papaioannou, F. Coccetti, P. Pons, and R. Plana, “Dielectric charging in silicon nitride films for MEMS capacitive switches: Effect of film thickness and deposition conditions,” Microelectronics Reliability, vol. 49, pp. 1309–1314, 2009.

As a consequence, open-loop control methods based on bipolar actuation are not effective in the long term, since they may not adapt to the drift in the characteristics of the materials involved or even in the environmental variables such as temperature, humidity etc. such as disclosed in R. Herfst, P. Steeneken, and J. Schmitz, “Time and voltage dependence of dielectric charging in RF MEMS capacitive switches,” in IEEE 45th Annual International Reliability Physics Symposium, Phoenix, 2007, pp. 417–421. This means that some amount of charge will still be accumulating and generating drifts in the device response.

Within this context, closed-loop control methods arise as one of the most promising ways to reduce the long-term effects of dielectric charging, as disclosed in T. Ikehashi, T. Miyazaki, H. Yamazaki, A. Suzuki, E. Ogawa, S. Miyano, T. Saito, T. Ohguro, T. Miyagi, Y. Sugizaki, N. Otsuka, H. Shibata, and Y. Toyoshima, “An RF MEMS variable capacitor with intelligent bipolar actuation,” in IEEE International Solid-State Circuits Conference (ISSCC 2008), Feb 3-7, 2008, pp. 581–583.

M. Dominguez, D. Lopez, D. Molinero, and J. Pons, “Dielectric charging control for electrostatic mems switches,” in Proc. of SPIE Conf. on Defense, Security and

Sensing DSS-2010, vol. 7679, pp. 1-11, Orlando, 2010; E. Blokhina, S. Gorreta, D. Lopez, D. Molinero, O. Feely, J. Pons-Nin, and M. Dominguez, “Dielectric charge control in electrostatic MEMS positioners / varactors,” IEEE JMEMS, vol. 21, pp. 559–573, 2012; and P. Giounanlis, E. Blokhina, O. Feely, M. Domínguez, J. Pons-Nin, and S. Gorreta, “Modelling of a charge control method for capacitive MEMS” in 21st European Conf. on Circuit Theory and Design, Dresden also disclose closed loop methods to control dielectric charging based on sensing the capacitance of the device that is linked to the amount of charge in the dielectric. Although these methods have shown good control of the charge of the devices under test, it has been observed that these methods do not withstand vertical shifts in the C-V curve due to creep or other variations in the environmental variables.

Summary of the invention

According to the present invention there is provided a controller for a micro-electromechanical system (MEMS) device incorporating a dielectric layer and a voltage supply contact, said controller including a capacitance sensor operatively connected to said MEMS device to selectively measure a capacitance of said MEMS device, an actuation controller interposed in a feedback loop between said capacitance sensor and said device voltage supply, said actuation controller being arranged to successively select between one of two voltage waveforms during actuation of said MEMS device, a first of said waveforms comprising a voltage of a given polarity to be applied for a majority of said waveform time and a voltage of an opposite polarity to be applied for a minority of said waveform time, and a second of said waveforms comprising the voltage of the opposite polarity for the majority of said waveform time and the voltage of the given polarity for the minority of the waveform time, the actuation controller being arranged to measure said capacitance during said waveform time before and after a transition between the given and the opposite polarity and to select a succeeding waveform by comparing a difference in measurements of capacitance and a threshold corresponding to desired device charge.

Using the present invention, the controller controls device supply to maintain net charge in the dielectric layer at a desired level. A ”quasi-differential” value of the

device capacitance is periodically sampled and, depending on whether it is above or below a threshold value, generally positive or generally negative polarity actuation waveforms are applied. That is, the amount of dielectric charge is fixed to a desired level by dynamically adjusting a stream of positive and negative voltage waveforms
5 applied to the device.

Embodiments of the invention can include devices whose C-V characteristic could otherwise suffer from horizontal displacement due to charging. This controller is also robust against drifts due to effects such as vertical shifts in the C-V curve resulting
10 from creep or other variations in the environmental variables, thereby improving the reliability of the device.

Using the present invention, device charge can be kept almost constant once a stable regime is achieved.

15

In some embodiments, a bit stream at the output of the controller indicating the successive selection of waveforms may be used to analyse whether the device has reached a stable regime of dielectric charge.

20 Furthermore, there is no minimum amount of charge below which the embodiments do not provide closed loop control.

Brief Description of the Drawings

25 Embodiments of the invention will now be described by way of example with reference to the accompanying drawings, in which:

Figure 1 shows a typical MEMS device;

Figure 2 illustrates a fragment of the C-V characteristics of a typical MEMS device where plot (a) corresponds to the discharged device (V_{sh} = 0, C_0 =6.356pF), and plot
30 (b) corresponds to the charged case reached when V = 4V is applied for 30 minutes (V_{sh} = -1.6V , C_0 = 6.366pF).

Figure 3 shows bipolar voltage symbols used to actuate a MEMS device according to an embodiment of the present invention;

Figure 4 is a schematic diagram of a digital control system for a MEMS device according to an embodiment of the invention;
Figure 5 illustrates a MEMS control method according to an embodiment of the present invention;
5 Figure 6 illustrates the effect of the control of Figure 5 on the C-V characteristics of a MEMS device;
Figure 7 illustrates a delta-sigma type implementation of the present invention;
Figure 8 illustrates a still further implementation of the present invention;
Figure 9 is a timing diagram illustrating the MEMS control method according to the
10 present invention when used in a single throw, double pole switch;
Figure 10 illustrates up-state control loops in a further implementation of the present invention;
Figure 11 shows a block diagram of a prior art MEMS resonator; and
Figure 12 shows a block diagram of a MEMS resonator according to an embodiment
15 of the present invention.

Description of the Preferred Embodiment

Referring back to Figure 1 for the purposes of the following discussion, we assume
20 that a charge density σ_d is uniformly distributed on the top surface of the dielectric layer, and thus the total amount of charge trapped in the dielectric, or the net charge, is *Qd* = $A\sigma_d$, where *A* is the area of the device. Then, a simple expression of the electrostatic force between the plates is:

$$F_{el}(t) = \frac{C(t)^2}{2A\varepsilon_0}\left(V - \frac{Q_d}{C_d}\right)^2 \qquad (1)$$

25 where *C(t)* is the total MEMS capacitance as a function of time, ε_0 the air permittivity and *Cd* = $A\varepsilon_0\varepsilon_d/d$ the dielectric capacitance, with ε_d its relative dielectric constant.

Taking into account that the term *Qd/Cd* may be seen as a voltage shift with regard to how the electrostatic force depends on the applied voltage, we further define V_{sh} =
30 *Qd/Cd*. As indicated above, this means that the electrostatic force F_{el} is proportional to the square of an “effective” voltage ($V-V_{sh}$). Then the capacitance-voltage (C-V) characteristic of the device is an even function centred on V =V_{sh}, and the value of

WO 2015/082377 PCT/EP2014/076052

the net charge *Qd* can be inferred from the horizontal shift of the C-V curve of the device.

Since the electrostatic attraction force in the device of Figure 1 is proportional to $(V - V_{sh})^2$, the C-V curve can be approximated by a parabola for voltage values below pull-in, i.e., for relatively small displacements of the device. Accordingly, the expression of the capacitance for the state below pull-in can take the following form:

$$C(V,t) = \alpha(V - V_{sh}(t))^2 + C_0 \qquad (2)$$

for some parameters α and C_0. However, as it has been mentioned above, the C-V curve may suffer from vertical displacements and therefore the constant term may have a slow time dependence, $C_0(t)$, that will account for the influence of certain parameters such as creep, temperature and other variables.

For example, Figure 2 shows the bottom section of the C-V curve of a typical MEMS device, before and after a voltage of 4V is applied for 30 minutes. As can be observed both V_{sh} and C_0 have noticeable variations, but both curves can still be fitted with the same value of α. In Figure 2, squares denote experimental data and dashed lines are the fits obtained with parabola according to the expression (2) where $\alpha = 1.4fF/V^2$;

Now let us suppose that the device is actuated with two voltage values, $V^+ > 0$ and $V^- < 0$. We can define $C^+(t)$ and $C^-(t)$ as the capacitance values measured when respectively applying V^+ and V^- in equation (2). Since the time constants involved in the dielectric charge dynamics can have large values, typically in the range of minutes or hours, we can assume that the C-V curve remains unchanged for time lapses Δt which are small when compared to those dynamical constants, that is

$V_{sh}(t) \approx V_{sh}(t + \Delta t)$ and $C_0(t) \approx C_0(t + \Delta t)$. We now define a “quasi-differential” capacitance magnitude $\Delta C(t)$ as follows:

$$\begin{aligned} \Delta C(t) = C^+(t) - C^-(t \pm \Delta t) = \\ C(V^+,t) - C(V^-, t \pm \Delta t) = \\ \alpha[(V^+)^2 - (V^-)^2] - 2\alpha V_{sh}(t)[V^+ - V^-] \end{aligned} \qquad (3)$$

Under the above assumptions, namely that $C_0(t)$ and $V_{sh}(t)$ change slowly with time, compared with the time between two consecutive measurements, we have that $\Delta C(t)$ is fairly independent of $C_0(t)$.

5 Let us note that formula (3) expresses that ΔC is a monotonic function of V_{sh}.

However, this is the case not only for C(V) dependencies expressed by nearly-parabolic functions. First of all, functions $C(V^+ - Vsh)$ and $C(V^- - Vsh)$ can be written as Taylor expansions, and therefore,

$$\Delta C = C(V^+) - C(V^-) + \\ + \sum_n (-1)^n \frac{V_{sh}^n}{n!} \left(\frac{d^n C(V^+)}{dV^n} - \frac{d^n C(V^-)}{dV^n} \right) \quad (4)$$

10 We consider the case when $V^+ = -V^-$. For the C-V characteristics that are symmetrical in the absence of dielectric charge, all odd-order derivatives are odd functions, and all even-order derivatives are even functions. Thus,

$$\Delta C = -2 \sum_{n=2k+1} \frac{V_{sh}^n}{n!} \frac{d^n C(V^+)}{dV^n} \quad (5)$$

On the condition that all derivatives $\frac{d^{2k+1}C(V^+)}{dV^{2k+1}}$ have the same sign, equation (5)

15 indicates that ΔC is a monotonic function of Vsh. For the particular case when Vsh/V^+ is small, eq. (5) simplifies as:

$$\Delta C = -2V_{sh} \frac{dC(V^+)}{dV} \quad (6)$$

and one can see that in the case $C = \alpha V^2/2$, equation (4) turns into equation (3). In general, equation (5) expresses the monotonic dependence of ΔC on Vsh for all

20 absolutely monotonic C(V) functions, and for a number of C(V) functions that are not necessary absolutely monotonic.

While equation (5) describes a more general case, the C-V curve of a contactless electrostatic MEMS can be very accurately approximated by a parabolic function.

25 Therefore, we will continue using expression (3) from here on as an example. Although this is not a general rule, for simplicity and the purposes of the present

specification, we assume that for devices below pull-in, applying positive voltages will shift the C-V curve to the left, whereas for negative voltages the C-V curve shifts to the right.

5 Equation (3) is used to establish the desired actuation parameters of the control system and method of the present invention. The aim of the control applied according to the present invention is to fix the capacitance difference $\Delta C(t)$ around a specified threshold value, ΔC_{th}. In order to accomplish this, the control system and method applies different sequences of positive and negative voltages, V^+ and V^-.
10 Voltages are switched during the sampling period and a quasi-differential capacitance measurement is made at each sampling time.

Figure 3 shows the voltages applied to the MEMS: In Figure 3(a) BIT0 applies a constant voltage V^- for a time $(1-\delta)T_s$, followed by V^+ for a relatively shorter time δT_s;
15 and in Figure 3(b) for BIT1, V^+ is applied during $(1-\delta)$Ts, then V^- for δT_s. For appropriate values of V^+, V^- and δ, applying BIT0 to the device increases the positive charge and reduces the negative charge in the dielectric. Applying BIT1 has opposite effects on the charge components of each sign.

20 Referring now to Figure 4, which illustrates schematically a digital control system for a MEMS device according to an embodiment of the invention. An actuation block 30 controlled by a digital controller 32 applies to the MEMS, synchronous voltage waveforms composed of positive V^+ and negative V^- values, such as shown in Figure 3. A sensing module 40 stores values of C^+ and C^- obtained from a capacitance
25 sensor at the two last clock periods of each symbol and compares its difference with a threshold value Cth, in order to determine the next symbol to apply to the MEMS.

In an experimental implementation, the MEMS device comprises a capacitive switch-like device made with Poly-MUMPS technology that shows evidence of dielectric
30 charging below the pull-in state. The upper moveable electrode is a polysilicon plate held by four suspension arms in “L” over a doped silicon substrate, which is the bottom-fixed electrode. The dielectric layer comprises a silicon nitride layer. The pull-

in voltage is around 12V and the parasitic capacitance associated to tracks and pads is *Cp* = 5.63 pF. An Agilent E4980A precision LCR meter is used both to measure the MEMS capacitance and to apply the bipolar actuation symbols BIT0 and BIT1.

5 In operation, a voltage symbol, BIT0 or BIT1, is applied to the device for n clock periods, therefore Ts = nTclk. For each symbol, the device capacitance is measured at both (n - 1)Tclk and nTclk instants, and a new value of the "quasi-differential" capacitance ΔC is obtained at the end of each symbol. Such value is compared with ΔCth and the next symbol to apply is decided according to the following equation:

$$\text{Next Symbol} = \begin{cases} BIT0 & \text{if } \Delta C > \Delta C_{\text{th}} \\ BIT1 & \text{otherwise} \end{cases} \qquad (7)$$

10

The clock period used in all the experiments is Tclk = 0.5s, a value far below the time constants of the dielectric charge and discharge dynamics for the device.

Figure 5 illustrates this closed-loop control used by the controller 32 to control the

15 net charge in the dielectric as follows:

1) Choose a suitable set of values for V^+, V^- and a threshold value ΔCth which, from equation (3), will lead to a target voltage shift Vsh = Vth and a target net charge Qd = Qtarget.
2) Actuate the device with any of the symbols shown in Figure 3, BIT0 or BIT1.
3) Perform capacitance measurements at symbol times $(1-\delta)$Ts and Ts. Values of C^+ and C^- are obtained and, for δTs far below the time constants of the charge dynamics, obtain ΔC as $C^+ - C^-$. (20)
4) The next symbol to be applied to the device comes from the comparison between ΔC and the threshold ΔCth, according to equation (7).
5) Apply the next symbol and go back to step 3. (25)

Figure 6 shows an example of how the above control works. Here, a target C-V is shown in Figure 6(a), with $V_{th} = Q_{target} = C_d < 0$. Figure 6(b) corresponds to the case *Qd* > *Qtarget*, where the next symbol to apply, BIT1, will shift the C-V to the left, that

is to decrease values of *Qd*. Symmetrically, in Figure 6(c) *Qd* < Qtarget and the next symbol, BIT0, would increase *Qd*.

From the point of view of the net dielectric charge the above method can be seen as an implementation of a delta-sigma modulator as shown in Figure 7. Conventionally, delta-sigma modulator circuits compensate for using a very coarse quantization scheme by oversampling an input signal. Quantization noise is shaped out of the band of interest, in what is called noise shaping. This is accomplished by implementing a feedback of the error signal provided by the coarse quantizer.

In Figure 7, after the completion of a sampling period, on which either a BIT0 or BIT1 has been applied, the resulting net charge is the result of the integral of both leaked and injected charge contributions during the sampling period taking into account the voltages applied, the characteristics of each exponential and the initial value of the charge in each exponential.

After suitable normalization, the stored charge at multiples of the sampling period follows the time evolution of a first-order sigma-delta modulator. Two consecutive measurements made within each sampling period are carried out to provide an indirect measurement Q_n of the net dielectric charge. This is the input fed into the comparator i.e. the difference between the net charge Q_n and a desired target charge value Q_{target}.

This charge control method approaches a net charge value Q_{target}, by applying a series of pulses, bitstream b(k), to compensate the charge being continuously leaked out of the dieletric reservoir.

Analogous to expression (7) above, b(k) the bit produced at the k-th decision instant can be defined as follows:

$$b_k = \begin{cases} -1 & \text{when } BIT0 \text{ is applied at } t \in [kT_s, (k+1)T_s) \\ +1 & \text{when } BIT1 \text{ is applied at } t \in [kT_s, (k+1)T_s) \end{cases}$$

The arrangement illustrated in Figure 7 allows real-time information on the state of the device, from the point of view of dielectric charging, to be extracted directly from the generated digital output b(k).

5 As will be seen from the above, using the present invention, the net dielectric charge in a MEMS device can be controlled and fixed at any level available from the parameters of the device.

The implementation described above for the scheme illustrated in Figure 4 is 10 primarily for experimental purposes. Commercial implementations of the control system would be rationalised for example by using a programmable platform such as a microcontroller or FPGA (field-programmable gate array) based system in conjunction with discrete comparator and gain stages. This approach allows for a degree of reconfiguration of the control method through variation of the sampling 15 rate, capacitive comparator resolution, etc.

Figure 8 shows a possible implementation of the system with the feedback control realised on an ASIC (application specific integrated circuit) with the MEMS device directly connect to the die. This solution represents a flexible option with the 20 ASIC\MEMS connection determining the level of flexibility. For instance, if a socket mount is used, a plug-and-play implementation would be possible whereby different MEMS devices could be interchanged with the same ASIC. In order for devices to be interchanged in this manner the circuit would need an additional level of intelligence to account for different device parameters, e.g. higher comparator resolution, speed, 25 etc. The highest level of integration for MEMS\electronics is monolithic integration and this is possible for the embodiment shown in Figure 8 so long as CMOS compatible materials are used in the fabrication of the MEMS (i.e. non-piezoelectric materials). The electronics comprises a capacitive comparator, decision logic, a charge pump and a control signal generator all of which can be designed on a 30 standard AMS (analog and mixed signal) process.

In terms of applications, the MEMS device can be operated in both the down-state (i.e. the device acts like a closed switch) or in the up-state (i.e. the device operates

as a variable capacitor – varactor). Figure 9 shows how the dielectric control method would be used in a simple single throw, double pole switch. During the off state 0V is applied to the actuation electrode and no charging takes place while in the on state either V^- or V^+ is applied as described in relation to Figures 3-7. In this scenario the
5 control loop is interleaved within the on-off switch control.

Referring to Figure 10, in the up-state state the MEMS device operates as a variable capacitor (varactor); a device often used in reconfigurable RF front-ends especially in mobile applications. For example, a simple RF transmitter circuit uses capacitive
10 and inductive elements to determine the frequency band of the transmitted signal. By replacing a passive capacitor with an active varactor it is possible to tune the output signal to desired frequency ranges. Such a system would require a recalibration routine to set the varactor value for each frequency shift. Without dielectric charge control, MEMS based varactors are prone to a drift in the capacitance value over
15 time or even pull-in events caused by an accumulation in dielectric charge. Also, since the method controls the dielectric charge, and not the position of the moveable electrode in a precise way, for up-state applications the dielectric control loop is embedded within a second control loop. In the case of a varactor the second control loop controls position by changing the absolute value of the applied voltage
20 magnitudes V^+,V^-, while the signs of the voltages will be controlled by the charge control loop. In Figure 10, the inner loop determines the polarity of the actuation sign (i.e. Bit0 or Bit1) while the magnitude of the pulses is set by the outer loop.

Another possible application is in the field of resonant sensors where experimental results indicate that the resonant frequency of electrostatically actuated MEMS
25 resonators is affected by dielectric charging. Figure 11 shows a block diagram of a MEMS resonator where the resonator motion is sensed capacitively and the resultant signal is fed back to differential electrostatic actuators to create a free running oscillator. This previous work, K. L. Dorsey and G. K. Fedder, “Dielectric Charging Effects in Electrostatically Actuated CMOS MEMS Resonators”, IEEE
30 Sensors 2010 Conference, pp. 197-200, 2010, speculated on design and compensation methods to decrease resonant frequency drift and improve the limit of detection for gravimetric sensing applications based on manipulation of the actuation voltage and magnitude. Figure 12 shows the embodiment of a solution where the

dielectric charge control feedback loop is embedded within the oscillation circuit block diagram. The circuit operates as in the previous case with the differential feedback signal driving the oscillation motion, however in the embodiment shown in figure 12 the dielectric charge control loop also operates. The dielectric charge
5 control loop senses the dielectric capacitance and applies the waveform (either Bit0 or Bit1) to ensure the required dielectric charge control. The control block merges the functionality of the two control loops (oscillator control and dielectric control) so that both combine to realise the dielectric charge control function as well as the free running oscillator function.

10

Claims:

1. A controller for a micro-electromechanical system (MEMS) device incorporating a dielectric layer and a voltage supply contact, said controller including a capacitance sensor operatively connected to said MEMS device to selectively
5 measure a capacitance of said MEMS device, an actuation controller interposed in a feedback loop between said capacitance sensor and said device voltage supply, said actuation controller being arranged to successively select between one of two voltage waveforms during actuation of said MEMS device, a first of said waveforms comprising a voltage of a given polarity to be applied for a majority of said waveform
10 time and a voltage of an opposite polarity to be applied for a minority of said waveform time, and a second of said waveforms comprising the voltage of the opposite polarity for the majority of said waveform time and the voltage of the given polarity for the minority of the waveform time, the actuation controller being arranged to measure said capacitance during said waveform time before and after a transition
15 between the given and the opposite polarity and to select a succeeding waveform by comparing a difference in measurements of capacitance and a threshold corresponding to desired device charge.

2. A controller as claimed in claim 1 further comprising a sensing module
20 arranged to store said measurements of capacitance.

3. A controller as claimed in claim 1 wherein said first waveform comprises a constant voltage V^- for a time $(1-\delta)T_s$, followed by a constant voltage V^+ for a relatively shorter time δT_s; and wherein said second waveform comprises V^+ applied
25 during $(1-\delta)$Ts, then V^- for δT_s.

4. A controller as claimed in claim 3 wherein T_s = nTclk, Tclk being a clock period substantially below the time constants of the dielectric charge and discharge dynamics for the MEMS device.

30

5. A controller as claimed in claim 4 wherein Tclk = 0.5s.

6. A controller as claimed in claim 1 wherein said actuation controller is arranged to sense a dielectric charge of said MEMS device as a measurement of capacitance and to select a succeeding waveform by comparing a difference Qn in measured charges and a desired target charge value Q_{target} corresponding to said threshold.

5

7. A controller as claimed in claim 6 providing a bit stream output indicating the successive selection of waveforms to indicate whether the MEMS device has reached a stable regime of dielectric charge.

10 8. A controller as claimed in claim 1 comprising a microcontroller implemented in a field programmable gate array (FPGA), a plurality of discrete gain stages for providing said measurements of capacitance and said threshold and a discrete comparator for comparing said difference in said measurements of capacitance and said threshold.

15

9. A controller as claimed in claim 1 comprising an application specific integrated circuit (ASIC) formed on a die, said die being arranged to receive said MEMS device.

10. A controller as claimed in claim 1 integrated with a MEMS device, said MEMS
20 device comprising non-piezoelectric materials.

11. A controller as claimed in claim 1 further comprising an on-off controller operably connected to said device voltage supply to selectively close said MEMS device.

25

12. An RF circuit including the controller as claimed in claim 1 and a MEMS device, said MEMS device forming a variable capacitor within said RF circuit with a desired capacitance corresponding to said threshold and enabling tuning of said RF circuit.

30

13. A resonator including the controller as claimed in claim 1 and a MEMS device, said MEMS device forming an oscillator within said resonator circuit.

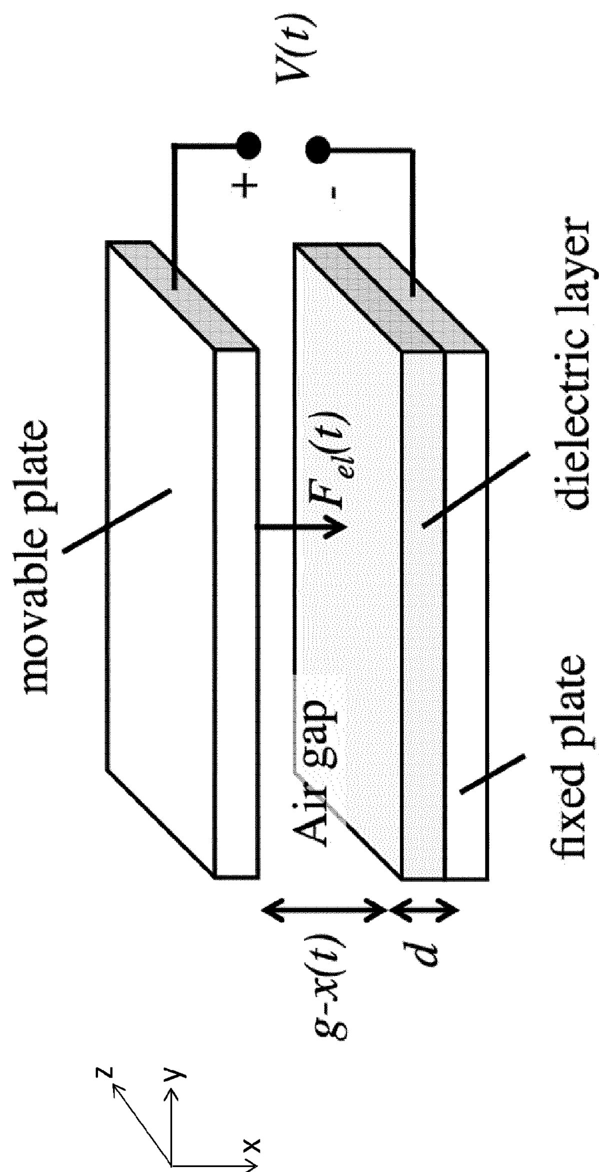

Figure 1 (Prior Art)

WO 2015/082377 PCT/EP2014/076052

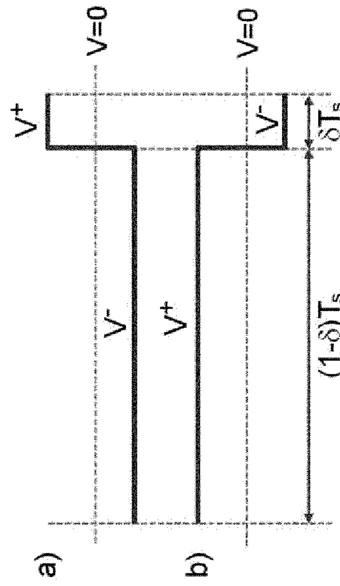

Figure 3

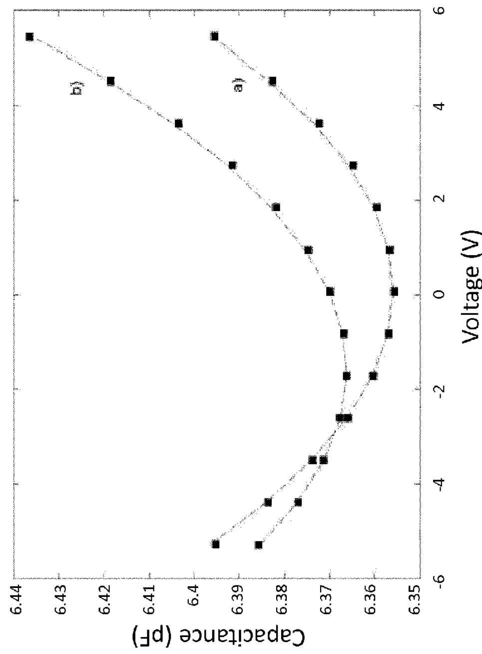

Figure 2

WO 2015/082377 **PCT/EP2014/076052**

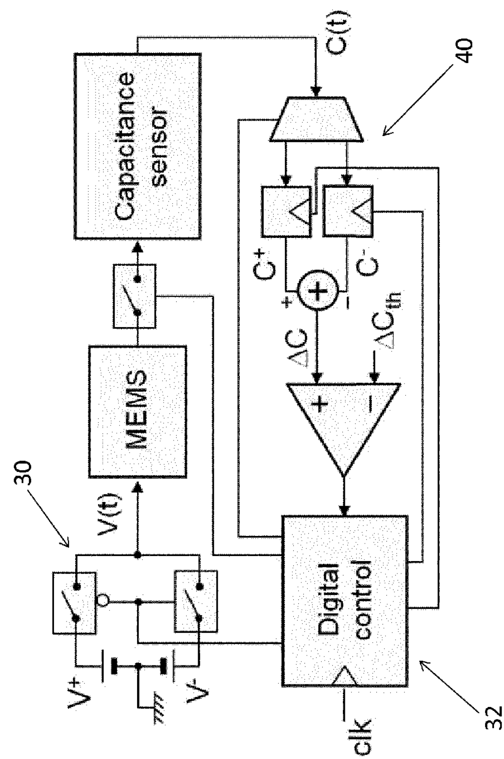

Figure 4

WO 2015/082377 PCT/EP2014/076052

4/9

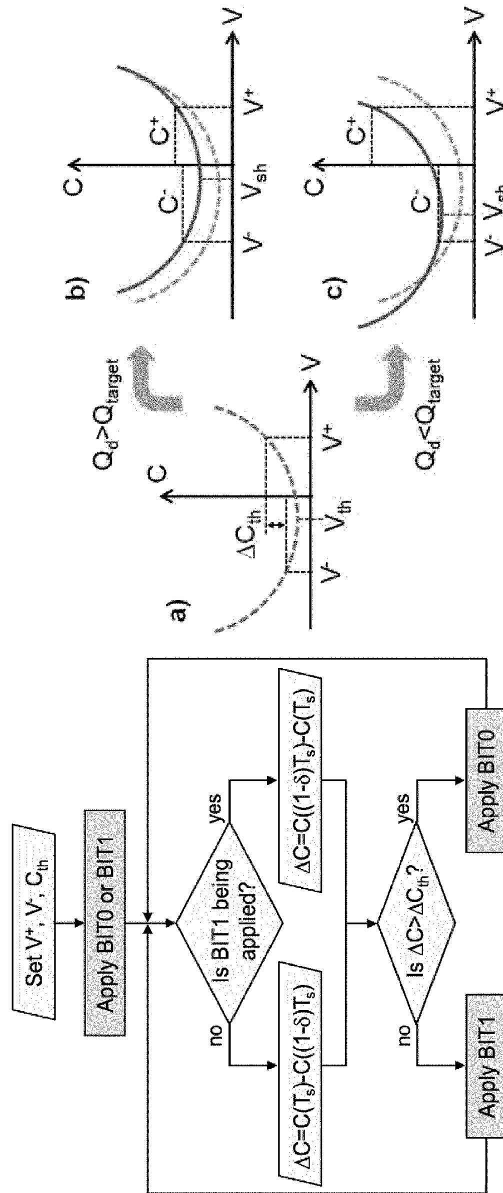

Figure 5

Figure 6

WO 2015/082377 **PCT/EP2014/076052**

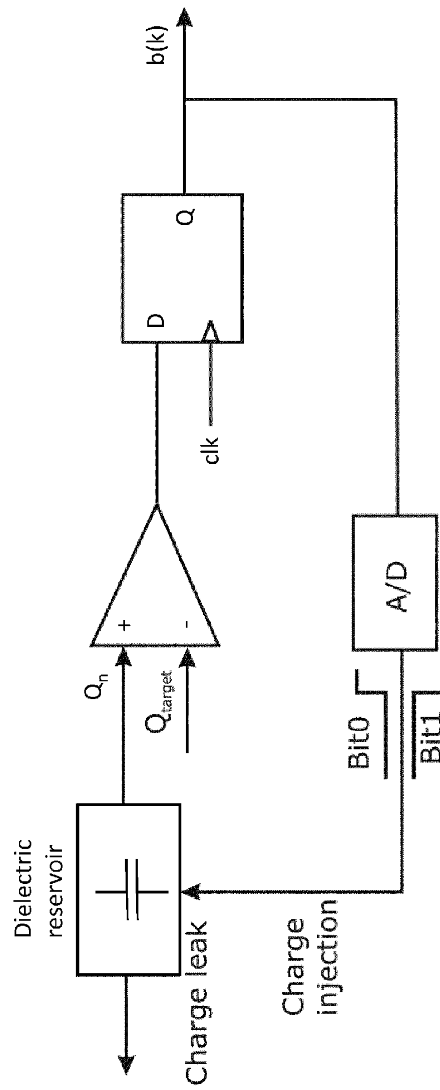

Figure 7

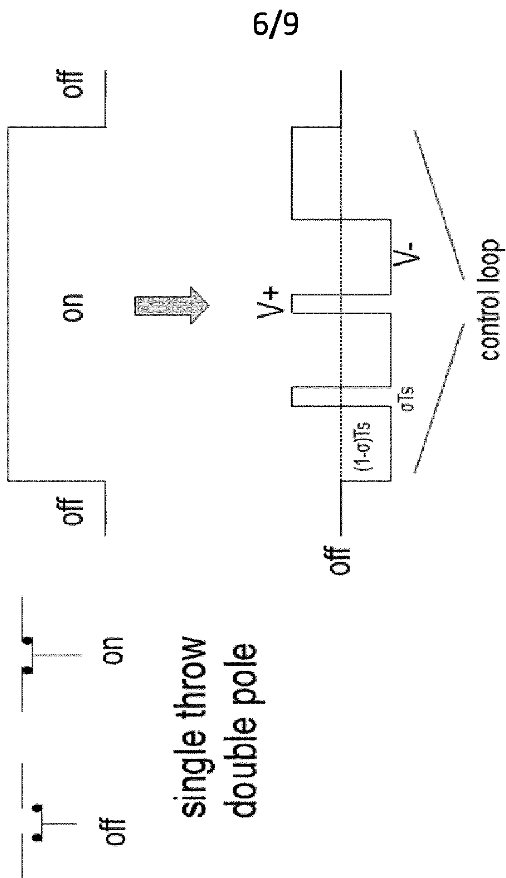

Figure 9

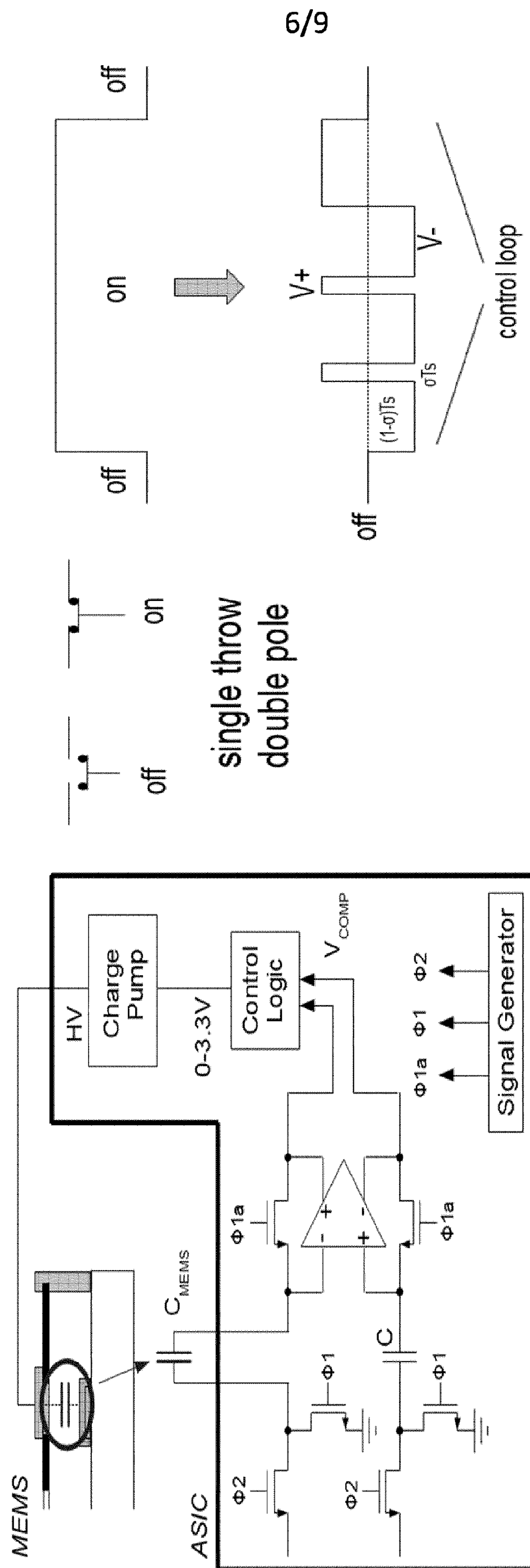

Figure 8

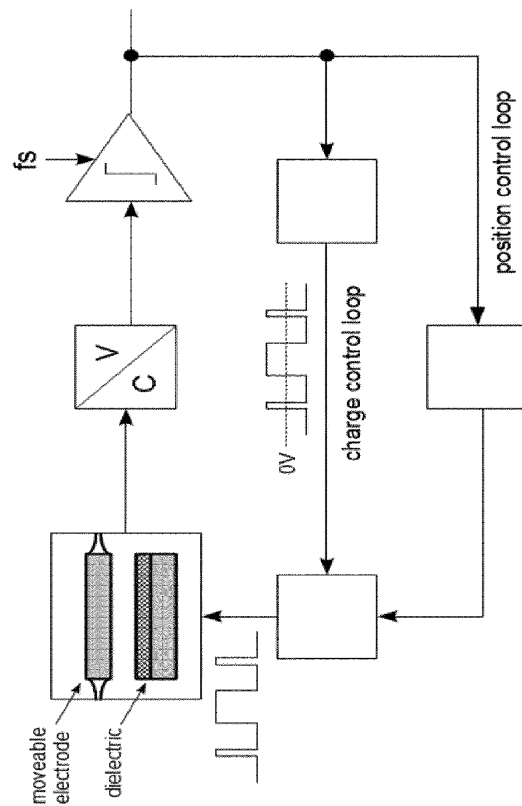

Figure 10

WO 2015/082377 **PCT/EP2014/076052**

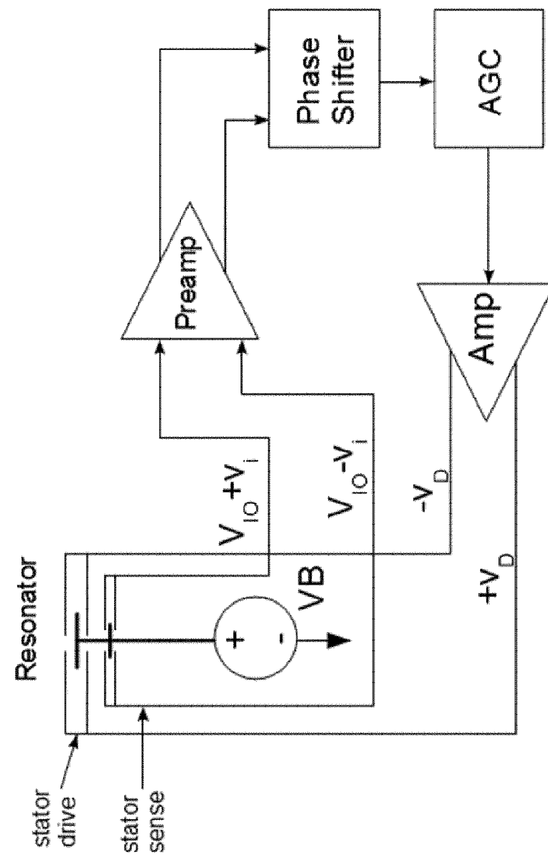

Figure 11 (Prior Art)

WO 2015/082377 **PCT/EP2014/076052**

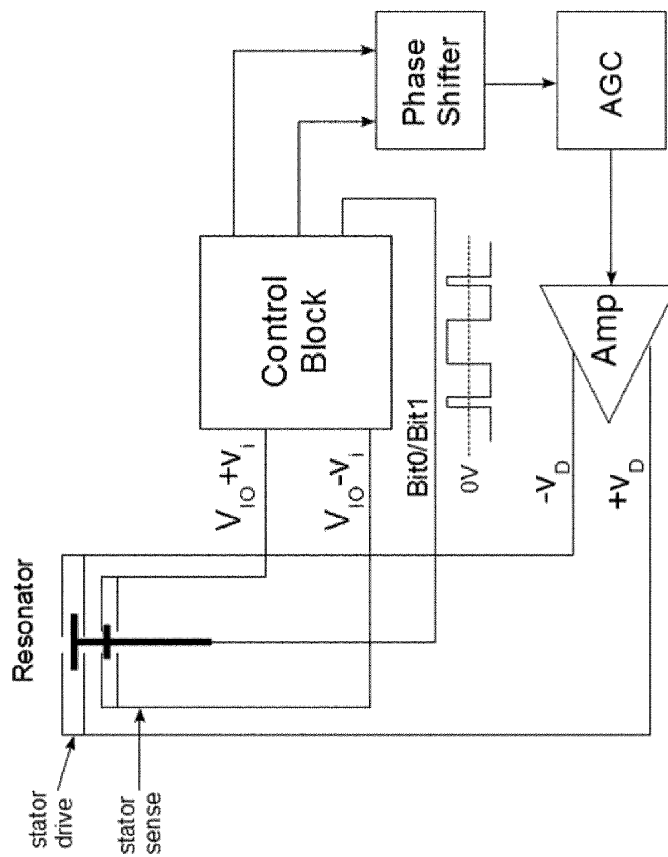

Figure 12

Appendix C

Other Thesis-related conference publications

This appendix contains the conference publication related to the main subject of this Thesis which have not been included in the compendium of publications.

Works:

1. **Modelling of a charge control method for capacitive MEMS.** *2013 European Conference on Circuit Theory and Design (ECCTD),* Sep.2013, p. 207
   http://ieeexplore.ieee.org/document/6662324/

2. **Sigma-Delta inspired control technique for the improvement of MEMS reliability.**, *2014 IEEE International Symposium on Circuits and Systems (ISCAS)*, Jun. 2014, p.211

   http://ieeexplore.ieee.org/document/6865367/

3. **Understanding complexity in multiphysics systems-on-a-chip: mod- ern approaches for design.** *2015 IEEE International Symposium on Circuits and Systems (ISCAS)*, May. 2015, p.2015

   http://ieeexplore.ieee.org/document/7168941/

4. **Sigma-Delta closed loop control of multiexponential systems.** *NOMA National Conferenece,* Oct. 2015, p. 219

   https://noma2015.wordpress.com/proceedings-2/

5. **Circuit considerations and design for MEMS capacitance measurements.** *Ph.D. Research in Microelectronics and Electronics (PRIME), 2016 12th Conference on*, Jun. 2016, p.225

   http://ieeexplore.ieee.org/document/7519540/

6. **Circuit modeling of a MEMS varactor including dielectric charging dynamics.** *MME 2016 27th Micromechanics and Microsystems Europe Workshop*, Aug. 2016, p.229
   http://iopscience.iop.org/article/10.1088/1742-6596/757/1/012012

Attention¡¡

For copyright reasons, pages 204 to 234 of the thesis,
containing the texts mentioned above,
should be consulted on the web pages of the respective publishers.

Appendix D

PDO-related journal publications

This appendix contains the journal papers related to the use of electrostatic MEMS in PDOs. This work has been done as a side project of this Thesis.

Works

1. **Control of MEMS vibration modes with Pulsed Digital Oscillators: Part II — Simulation and experimental results** *IEEE Transactions on circuits and systems I: Regular papers,* vol. 57, no. 8, pp. 1879-1890, Aug. 2010, p. 237. http://ieeexplore.ieee.org/document/5427094/

2. **Pulsed Digital Oscillators for electrostatic MEMS.** *IEEE Transactions on circuits and systems I: Regular papers*, vol. 59, no. 12, pp. 2835-2845, Dec. 2012, p. 249 http://ieeexplore.ieee.org/document/6248713/

3. **A CubeSAT payload for in-situ monitoring of pentacene degradation due to atomic oxygen etching in LEO**. *Acta Astronautica,* vol. 126, pp. 456-462, Oct. 2016, p.261 www.sciencedirect.com/science/article/pii/S0094576

Attention¡¡
For copyright reasons, pages 236 to 267, containing the texts mentioned above, should be consulted on the web pages of the respective publishers.